

## Department of Precision and Microsystems Engineering

### Synthesis Of A Compliant Mechanism That Translates A Reciprocating Reversible Path To A History Dependent Area Describing Path

M. den Daas

Report no : MSD 2024.033  
Coach : Dr. ir. W.W.P.J. van de Sande  
Professor : Prof. dr. ir. J.L. Herder  
Specialisation : MSD  
Type of report : Master thesis  
Date : 11th of June 2024



# Synthesis Of A Compliant Mechanism That Translates A Reciprocating Reversible Path To A History Dependent Area Describing Path

by

M. den Daas

to obtain the degree of Master of Science  
at the Delft University of Technology,  
to be defended publicly on Tuesday June 25th, 2024 at 14:30.

Student number: 5659949  
Project duration: December, 2022 – June, 2024  
Thesis committee: Prof. dr. ir. J. L. Herder, TU Delft, Chair  
Dr. ir. W.W.P.J. van de Sande, TU Delft, Supervisor  
Dr. D. Farhadi Machekposhti, TU Delft, Committee member

An electronic version of this thesis is available at <http://repository.tudelft.nl/>.

# Preface

---

This thesis was written as part of the master High Tech Engineering at the department of mechanical engineering at the Technical University Delft. I had started with the goal of designing a compliant mechanism that could transfer motion intermittently. However, during literature research and the start of the design process it became clear that the necessary building blocks to design such a mechanism did not exist yet. Which led me to a more fundamental research topic. Over the past year I have spent my time researching a novel type of compliant path generator.

I would like to thank my supervisor W.W.P.J. van de Sande for his time, expertise, knowledge and the many fruitful discussions. And I would like to thank my parents and friends for their continued support during my research.



# Introduction

---

Path generation mechanisms are those mechanisms that produce a predetermined path. Such mechanisms are prevalent in daily life, and many devices depend on path generation mechanisms or are derived from path generation mechanisms. One might think of examples such as vehicle suspension, film advance mechanisms or sewing machines. These are generally made with rigid body mechanics, such as linkages. However, these rigid body mechanisms suffer from effects such as friction, play and wear. These problems are well known to be solved using compliant mechanisms. But some path generation such as that necessary for a film advance mechanism can currently not be made using a fully compliant system. This is because full-cycle motion is necessary to produce the path that is generated by such mechanisms, and compliant mechanisms fundamentally are not able of producing full-cycle motion.

This thesis presents the synthesis of a compliant mechanism that is able to translate reversible reciprocating motion to a history dependent path that describes an area. This process is detailed in three separate texts. The first text is set up as a paper, and outlines the generated academic contribution. The second text is the design report, herein the full design and modelling process is described. The third text is the literature review in which the gap in research is detailed.

# Contents

---

<b>1</b>	<b>A Novel Compliant Mechanism Transforming A Reversible Path To A Circumscribed Area Path</b>	<b>1</b>
	I. Introduction . . . . .	1
	II. Model . . . . .	2
	III. Case study . . . . .	5
	IV. Experiment . . . . .	7
	V. Results . . . . .	8
	VI. Discussion . . . . .	10
	VII. Conclusion . . . . .	11
<b>2</b>	<b>Synthesis Of A Compliant Mechanism That Translates A Reciprocating Reversible Path To A History Dependent Area Describing Path</b>	<b>14</b>
	I. Introduction . . . . .	14
	II. Design process . . . . .	14
	III. Bistable model . . . . .	19
	IV. Four bar model . . . . .	24
	V. Combined model . . . . .	24
	VI. Production . . . . .	30
	VII. Experiment . . . . .	32
	VIII. Data processing . . . . .	33
	IX. Results . . . . .	35
	X. Discussion . . . . .	36
	XI. Conclusion . . . . .	38
<b>3</b>	<b>A Review of Existing Intermittent Motion Mechanisms and Their Compliant Counterparts</b>	<b>43</b>
	I. Introduction . . . . .	43
	II. Method . . . . .	44
	III. Mechanical state of the art . . . . .	44
	IV. Compliant state of the art . . . . .	48
	V. Results . . . . .	52
	VI. Discussion . . . . .	52
	VII. Conclusion . . . . .	54



# A Novel Compliant Mechanism Transforming A Reversible Path To A Circumscribed Area Path

Michiel den Daas

**Abstract**—In this paper, a fully compliant mechanism is presented which can translate reciprocating reversible motion to a circumscribed area path imitating full cycle motion. The mechanism functions by replacing one axle with a bistable element, which introduces a predetermined hysteresis loop into the output motion. This mechanism is analysed through the development of a PRB model, a FE model, and experimentation. Between these analyses agreement was found, confirm the mechanism works and is capable of translating reciprocating motion to a circumscribed area.

**Index Terms**—Micro-Scale actuation, Motion translation mechanism, Compliant mechanism, Bistable, Reciprocating motion, Hysteresis

## I. INTRODUCTION

Path generation is one of three categories of kinematic synthesis [1], [2]. Path generators produce a predetermined path with respect to fixed ground at a point existing on a floating link. Straight lines, circle section paths, paths through points etc. are examples of path generation. Path generation linkages such as the Watt's straight line linkage Robert's Linkage and the Scott-Russel linkage have been developed during the 19th century and contributed to the rapid industrialisation by enabling the effective use of steam power [3]–[5]. These mechanisms are still prevalent in various everyday devices. In recent research, these linkages are also used to obtain accurate straight line motion for high precision applications [6], [7]. These high precision applications mainly focus on micro-scale mechanisms, and at micro-scales compliant mechanisms are replacing traditional mechanisms[8]. Compliant mechanisms are mechanisms that elastically deform to provide motion. When designed well, compliant mechanisms will not suffer from wear or friction, and can be made from one continuous piece of material. As a result, the complexity of assembly and maintenance is reduced [9], and the mechanism will not exhibit play. During the last two decades compliant path generation devices have been developed for various applications such as: gripping [10]–[12], transmission [13], [14], micropositioning [15] etc.

Wang and Tai use symmetric path generators to synthesise a fully compliant symmetric gripper [12]. This gripper is able to pick and move objects using the symmetry of the end-effector paths. Sanò et al. developed a fully compliant combdrive actuated straight line mechanism [11], developed for the design of a compliant gripper [10]. This mechanism makes use of a simplified variant of conjugate surface flexure hinges without the guiding surface. Tai et al. present the synthesis of compliant path generators using evolutionary optimisation [16]. The authors make use of skeleton and "flesh" arrangements to generate the mechanisms. They provide the

algorithm with a one DOF loading direction located in a region, a support region, an output region and a desired path. Saxena described a method for the design of compliant path generation mechanisms based on a genetic algorithm [17]. The genetic algorithm is given a structure of nodes, one input, one output, and a support area. With this information it addresses the synthesis in binary form. Zhao and Schmiedeler developed a method for the synthesis of compliant path generators based on rigid body synthesis and a genetic algorithm [18]. The mechanisms that they present are capable of following a predetermined straight-line and curved path. These synthesis methods focus on the development of one DOF compliant linkages and mechanisms. Garcia and Snięowski present a partially compliant combdrive actuated microengine[13]. This microengine is driven by a partially compliant bar mechanism actuated with two combdrives. In the review paper presented by Kota, a three-DOF compliant combdrive actuated microengine is shown [14]. This microengine is driven by three combdrives, with compliant amplification mechanisms to produce the necessary displacement. The mechanisms presented in both papers require the generation of a path that describes an area and this is achieved through control. Botta et al. present the design of a piezoelectrically actuated MEMS which can produce arbitrary XY paths[15]. The actuation is based on 4 sets of piezoelectric elements which are placed such that they incur a moment on the respective cantilever. This displaces the end-effector in two degrees-of-freedom. Mankame and Ananthasuresh present a fully compliant mechanism which can accept reciprocating motion to describe an area at the output [19]. To circumvent the requirement of infinite rotation, they make use of two end-effectors. Tekes presents a two DOF compliant five bar mechanism that can trace predetermined paths based using two actuators and a controller[20].

These strategies either produce reversible reciprocating motion, or they are dependent on two or more degrees of actuation. As a result a designer might be limited to reversible motion, or they have to incorporate more complex control into the design of their system. This may have two reasons, fully compliant mechanisms can only deform over a limited range as shown in fig. 1b[9], [21], [22], and most microscale actuators produce reciprocating motion [23]–[28].

Various applications such as the MEMS micro-engine [13] and the medical applications mentioned by Mankame [19] require a circumscribed perimeter path. Traditional linkages are capable of producing these paths using full cycle motion like in sewing machines or film advancers [3]. But as mentioned earlier, at smaller scales most actuators only produce reciprocating motion. Here, mechanisms such as rocker-crank and slider-crank linkages could translate the reciprocating motion to full

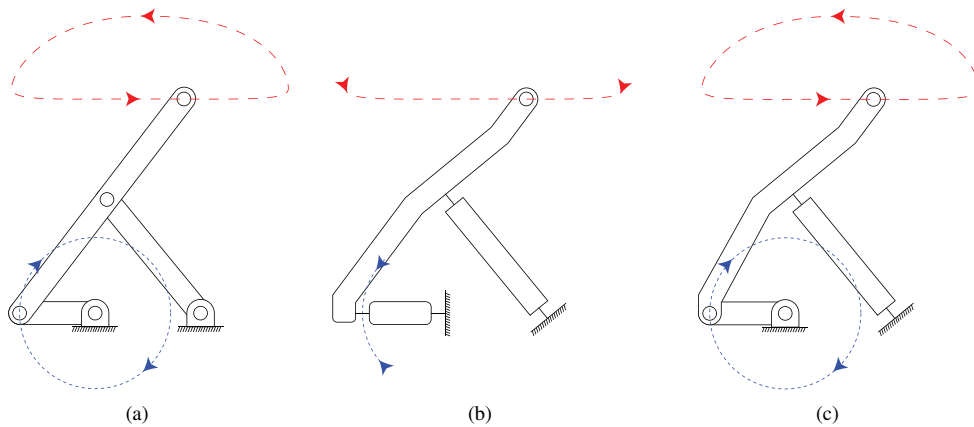


Fig. 1. Three figures showing Chebyshev lambda mechanisms that follow a straight line. a) shows a traditional rigid body mechanism, b) shows a fully compliant mechanism and c) shows a partially compliant mechanism. Adapted from [29]. The input path is indicated with a blue line, and the output path is indicated with a red line.

cycle motion. However, these mechanisms are hampered by the forward kinematic singularity, at this singularity the actuated bar has no DOF with respect to the output. Van den Doel proposes a four-bar mechanism which can translate reciprocating motion to full cycle motion by harnessing the elastic energy in an external spring to overcome the lack of torque transmission near its kinematic singularities. In their paper they show how such a spring should be placed and configured for the optimal behaviour of the four-bar mechanism [30]. But at smaller scales the necessary joint clearance impairs output accuracy [19], and wear causes earlier failure[31].

Ideally one would use a compliant mechanism at this scale to solve this problem. However, to produce circumscribed perimeter motion, compliant mechanisms require a circumscribed path as input as demonstrated in fig. 1c[29]. As a result, the production of motion that circumscribes a perimeter has been limited to traditional, partially compliant, or multi-DOF mechanisms.

In this paper, the authors present a fully compliant four-bar mechanism which can translate reversible reciprocating motion to motion that circumscribes a perimeter. The paper describes the physical modelling and a case study of a new kinematic concept. This concept is inspired by the paper by Mankame and Ananthasuresh [19]. By implementing a bistable element, a hysteresis loop is introduced in a generic compliant four-bar mechanism, forcing the coupler link to follow a path that describes a perimeter. The physical modelling is based on a Pseudo Rigid Body Model (PRBM).

Section II details the kinematics of a four-bar mechanism, the PRBM model used to describe the stiffness, and the interaction between the four-bar mechanism and the bistable element. In section III the parameters of a case study are presented, and the mechanism is modelled in Ansys APDL to compare the predictions with the PRBM. Section IV details the experiments performed on the 3D-printed samples. In section V the results obtained from the PRBM, Ansys APDL and the

experimentation are compared. Finally in sections VI and VII the pertinent conclusions and observations obtained during research are presented.

## II. MODEL

The model described is based on the following hypothesis: A compliant mechanism with an incorporated bistable element is able to translate a reversible oscillation into a motion path that circumscribes a perimeter. This bistable element must be implemented such that it can affect the kinematics of the compliant mechanism. Figure 2 shows the hypothesised behaviour of a compliant four-bar mechanism with a bistable element incorporated into one of its hinges.

The path that the end-effector follows is a result of the hysteresis loop introduced by the bistable element. When actuating a bistable mechanism using a force-determined method, the mechanism will snap-through once the force exceeds the first peak. When consequently the force is decreased, the mechanism will not snap-through at the same point in the force-displacement graph, because the second peak needs to be exceeded. This behaviour results in a hysteresis loop as is shown in fig. 3. In this graph the direction of the hysteresis loop is indicated with the arrows.

In the configuration shown in fig. 2, upon actuating the four-bar mechanism leftwards as indicated by the blue arrow, the four-bar mechanism will start exerting a force and moment on the bistable element. This force and moment builds until the bistable element snaps through, as is shown by the hatched outline of the deformed mechanism. After this snap the effective length of the right link has increased, changing the kinematics of the four-bar mechanism and compelling the end-effector to follow a different path. When actuating the compliant mechanism back to its rest position, or releasing it, the bistable element will remain in its snapped-through state. Only when the four-bar mechanism exerts enough force on the bistable element in the opposite direction will it snap-through to its original position. Considering that the force-displacement graph of the bistable element describes a hysteresis loop as shown in

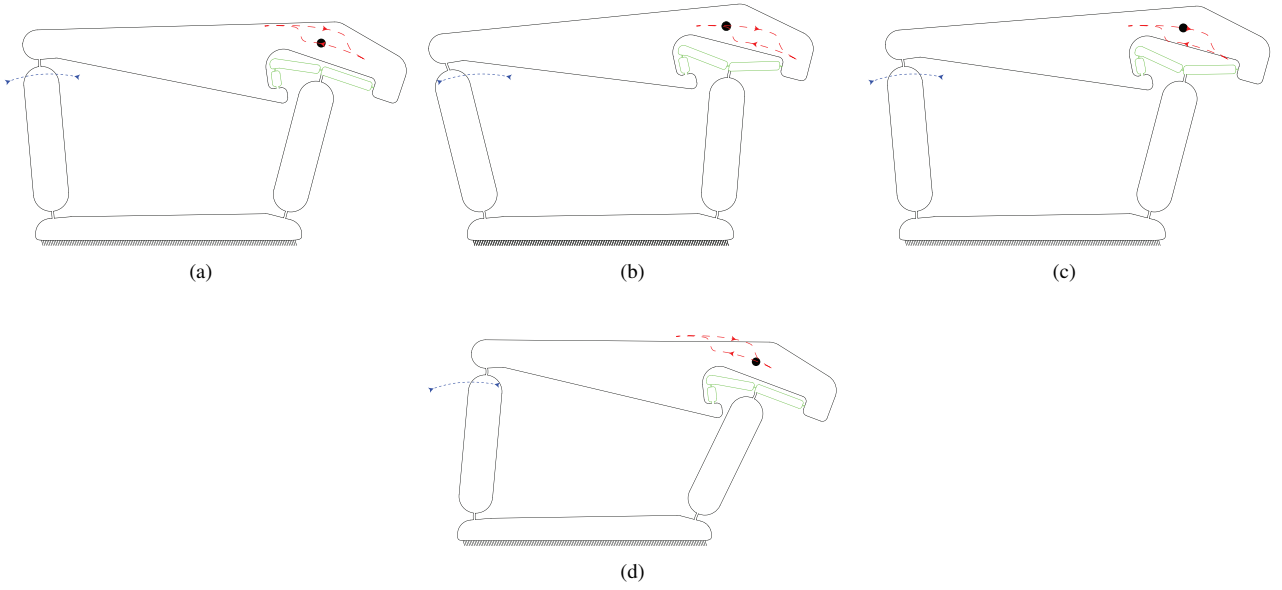


Fig. 2. Four figures showing schematic representations of a compliant four-bar mechanism demonstrating the hypothesised motion at different time frames. The actuation at the input side is shown with a blue line and the hypothesised path is shown with the red line. The bistable element is highlighted in green. a) shows the compliant mechanism before deformation, b) shows the compliant mechanism just after snap-through on the forward stroke, c) shows the mechanism following a different return path, d) shows the compliant mechanism just after snap-through on the return stroke.

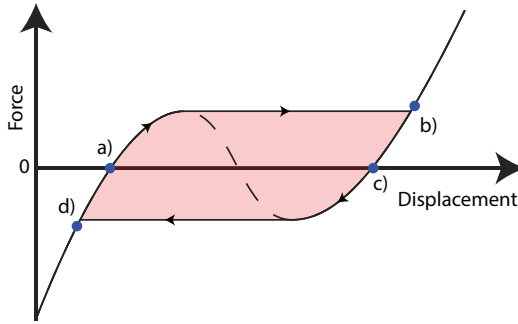


Fig. 3. A graph showing the force-displacement behaviour associated with bistability. The hysteresis loop resulting from force as an input is shown by the lines with arrows denoting the direction. The area in red shows the area of the graph that can not be reached using force as an input. The blue dots show where along the hysteresis path of the bistable element each of the timeframes shown in fig. 2 are.

fig. 3, this snap through on return should happen at a different configuration. Consequently, the end-effector will produce a motion path that describes an area.

The model is developed by implementing a PRBM to approximate the four-bar mechanism and the bistable element. Both mechanisms are approximated as four-bar mechanisms for which the kinematic and stiffness calculations will be presented in general form. Table I shows the equivalent variables for the four-bar mechanism and the bistable element. The interaction between the mechanisms is determined using force balances obtained from the PRBM.

In the first two paragraphs, the kinematics and stiffness of the mechanisms are presented. After which the internal forces of the four bar mechanism, and the interaction between the

four bar mechanism and the bistable element are described.

#### A. Kinematics

The kinematics of the four-bar mechanisms is solved using the Freudenstein equation.

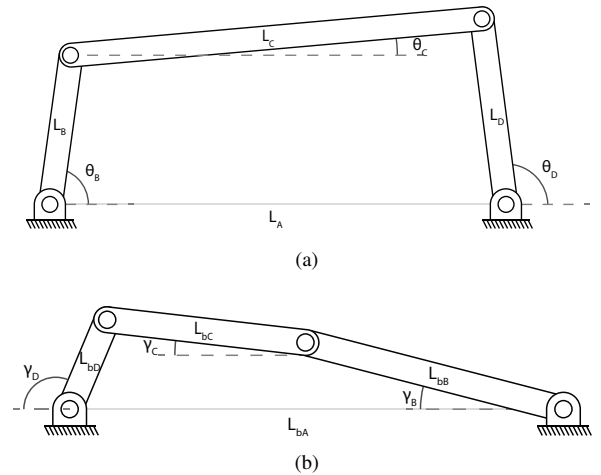


Fig. 4. Two figures showing a schematic representation of the kinematic model used for the four-bar mechanism (a) and the bistable element (b). Included in the figures are the corresponding variables.

Based on the model representation shown in fig. 4a, the vector loop equations are set up:

$$l_B \cos[\theta_B] + l_C \cos[\theta_C] - l_D \cos[\theta_D] - l_A = 0 \quad (1)$$

$$l_B \sin[\theta_B] + l_C \sin[\theta_C] - l_D \sin[\theta_D] = 0 \quad (2)$$

The vector loop equations can be rewritten as the Freudenstein equation.

TABLE I  
VARIABLES USED TO DESCRIBE THE FOUR-BAR MECHANISM AND BISTABLE ELEMENT

	link Angle	Internal Angle	Lengths
four-bar mechanism	$\theta$	$\phi$	$l$
Bistable Element	$\gamma$	$\alpha$	$l_b$

$$K_1(\theta_B)\sin[\theta_D] + K_2(\theta_B)\cos[\theta_D] + K_3(\theta_B) = 0 \quad (3)$$

With the following variables  $K_i$   $i = \{1, 2, 3\}$ :

$$K_1(\theta_B) = -2l_B l_D \sin[\theta_B] \quad (4)$$

$$K_2(\theta_B) = 2l_D(l_A - \cos[\theta_B]) \quad (5)$$

$$K_3(\theta_B) = l_A^2 + l_D^2 + l_B^2 - 2l_A l_B \cos[\theta_B] \quad (6)$$

The Freudenstein equation leads to the following solution.

$$\theta_D(\theta_B) = 2\text{atan2}\left(-2K_1 \pm \sqrt{4(K_1^2 + K_3^2 - K_2^2)}, 2(K_3 + K_2)\right) \quad (7)$$

$$\theta_C(\theta_B, \theta_D) = \text{atan2}(l_D \sin[\theta_D] - l_B \sin[\theta_B], l_A + l_D \cos[\theta_D] - l_B \cos[\theta_B]) \quad (8)$$

### B. Stiffness

Based on the kinematics obtained using the Freudenstein equation, the force behaviour of the mechanisms can be derived. The flexures are modelled as small length flexural pivots. This type of flexure may be modelled as a single hinge [9].

The reaction torsion provided by each of the pivots is determined using the material Young's modulus  $E$ , flexure area moment of inertia  $I_i$  and flexure length  $l_i$  for flexures  $i = \{1, 2, 3, 4\}$  as follows:

$$T_i = -k_i * \phi_i \quad (9)$$

$$T_i = -\frac{EI_i}{l_i} * \phi_i \quad (10)$$

Where  $\phi$  is defined as the deformation of  $\theta$  with respect to starting angles  $\theta_0$ :

$$\phi_1 = (\theta_B - \theta_{B0}) \quad (11)$$

$$\phi_2 = (\theta_B - \theta_{B0}) - (\theta_C - \theta_{C0}) \quad (12)$$

$$\phi_3 = (\theta_C - \theta_{C0}) - (\theta_D - \theta_{D0}) \quad (13)$$

$$\phi_4 = (\theta_D - \theta_{D0}) \quad (14)$$

Using these hinge torques, the reaction moment of the mechanisms around link B is calculated.

$$Mr_B = -T_1 - T_2 - (T_2 + T_3) * h_{32} + \quad (15)$$

$$(T_3 + T_4) * h_{42} \quad (16)$$

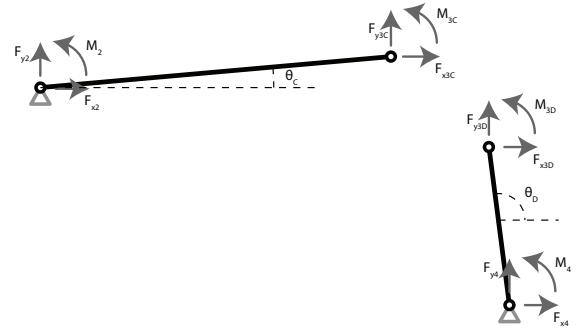


Fig. 5. Figure showing the free body diagram of links C and D for an arbitrary configuration.

With  $h_{32}$  and  $h_{42}$  defined as:

$$h_{32} = \frac{L_B \sin[\theta_D - \theta_B]}{L_C \sin[\theta_C - \theta_D]} \quad (17)$$

$$h_{42} = \frac{L_B \sin[\theta_C - \theta_B]}{L_D \sin[\theta_C - \theta_D]} \quad (18)$$

### C. Force in link D

The sum of moment exerted on the bistable element is calculated using the torque and force in hinge three as shown in section II-D. The internal force is a result of the four-bar mechanism stiffness, and is found per time step using static equations.

From the free body diagram, the force and moment balances can be determined for links C and D.

The balances for link C are:

$$\sum F_{xC} = F_{x2} + F_{x3C} = 0 \quad (19)$$

$$\sum F_{yC} = F_{y2} + F_{y3C} = 0 \quad (20)$$

$$\sum M_{2C} = M_2 + M_{3C} + l_C [F_{y3C} \cos[\theta_C] - F_{x3C} \sin[\theta_C]] = 0 \quad (21)$$

$$\sum M_{s3C} = M_2 + M_{3C} + l_C [F_{x2} \sin[\theta_C] - F_{y2} \cos[\theta_C]] = 0 \quad (22)$$

The balances for link D are:

$$\sum F_{xD} = F_{x4} + F_{x3D} = 0 \quad (23)$$

$$\sum F_{yD} = F_{y4} + F_{y3D} = 0 \quad (24)$$

$$\sum M_{4D} = M_4 + M_{3D} + l_D [F_{y3D} \cos[\theta_C] - F_{x3D} \sin[\theta_D]] = 0 \quad (25)$$

$$\sum M_{s3D} = M_4 + M_{3D} + l_D [F_{x4} \sin[\theta_D] - F_{y4} \cos[\theta_D]] = 0 \quad (26)$$

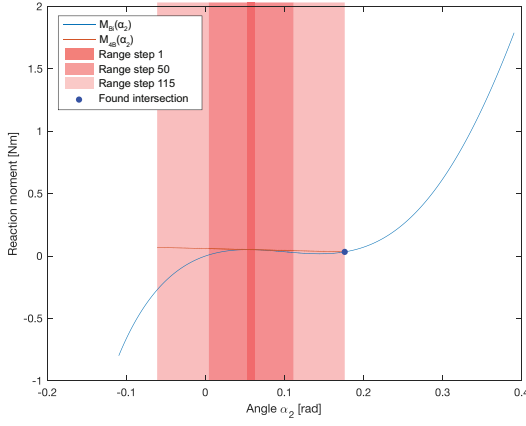


Fig. 6. A figure showing a graphical interpretation of the algorithm used to find the intersection. In orange is the line of the applied moment  $M_{4B}(\alpha_2)$ , in blue is the reaction moment  $M_{Bi}(\alpha_2)$ . The red areas show the search ranges for steps 1, 50, and 115. The blue dot shows the intersection that was found.

The force and moment balance in joint three of the four-bar mechanism is then:

$$\sum Fx_3 = Fx_{3C} + Fx_{3D} = 0 \quad (27)$$

$$\sum Fy_3 = Fy_{3C} + Fy_{3D} = 0 \quad (28)$$

$$\sum M_3 = M_{3C} + M_{3D} = 0 \quad (29)$$

These equations are solved for  $Fx_3$  and  $Fy_3$  to obtain the internal forces of link D at the location of joint three.

$$Fx_3(\gamma_B) = -\frac{L_C[M_3 + M_4]\cos[\theta_C] + L_D[M_2 - M_3]\cos[\theta_D]}{l_C l_D \sin[\theta_C - \theta_D]} \quad (30)$$

$$Fy_3(\gamma_B) = -\frac{L_C[M_3 + M_4]\sin[\theta_C] + L_D[M_2 - M_3]\sin[\theta_D]}{l_C l_D \sin[\theta_C - \theta_D]} \quad (31)$$

Because deformation of bistable element change the configuration of the four-bar mechanism, all moments and angles in eqs. (30) and (31) are functions of  $\gamma_B$  at each timestep.

#### D. Interaction

The interaction between the two four-bar mechanisms is modelled using a moment balance at the attachment point to find the deflection of the bistable element. This is the attachment point of link D of the four-bar mechanism to link B of the bistable element the forces exerted by the four bar are shown in fig. 7. From this deflection of the bistable element, the change in length of  $l_D$  can be calculated.

For each timestep of the simulation, an angle  $\theta_B$  is set. Using this set angle, the moment exerted by the four-bar mechanism can be calculated as a function of  $\gamma_B$ . By obtaining the internal forces as a function of  $\gamma_B$ , the effect of the changing kinematics is accounted for in the model. Equation (33) describes the moment that the four-bar mechanism applies on the bistable element.

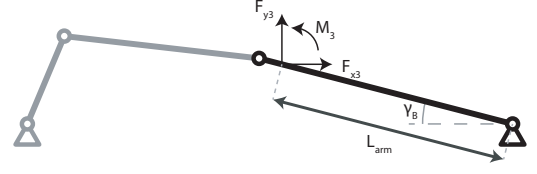


Fig. 7. A schematic representation of the force and moment exerted on link B of the bistable mechanism by the four bar mechanism.

$$M_{4B}(\gamma_B) = M_3(\gamma_B) - \quad (32)$$

$$(Fx_3(\gamma_B)\sin[\gamma_B] + Fy_3(\gamma_B)\cos[\gamma_B])L_{arm} \quad (33)$$

This exerted moment is then balanced with the reaction moment of the bistable mechanism obtained using eq. (16).

$$M_{Bi}(\gamma_B) = M_{4B}(\gamma_B) \quad (34)$$

At the intersections between  $M_{4B}(\gamma_B)$  and  $M_{Bi}(\gamma_B)$ , the four bar mechanism and the bistable element are in balance. Given that both  $M_{4B}(\gamma_B)$  and  $M_{Bi}(\gamma_B)$  can be calculated using eqs. (16) and (33), their intersection can be found at each timestep. However, between a certain range of moments, three intersections may be found between the graphs of  $M_{4B}(\gamma_B)$  and  $M_{Bi}(\gamma_B)$ , of which one is valid with respect to the previous timestep. To ensure that only the correct intersection is found, the intersection is searched for over a range of  $\gamma_2$ . When no intersection is found within the range, the range is increased until an intersection is found. Whenever multiple intersections are found, the range is decreased. This process is shown in fig. 6. From this intersection angle  $\gamma_B$  and the corresponding change in length  $dl_D$  is found for the current value of  $\theta_B$ .

The process is based on the following assumptions:

- The displacement of the bistable mechanism in y direction can be directly translated to a change in length of link D of the four-bar mechanism.
- The displacement of the bistable mechanism in x direction is small enough to not take into account with respect to the behaviour of the entire system.
- The force and moment exerted on the bistable element by the four-bar mechanism may be summed and modelled as one moment.

### III. CASE STUDY

Using the PRBM, parameters were obtained that would produce a functioning model. These parameters are shown in table II. These parameters have been chosen such that the compliant mechanism can be produced using a Bambulabs X1C 3D printer. This meant that the minimum feature size was limited to 0.4mm.

#### A. Sensitivity of the mechanism

The angle  $\theta_B$  at crossover was determined for the forward and return stroke. This plot is shown in fig. 9. To assess the effect of small variations of the mechanism configuration,



TABLE II  
PARAMETERS OF THE FINAL MECHANISM DESIGN. THE VARIABLE NAMES CAN BE REFERENCED FROM FIG. 4, AND AN F IN SUBSCRIPT DENOTES FLEXURE VARIABLES.

Segment	Length/angle	Width	Segment	Length/angle	Width
$l_A$	132 mm	20 mm	$l_{bA}$	54 mm	5 mm
$l_B$	86.4 mm	20 mm	$l_{bB}$	31 mm	5 mm
$l_C$	160 mm	20 mm	$l_{bC}$	26 mm	5 mm
$l_D$	80 mm	20 mm	$l_{bD}$	10 mm	5 mm
$l_{f1}$	4 mm	1.2 mm	$l_{bf1}$	1.4 mm	0.4 mm
$l_{f2}$	4 mm	1.2 mm	$l_{bf2}$	1.4 mm	0.4 mm
$l_{f3}$	4 mm	1.2 mm	$l_{bf3}$	1.4 mm <td 0.4 mm	
$l_{f4}$	4 mm	1.2 mm	$l_{bf4}$	1 mm	1.6 mm
$\theta_{B0}$	95 °		$\gamma_{B0}$	18.56 °	

TABLE III  
MATERIAL PARAMETERS AND SHEET THICKNESS

	Value	Unit
Material	PETG	
Young's modulus	1607	MPa
Thickness $t_p$	5	mm

this crossover angle was calculated for a set of mechanisms with varying stiffnesses for the bistable element and four-bar mechanism. This plot is shown in fig. 9.

The relative stiffness was obtained by changing the width of all flexures in the bistable element and four-bar mechanism with respect to the case study parameters. The stiffness of all flexures of either the bistable element or the four-bar mechanism is changed with a factor  $f_{Bi}$  or  $f_{AB}$  respectively. To obtain the new stiffness, the width of each flexure was changed with the cube root of the desired factor. With this new width, the corresponding area moment of inertia  $I_i$  is calculated using the plate thickness  $t_p$  and flexure width  $d_i$  with  $i = \{1, 2, 3, 4\}$ . After which the new value can be used in eq. (10).

$$I_i^{AB} = \frac{t_p [\sqrt[3]{f_{AB}} d_i^{AB}]^3}{12} \quad (35)$$

$$I_i^{Bi} = \frac{t_p [\sqrt[3]{f_{Bi}} d_i^{Bi}]^3}{12} \quad (36)$$

From fig. 9 it is visible that the ratio between the four-bar mechanism and the bistable element has an effect on the crossover moment of the mechanism. One can see that below  $\frac{f_{Bi}}{f_{AB}} = 0.24$  the two lines become one, this shows that below a certain stiffness ratio the crossover moment is the same on the forward stroke as on the return stroke. This is because the slope of the applied moment  $M_{4B}(\gamma_B)$  has become larger than the strongest slope between the peaks of the reaction moment  $M_{Bi}(\gamma_B)$ . From  $\frac{f_{Bi}}{f_{AB}} > 0.24$  the difference between the forward and return crossover angle  $\theta_B$  becomes greater with increasing bistable element stiffness.

### B. APDL Simulation

The bistable element and the four-bar mechanism were simulated in Ansys APDL to validate the PRBM. Both models are modelled using beam188 elements with nonlinear geometry turned on in the solver. The mechanisms were modelled with the same parameters as denoted in table II.

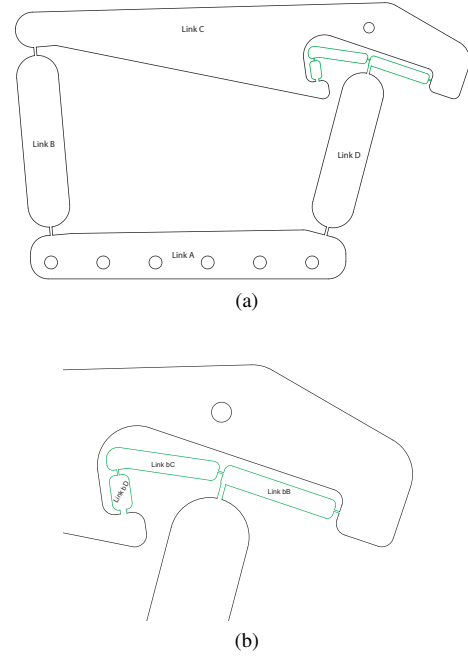


Fig. 8. Two figures showing the outline of the compliant mechanism being analysed in this paper. a) shows the full mechanism and b) shows the bistable element up close. The circle hole that exists above the bistable element is the point of interest which exists in the samples, and the PRBM and FEM models.

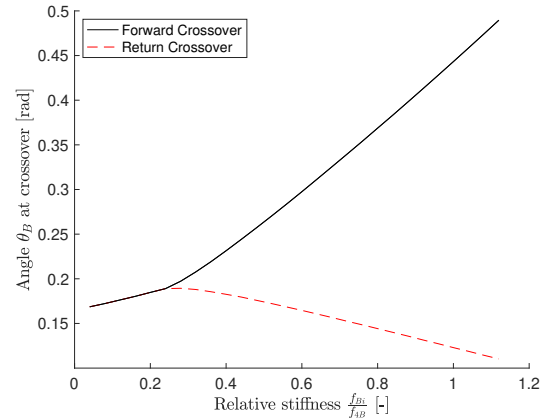


Fig. 9. A plot showing the effect of varying flexure stiffness on the crossover angle  $\theta_B$ . The black line shows angle  $\theta_B$  at the first crossover. The red line shows angle  $\theta_B$  at the return crossover. At relative stiffness = 1 exists the chosen configuration. Factors  $f_{Bi}$  and  $f_{AB}$  are the factors that are used to change the stiffness as in eqs. (35) and (36) for the bistable element and four-bar mechanism respectively.

1) *Bistable element*: The bistable element is actuated using a forced rotation of link B, which can be seen on the right in fig. 10. Based on this forced rotation, the moment-displacement graph shown in fig. 12a was obtained.

2) *Four-bar mechanism*: The four-bar mechanism is also actuated with a forced rotation of link B, present on the left in fig. 11. From this the moment-displacement graph shown in fig. 12b and the motion plot shown in fig. 12c were obtained.

The predictions for the mechanism behaviour generated by the APDL model and PRBM do not fully align. As is visible in

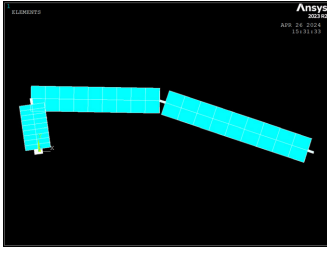


Fig. 10. A figure showing the FEM model produced for the bistable element in Ansys APDL.

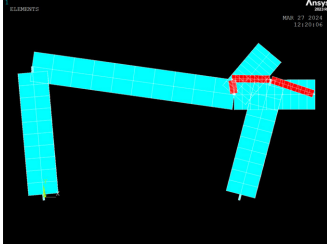


Fig. 11. A figure showing the FEM model produced for the bistable element in Ansys APDL. The blue elements are the four-bar mechanism, and the red elements are the bistable element connected to the four-bar mechanism.

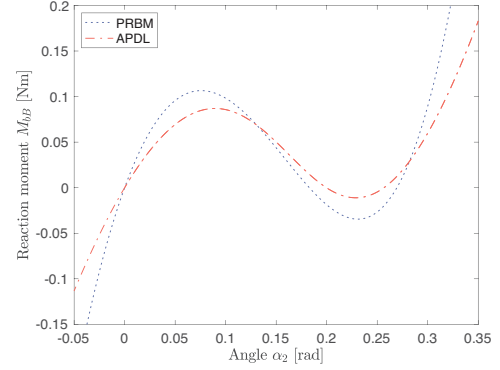
figs. 12b and 12c, the angle at which the mechanism switches between the paths is different between the PRBM and the APDL models. This difference may be explained by the difference in stiffness of the bistable element between the models. As was concluded based on fig. 9, a stiffer bistable element will result in a larger difference between the crossover angles. Regarding the moment-displacement plots of both models, one can see from fig. 12b that the PRBM and Ansys agree on the stiffness of the four-bar mechanism, but disagree on the stiffness of the bistable element. This indicates that the difference in predicted motion path is likely to originate from the PRBM of the bistable element.

Another explanation for the discrepancy might be the design of the bistable element. Due to the design limitations when designing for 3D printing, the widths of flexure four and link D of the bistable element shown in fig. 8b are too similar. As a result the stiffness ratio between link D and flexure four of the bistable element in the chosen configuration is too low to disregard the compliance of link D. When calculating the ratio  $r$  between flexure stiffness  $k_{bf4}$  and link stiffness  $k_{bD}$ , one can see that the assumption  $k_{bD} \gg k_{bf4}$  on which the PRBM is based does not hold.

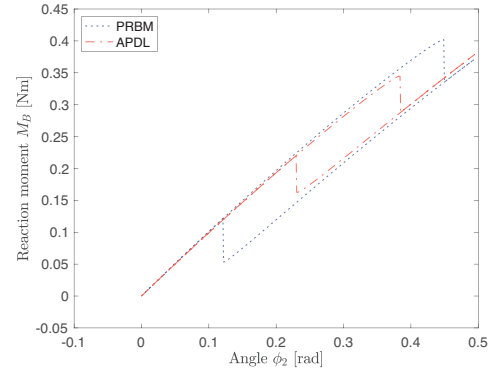
$$r = \frac{k_{bD}}{k_{bf4}} = 3.05[-] \quad (37)$$

The stiffness of joint four of the bistable element was adjusted to correct the PRBM for this error. This was done by taking the spring stiffness of link D and axle four as springs in series as in eq. (38). This change is taken into account into the results shown in table IV.

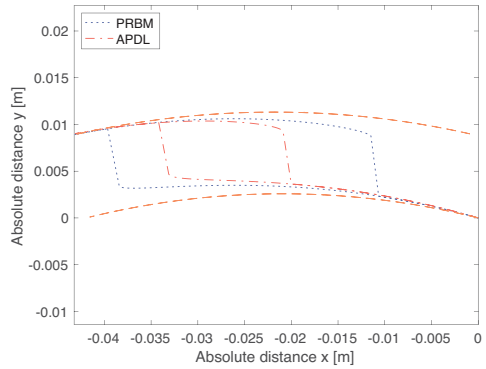
$$\frac{1}{k_4} = \frac{1}{k_{f4}} + \frac{1}{k_{bD}} \quad (38)$$



(a)



(b)



(c)

Fig. 12. Three plots showing the results from the PRBM and the APDL model. In the plots, the dotted blue line shows the result from PRBM, and the dot-dashed orange line shows the results from APDL. a) shows the moment-displacement results for the bistable element, b) shows the moment-displacement results for the full mechanism, and c) shows the motion plot for the point of interest. In c) additional lines are added, the dashed orange lines show the paths between which the mechanism switches.

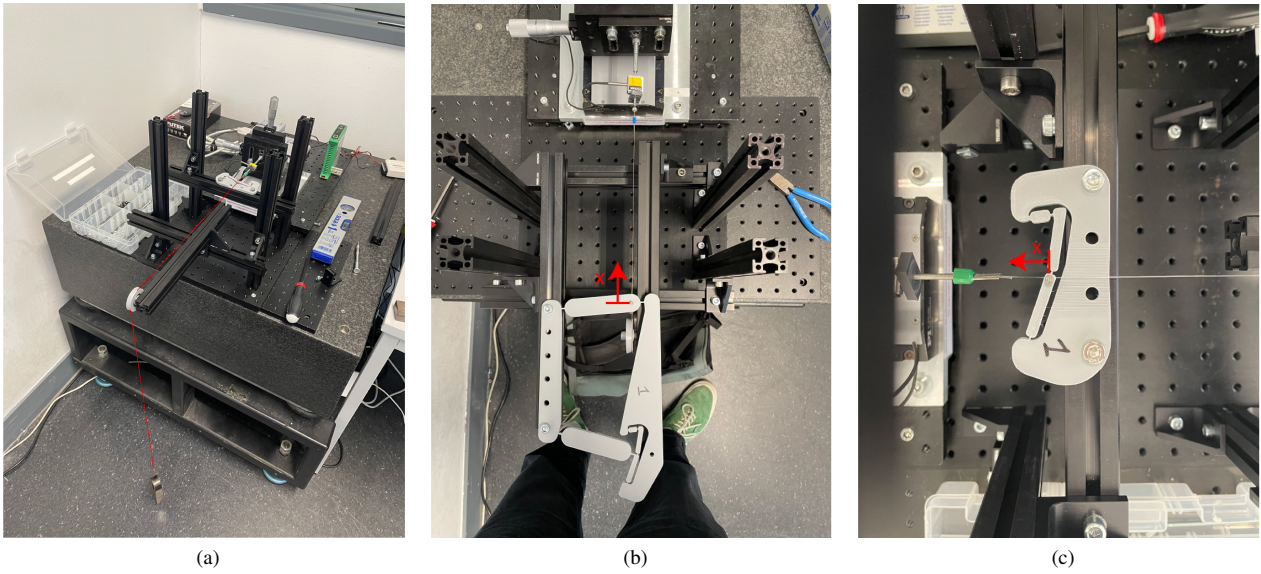


Fig. 13. Three pictures showing the experiment setup used to perform the force-distance experiments. a) shows an overview of the entire setup, the wire that was used is highlighted using a red line. b) shows the full compliant mechanism mounted in the setup with the positive displacement direction denoted with  $x$ . c) shows the bistable element mounted in the setup with the positive displacement direction denoted with  $x$ .

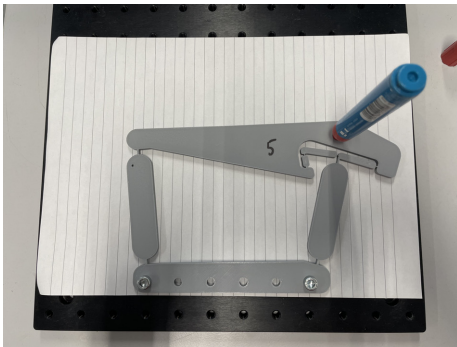


Fig. 14. four-bar sample mounted to a thorlabs breadboard with a pen attached to the point of interest to draw the motion path.

#### IV. EXPERIMENT

The predicted functioning of the designed mechanism was verified through experimentation. Three experiments were performed: the motion path of the point of interest was tested, and the force-displacement graphs of the compliant mechanism and bistable element were measured.

For all experiments the samples were printed using a bambulabs x1 carbon at 150 mm/s with wall speed of 75mm/s to ensure the single thickness flexures are printed as accurately as possible. The material used was polymaker PETG in grey, this material was selected as the best material available, see table III.

##### A. Motion path

1) *Method:* After the 3D-printed mechanism is taken out of the printer, it is moved to the testbed ensuring the mechanism is deformed as little as possible. The compliant mechanism is then fastened to a Thorlabs breadboard using the holes included

in the base of the mechanism. Underneath the compliant mechanism, a sheet of A4 paper is fastened using the same bolts as shown in fig. 14. Then, a ball-point pen is secured in the hole located at the point of interest. This pen is dragged over the paper by the compliant mechanism during the stroke. The stroke is actuated by hand from rest until beyond the bistable element switches over to the different path. After the the mechanism is actuated back to its starting position. This constitutes one cycle. This is repeated for a total of three cycles.

##### B. Force-Displacement

Based on fig. 9, the conclusion was drawn that the mechanism is sensitive to a variation of relative stiffness between the bistable element and the four-bar mechanism. As such, a lack of accuracy in the production of the mechanism can affect the measured results. To validate whether the difference observed is due to modelling methods or production methods two further experiments are performed: The force displacement of both the bistable element isolated, and the full compliant mechanism.

1) *Method:* The sample is mounted to a frame on a Thorlabs breadboard such that no moving parts are in contact with any surface. A second Thorlabs breadboard with a PI linear stage with a plutek lsb200 44 N force sensor is attached to the previous breadboard.

First, a wire (0.3mm copper) was attached to the load cell using a bolt. As it was predicted that the bistable element would produce a negative force over the course of its path, this wire is strung over a pulley and preloaded using a weight as shown in fig. 13a.

To this wire a small clamp was added after which the force measurement of the load cell was zeroed. After this, the sample is mounted to the small clamp.

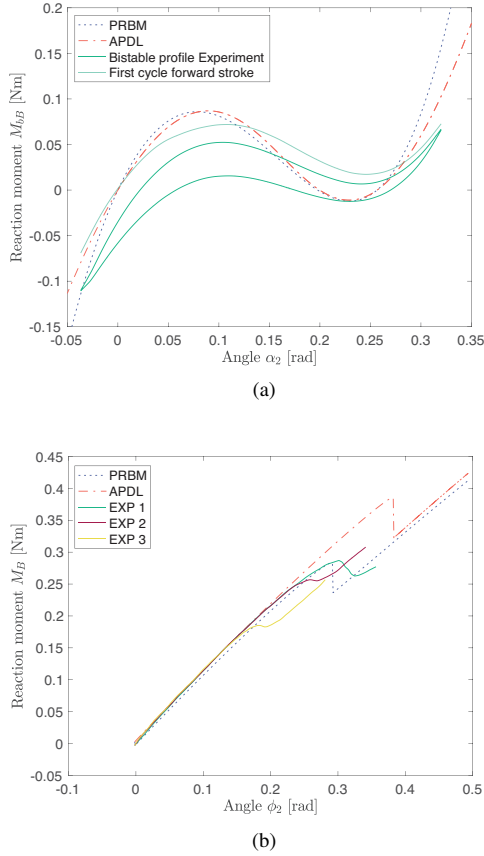


Fig. 15. Two plots showing the force-Displacement profiles resulting from the experiments. a) shows the results of the bistable mechanism, b) shows the results from the force-displacement experiments of the four-bar. In a), the dotted blue and dot-dashed orange lines represent the PRBM and Ansys APDL models respectively, the cyan line indicates the first forward stroke, and the black line represents the forward and return strokes from stroke 2-N. In b), the dotted blue and dot-dashed orange lines represent the PRBM and Ansys APDL models respectively, and the solid lines show the experimental results.

Because during the attachment of the compliant mechanism to the wire, the compliant mechanism is most likely preloaded. The next step is to move the linear stage to a position where the load cell again reads 0 N, after which the stage location is zeroed.

Next, the samples are displaced.

The bistable element is first displaced to -1 mm and then 9mm in the positive direction. This is repeated until five cycles have been completed, ending at -1 mm.

The four-bar mechanism is displaced 25 mm in the positive direction. After this forward stroke the four-bar mechanism is moved back to 0 mm.

## V. RESULTS

### A. Force-Displacement

Figure 15 shows the results obtained from the force-displacement experiments. In fig. 15a, the stiffness of the mechanism during the forward stroke of the first actuation is higher than on subsequent actuations. The return stroke of cycle one and cycles two until five follow a hysteresis path which is lower than the moment-displacement path predicted.

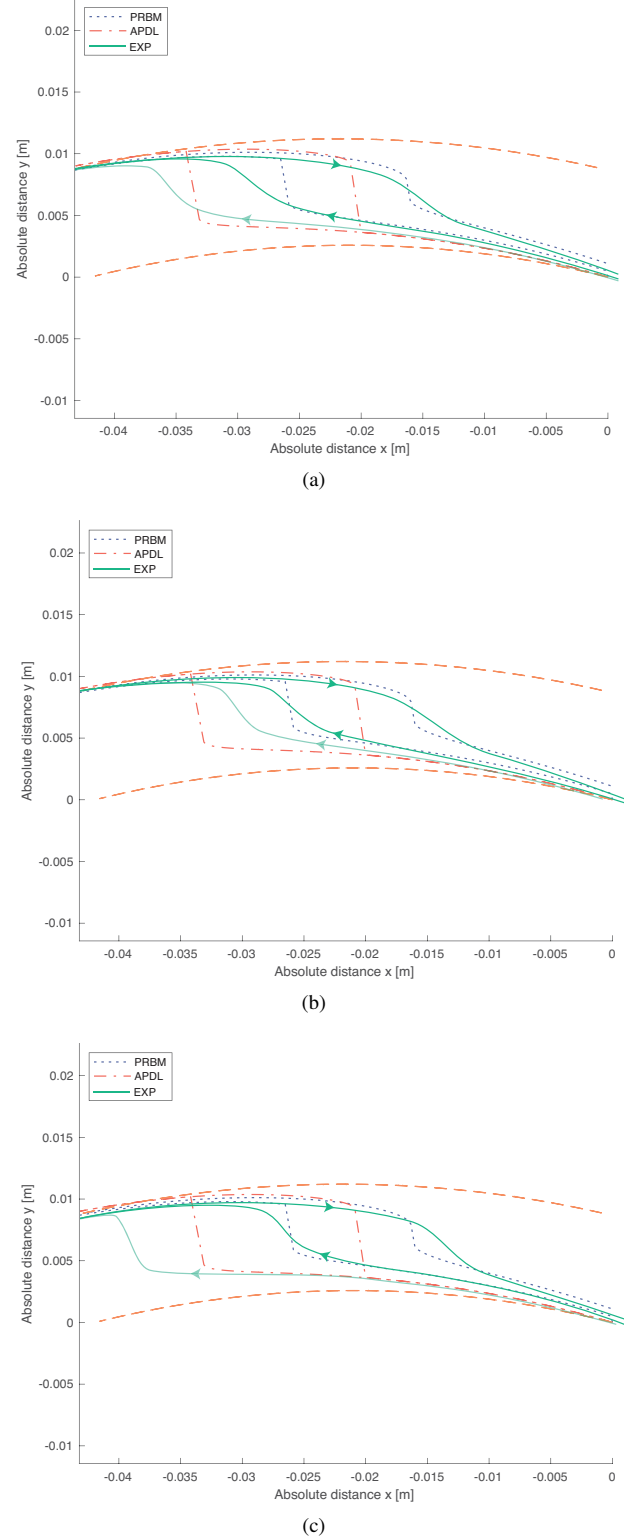


Fig. 16. Three plots showing the results of the path experiment. The dotted blue and dot-dashed orange lines represent the PRBM and Ansys APDL models respectively. The solid green lines show the measured paths, from each experiment the forward stroke of cycle one is shown in a less saturated green. a) shows the results for path experiment 1, b) shows the results for path experiment 2 and c) shows the results for path experiment 3.

The maximum of the bistable element on the forward stroke is lower than predicted. Additionally the minimum on the return stroke is at a higher negative value than predicted.

Figure 15b shows the experiment results for the force-displacement experiment of the four-bar mechanism. This figure shows that the measured results agree with the predictions obtained from the PRBM and APDL model. The agreement of the slope of the moment-displacement line between the measured results and the models indicates that the models are good predictors for the four-bar mechanism stiffness.

### B. Motion path

Figure 16 shows that the models provide a reasonable prediction for path generation. Based on section III-A the stiffness of the bistable mechanism is determinative for the switchover angle of the full mechanism.

In the motion experiment results in fig. 16 the prototypes actuated earlier than predicted by the models on the forward stroke and tended to actuate later than predicted on the return stroke. This can be explained when looking at the measured force-displacement graph of the bistable element in fig. 15a. Comparing the observations in section V-A with fig. 9, this may provide an explanation for the difference between the PRBM and the samples.

This is further supported by the results of the model when incorporating the experimental data into the PRBM. The results of this can be seen in table V, which shows the prediction error of the model compared to the experiment results shown in fig. 16. As is visible when comparing to the results of the PRB model with the correction from eq. (38) shown in table IV, implementing the data of the moment-displacement provides a better prediction than purely the PRBM. On the other hand, table V also shows a larger discrepancy with the predicted crossover on the first cycle. The percentages in tables IV and V are taken as percentage of the actuation distance of the model, which is 0.49 rad. This percentage is calculated as in eq. (39). From this table one can see that the predictions of the model improve by a few percent when using the experiment data. Especially the prediction of the forward stroke improves by using the measured data.

Furthermore from fig. 16 it is found that the forward crossover angle changes significantly after the first cycle. This is consistent with the experiment results obtained from fig. 15a. On this first cycle, the motion path seems to follow predictions relatively well. But based on the sensitivity predicted in fig. 9, from the second cycle it seems like the stiffness of the bistable element relative to the four-bar becomes significantly smaller. As a result, the forward crossover angle decreases after the first cycle.

The equation used to calculate the absolute percentage error of the predicted crossover  $\theta_{BCE}$  with respect to the measured crossover  $\theta_{BCM}$  as a percentage of the swept angle  $\theta_{BS}$ :

$$Error\% = \frac{|\theta_{BCE} - \theta_{BCM}|}{\theta_{BS}} \quad (39)$$

TABLE IV  
THE CROSSOVER ANGLE  $\theta_B$  PREDICTION ERROR OF THE PRBM AS A PERCENTAGE OF THE SWEEP ANGLE  $\theta_B = 0.49[rad]$ .

	PRBM Cyc 1	PRBM Forward	PRBM Return
EXP1	3.84	12.21	4.31
EXP2	7.92	17.85	6.23
EXP3	13.7	16.47	8.71

TABLE V  
THE CROSSOVER ANGLE  $\theta_B$  ERROR AS A PERCENTAGE OF THE SWEEP ANGLE  $\theta_B = 0.49[rad]$  AS PREDICTED BY THE PRBM WITH EXPERIMENT DATA IMPLEMENTED.

	EXP Bi Cyc 1	EXP Bi Forward	EXP Bi Return
EXP1	5.74	3.25	2.37
EXP2	6.02	2.39	4.29
EXP3	15.6	1.01	6.77

## VI. DISCUSSION

In this paper, the method and modelling of a planar compliant translation mechanism have been presented. The mechanism has successfully been designed such that it is able to translate reversible oscillatory path to a circumscribed area path. Based on experimental data and the APDL model it is shown that the PRBM model provides a reasonable prediction the behaviour of the system. The application that is worked out in this paper is a proof of concept, and the concept could translate to more complex mechanisms, as long as the force interaction is maintained.

Between the models good agreement was found. The differences found between the models is suspected to be due to the fidelity of the Ansys APDL model. Regarding that care was taken to remain within the range of deformation that can reasonably be predicted using PRBM, the main difference may result from things such as how relatively constricting the kinematics of a four bar linkage model are. The bistable element seems to be the biggest contributing factor in the differences between both models and the experimental results. Correspondingly, for implementation it is relevant to gather an experimental understanding of the bistable element, or to use FEM to get a more accurate prediction of the bistable element. This is supported by fig. 9, from which one can gather that the mechanism is sensitive to a change in stiffness in the bistable element. Especially the dimensions of the bistable element flexures have a big effect on the path followed by the end-effector of the mechanism. This is further supported by the fact that when fed with experimental data for the bistable element, the PRBM model is able to provide a prediction of the crossover moments with improved accuracy. Moreover the mechanism will only work if the function of the reaction moment  $M_{Bi}(\gamma_B)$  between the peaks is steeper than function of moment  $M_{AB}(\gamma_B)$  applied by the four-bar. When  $M_{AB}(\gamma_B)$  becomes steeper than  $M_{Bi}(\gamma_B)$ , these two functions will only have one point of intersection for all values of  $\theta_B$ . As a result, the bistable element will not produce a hysteresis loop in such a mechanism configuration. This is what happens when  $\frac{f_{Bi}}{f_{AB}} < 0.24$ .



It is also expected that the  $\alpha_2$ -location of the peaks in the moment-displacement graph of the bistable element has an effect on the mechanism behaviour. This might have an effect on at what point crossover happens, but also how much the bistable element deforms before snapping through.

The parameters that were chosen for the prototypes were driven by experiment and manufacturing methods. However, they have proven not to be ideal. Specifically flexure four of the bistable element proved problematic for modelling. Due to its thickness, this flexure was only 3.05 times more compliant than the bar which was attached to it. Initially the assumption was made that this would not affect accuracy to an undesired degree, however after comparing the results of the PRBM to that of APDL. The decision was made to take the stiffness of the bar into account for the model. The reason the flexure had this thickness was because prototypes were FDM 3D printed on a bambulabs x1 carbon with a 0.4 mm nozzle, which meant that the minimum feature size was 0.4 mm. Ideally the stiffness of flexures one, two, and three in the bistable element is as low as possible. In his book, Howell makes use of living hinges for these joints [9], these are flexures which are so compliant that their stiffness may be neglected. To make flexures more compliant, either the flexure has to be made longer, or the flexure should be made thinner. The thickness of these flexures was constrained at 0.4 mm by the production methods, and the length of the flexures was constrained at 1.2 mm by the assumptions of PRBM: Flexures might only be considered as small length flexures as long as the bar attached to the flexure is 10x its length. From here the minimal stiffness of flexures one two and three has been set, and the bistable element could only be tuned with the thickness of flexure four, and the geometry of the linkage. Additionally, the accuracy of the model can undergo improvement by accounting for the anisotropy of 3D printed parts and the effect of creep in plastics.

The results from the path experiment confirm the expected behaviour of the compliant mechanism. However, the results for the motion path of the mechanism do not fully agree with the predictions made by the PRBM and FEM models. As is visible in fig. 14, the samples displayed an earlier first crossover than the models.

The results from the force-displacement experiments provide an explanation for the difference in behaviour of the samples versus the models. The stiffness measured for the full system as shown in fig. 15b shows good agreement with the models. This indicates that the modelled stiffness of the four-bar mechanism is implemented correctly.

The stiffness-displacement of the bistable element was measured to be less stiff than predicted, this does provide some explanation for the results that were observed in fig. 14. Because the bistable is less stiff than predicted on the forward stroke, and stiffer on the return stroke. Forward crossover happens earlier than predicted, and return crossover happens later. This hypothesis is strengthened by the results shown in fig. 9.

The geometry of the bistable element was designed such that the force-displacement would be reversible between the forward and the backward stroke. However, it was observed that the element produces a hysteresis loop. Because of this

hysteresis loop, the hysteresis induced in the full mechanism is also larger, increasing the difference between the forward and return crossover. It is visible that the mechanism is more stiff on the first cycle, and then exhibits a hysteresis loop for the following cycles. This hysteresis is likely due to creep in the PETG material. Additionally after repeated cycles, the flexures of the samples did start to show visible defects such as necking, delamination and small tears. These defects appeared in the compliant flexures of the bistable element first, and then started to appear in the flexures of the four-bar mechanism. It is expected that this is due to high stresses that build up in the flexures and bad layer and seam adhesion. Moreover, 3D prints suffer from irregularities between different samples which are greater than might be obtained from other manufacturing methods. Examples of these irregularities are: layer adhesion, anisotropy, internal stresses, varying layer heights and widths etc. This is something that can be optimised in further research. Which might be solved by changing the design to a better configuration which suffers less stress, as well as improving on the material and manufacturing choice. An example would be to replace the flexures with metal leaf flexures. Metal does not suffer from the properties that 3D printed polymer materials exhibit.

*Applications of the presented mechanism would include:*

- 1) The translation of reciprocating motion to full cycle motion.
- 2) Intermittent driving of a toothed wheel.
- 3) The mechanism could behave as a mechanical diode, only letting through one rotation direction between axles.

*Applications of the presented method can include:*

- 1) Any compliant mechanism where the designer requires the output path to describe an area, but where it is not possible to provide the input with an area.
- 2) Compliant mechanisms where the designer desires switchable kinematics.

## VII. CONCLUSION

In this paper a compliant mechanism for the translation of reciprocating reversible motion to a path circumscribing an area is presented. The mechanism utilises the force-displacement hysteresis produced by a bistable mechanism to produce a four-bar path generator which has a history dependent output path. The mechanism was analysed using both PRBM and FEM modelling to provide a prediction of its functioning. Using FDM 3D printing, the mechanism was also realised for experimentation. The results of the experiments corresponds with the predictions of the PRBM and FEM models.

## REFERENCES

- [1] A. G. Erdman, *Modern kinematics: developments in the last forty years* (Wiley series in design engineering), English. New York: Wiley, 1993, Section: xiii, 604 pages : illustrations ; 25 cm., ISBN: 978-0-471-55459-2.
- [2] N. Sclater, *Mechanisms and mechanical devices source-book*, English, 5th ed. New York: McGraw-Hill Professional ; 2011, Section: 546 pages . : illustrations ; 29 cm, ISBN: 978-0-07-170442-7.

- [3] G. N. Sandor and A. G. Erdman, *Mechanism design: analysis and synthesis / Vol. 2*, English. Englewood Cliffs, NJ: Prentice-Hall, 1984, Section: XII, 688 p. : ill. ; 25 cm., ISBN: 978-0-13-011437-2.
- [4] F. V. Morley, "Linkages," *The Scientific Monthly*, vol. 9, no. 4, pp. 366–378, 1919, Publisher: American Association for the Advancement of Science, ISSN: 0096-3771. [Online]. Available: <https://www.jstor.org/stable/6288> (visited on 06/06/2024).
- [5] H. Nolle, "Linkage coupler curve synthesis: A historical review — I. Developments up to 1875," en, *Mechanism and Machine Theory*, vol. 9, no. 2, pp. 147–168, Jun. 1974, ISSN: 0094114X. DOI: 10.1016/0094-114X(74)90034-2. [Online]. Available: <https://linkinghub.elsevier.com/retrieve/pii/0094114X74900342> (visited on 01/09/2023).
- [6] S. H. Chang and B. C. Du, "A precision piezodriven micropositioner mechanism with large travel range," en, *Review of Scientific Instruments*, vol. 69, no. 4, pp. 1785–1791, Apr. 1998, ISSN: 0034-6748, 1089-7623. DOI: 10.1063/1.1148842. [Online]. Available: <http://aip.scitation.org/doi/10.1063/1.1148842> (visited on 12/06/2022).
- [7] P. Xu, J. Yu, G. Zong, and S. Bi, "Design of compliant straight-line mechanisms using flexural joints," en, *Chinese Journal of Mechanical Engineering*, vol. 27, no. 1, pp. 146–153, Jan. 2014, ISSN: 1000-9345, 2192-8258. DOI: 10.3901/CJME.2014.01.146. [Online]. Available: <http://link.springer.com/10.3901/CJME.2014.01.146> (visited on 12/07/2022).
- [8] S. Kota, "Design of compliant mechanisms: Applications to MEMS," en, V. K. Varadan, Ed., Newport Beach, CA, Jul. 1999, pp. 45–54. DOI: 10.1117/12.354294. [Online]. Available: <http://proceedings.spiedigitallibrary.org/proceeding.aspx?articleid=982825> (visited on 05/20/2024).
- [9] L. L. Howell, *Compliant Mechanisms*, en. John Wiley & Sons, Aug. 2001, Google-Books-ID: tiiSOuhsIfgC, ISBN: 978-0-471-38478-6.
- [10] N. P. Belfiore, A. Bagolini, A. Rossi, G. Bocchetta, F. Vurchio, R. Crescenzi, A. Scorza, P. Bellutti, and S. A. Sciuto, "Design, Fabrication, Testing and Simulation of a Rotary Double Comb Drives Actuated Microgripper," en, *Micromachines*, vol. 12, no. 10, p. 1263, Oct. 2021, ISSN: 2072-666X. DOI: 10.3390/mi12101263. [Online]. Available: <https://www.mdpi.com/2072-666X/12/10/1263> (visited on 05/20/2024).
- [11] P. Sanò, M. Verotti, P. Bosetti, and N. P. Belfiore, "Kinematic Synthesis of a D-Drive MEMS Device With Rigid-Body Replacement Method," en, *Journal of Mechanical Design*, vol. 140, no. 7, p. 075 001, Jul. 2018, ISSN: 1050-0472, 1528-9001. DOI: 10.1115/1.4039853. [Online]. Available: <https://asmedigitalcollection.asme.org/mechanicaldesign/article/doi/10.1115/1.4039853/369015/Kinematic-Synthesis-of-a-DDrive-MEMS-Device-With> (visited on 05/20/2024).
- [12] N. F. Wang and K. Tai, "Design of Grip-and-Move Manipulators Using Symmetric Path Generating Compliant Mechanisms," en, *Journal of Mechanical Design*, vol. 130, no. 11, p. 112 305, Nov. 2008, ISSN: 1050-0472, 1528-9001. DOI: 10.1115/1.2976790. [Online]. Available: <https://asmedigitalcollection.asme.org/mechanicaldesign/article/doi/10.1115/1.2976790/470413/Design-of-GripandMove-Manipulators-Using-Symmetric> (visited on 06/10/2024).
- [13] E. J. Garcia and J. J. Sniegowski, "Surface micromachined microengine," *Sensors and Actuators A: Physical*, vol. 48, no. 3, pp. 203–214, May 1995, ISSN: 0924-4247. DOI: 10.1016/0924-4247(95)00999-X. [Online]. Available: <https://www.sciencedirect.com/science/article/pii/092442479500999X> (visited on 05/02/2024).
- [14] S. Kota, J. Hetrick, Z. Li, and L. Saggere, "Tailoring unconventional actuators using compliant transmissions: Design methods and applications," *IEEE/ASME Transactions on Mechatronics*, vol. 4, no. 4, pp. 396–408, Dec. 1999, Conference Name: IEEE/ASME Transactions on Mechatronics, ISSN: 1941-014X. DOI: 10.1109/3516.809518.
- [15] F. Botta, A. Rossi, and N. P. Belfiore, "A Cantilever-Based Piezoelectric MEMS for Arbitrary XY Path Generation," en, *Micromachines*, vol. 13, no. 9, p. 1514, Sep. 2022, ISSN: 2072-666X. DOI: 10.3390/mi13091514. [Online]. Available: <https://www.mdpi.com/2072-666X/13/9/1514> (visited on 05/20/2024).
- [16] K. Tai, G. Y. Cui, and T. Ray, "Design Synthesis of Path Generating Compliant Mechanisms by Evolutionary Optimization of Topology and Shape," *Journal of Mechanical Design*, vol. 124, no. 3, pp. 492–500, Aug. 2002, ISSN: 1050-0472. DOI: 10.1115/1.1480818. [Online]. Available: <https://doi.org/10.1115/1.1480818> (visited on 01/20/2023).
- [17] A. Saxena, "Synthesis of Compliant Mechanisms for Path Generation using Genetic Algorithm," en, *Journal of Mechanical Design*, vol. 127, no. 4, pp. 745–752, Jul. 2005, ISSN: 1050-0472, 1528-9001. DOI: 10.1115/1.189 9178. [Online]. Available: <https://asmedigitalcollection.asme.org/mechanicaldesign/article/127/4/745/729159/Synthesis-of-Compliant-Mechanisms-for-Path> (visited on 05/16/2024).
- [18] K. Zhao and J. P. Schmiedeler, "Using Rigid-Body Mechanism Topologies to Design Path Generating Compliant Mechanisms," en, *Journal of Mechanisms and Robotics*, vol. 8, no. 1, p. 014 506, Feb. 2016, ISSN: 1942-4302, 1942-4310. DOI: 10.1115/1.4030623. [Online]. Available: <https://asmedigitalcollection.asme.org/mechanismsrobotics/article/doi/10.1115/1.4030623/421982/Using-RigidBody-Mechanism-Topologies-to-Design> (visited on 06/10/2024).
- [19] N. D. Mankame and G. K. Ananthasuresh, "A Novel Compliant Mechanism for Converting Reciprocating Translation Into Enclosing Curved Paths," en, *Journal of Mechanical Design*, vol. 126, no. 4, pp. 667–672, Jul. 2004, ISSN: 1050-0472, 1528-9001. DOI: 10.1115/1.1759360. [Online]. Available: <https://asmedigitalcollection.asme.org/mechanicaldesign/article/126/4/667/458721/A-Novel-Compliant-Mechanism-for-Converting> (visited on 12/23/2022).

- [20] A. Tekes, "Compliant Five Bar Mechanism Control to Achieve a Desired Trajectory," en, in *Volume 4B: Dynamics, Vibration, and Control*, Tampa, Florida, USA: American Society of Mechanical Engineers, Nov. 2017, V04BT05A001, ISBN: 978-0-7918-5838-7. DOI: 10.1115/IMECE2017-70077. [Online]. Available: <https://asmedigitalcollection.asme.org/IMECE/proceedings/IMECE2017/58387/Tampa,%20Florida,%20USA/288534> (visited on 06/10/2024).
- [21] M. Verotti, A. Dochshanov, and N. P. Belfiore, "A Comprehensive Survey on Microgrippers Design: Mechanical Structure," en, *Journal of Mechanical Design*, vol. 139, no. 6, p. 060801, Jun. 2017, ISSN: 1050-0472, 1528-9001. DOI: 10.1115/1.4036351. [Online]. Available: <https://asmedigitalcollection.asme.org/mechanicaldesign/article/doi/10.1115/1.4036351/472999/A-Comprehensive-Survey-on-Microgrippers-Design> (visited on 12/23/2022).
- [22] A. Dochshanov, M. Verotti, and N. P. Belfiore, "A Comprehensive Survey on Microgrippers Design: Operational Strategy," en, *Journal of Mechanical Design*, vol. 139, no. 7, p. 070801, Jul. 2017, ISSN: 1050-0472, 1528-9001. DOI: 10.1115/1.4036352. [Online]. Available: <https://asmedigitalcollection.asme.org/mechanicaldesign/article/doi/10.1115/1.4036352/383735/A-Comprehensive-Survey-on-Microgrippers-Design> (visited on 06/06/2024).
- [23] A. S. Algamili, M. H. M. Khir, J. O. Dennis, A. Y. Ahmed, S. S. Alabsi, S. S. Ba Hashwan, and M. M. Junaid, "A Review of Actuation and Sensing Mechanisms in MEMS-Based Sensor Devices," *Nanoscale Research Letters*, vol. 16, no. 1, p. 16, Jan. 2021, ISSN: 1556-276X. DOI: 10.1186/s11671-021-03481-7. [Online]. Available: <https://doi.org/10.1186/s11671-021-03481-7>.
- [24] R. G. Gilbertson and J. D. Busch, "A survey of micro-actuator technologies for future spacecraft missions," *Journal of the British Interplanetary Society*, vol. 49, no. 4, pp. 129–138, 1996, Publisher: Citeseer.
- [25] V. Bučinskis, J. Subačiūtė-Žemaitienė, A. Dzedzickis, and I. Morkvėnaitė-Vilkončienė, "Robotic micromanipulation: A) actuators and their application," en, *Robotic Systems and Applications*, vol. 1, no. 1, pp. 2–23, Jun. 2021, ISSN: 2669-2473. DOI: 10.21595/rsa.2021.22071. [Online]. Available: <https://www.extrica.com/article/22071> (visited on 05/01/2024).
- [26] L. Tan, A. C. Davis, and D. J. Cappelleri, "Smart Polymers for Microscale Machines," en, *Advanced Functional Materials*, vol. 31, no. 9, p. 2007125, 2021, ISSN: 1616-3028. DOI: 10.1002/adfm.202007125. [Online]. Available: <https://onlinelibrary.wiley.com/doi/abs/10.1002/adfm.202007125> (visited on 05/01/2024).
- [27] A. Veroli, A. Buzzin, F. Frezza, G. De Cesare, M. Hamidullah, E. Giovine, M. Verotti, and N. Belfiore, "An Approach to the Extreme Miniaturization of Rotary Comb Drives," en, *Actuators*, vol. 7, no. 4, p. 70, Oct. 2018, ISSN: 2076-0825. DOI: 10.3390/act7040070. [Online]. Available: <http://www.mdpi.com/2076-0825/7/4/70> (visited on 05/20/2024).
- [28] S. Kim and S. Bergbreiter, "Fabrication and Characterization of 3D Printed Out-of-Plane Torsional Comb-Drive Actuators for Microrobotics," en, in *2021 21st International Conference on Solid-State Sensors, Actuators and Microsystems (Transducers)*, Orlando, FL, USA: IEEE, Jun. 2021, pp. 6–9, ISBN: 978-1-66541-267-4. DOI: 10.1109/Transducers50396.2021.9495753. [Online]. Available: <https://ieeexplore.ieee.org/document/9495753/> (visited on 05/20/2024).
- [29] M. Sattari Sarebangholi and F. Najafi, "Design of a path generating compliant mechanism using a novel rigid-body-replacement method," en, *Meccanica*, vol. 57, no. 7, pp. 1701–1711, Jul. 2022, ISSN: 1572-9648. DOI: 10.1007/s11012-022-01527-3. [Online]. Available: <https://doi.org/10.1007/s11012-022-01527-3> (visited on 03/20/2023).
- [30] G. J. Van Den Doel, J. L. Herder, and D. Farhadi, "Harnessing elastic energy to overcome singularity issues in four-bar mechanisms with a crank link," en, *Mechanism and Machine Theory*, vol. 183, p. 105274, May 2023, ISSN: 0094114X. DOI: 10.1016/j.mechmachtheory.2023.105274. [Online]. Available: <https://linkinghub.elsevier.com/retrieve/pii/S0094114X23000484> (visited on 03/29/2024).
- [31] D. M. Tanner, N. F. Smith, L. W. Irwin, *et al.*, "MEMS Reliability: Infrastructure, Test Structures, Experiments, and Failure Modes," English, Sandia National Lab. (SNL-NM), Albuquerque, NM (United States); Sandia National Lab. (SNL-CA), Livermore, CA (United States), Tech. Rep. SAND2000-0091, Jan. 2000. DOI: 10.2172/750344. [Online]. Available: <https://www.osti.gov/biblio/750344> (visited on 06/06/2024).



# Synthesis Of A Compliant Mechanism That Translates A Reciprocating Reversible Path To A History Dependent Area Describing Path

Michiel den Daas

**Abstract**—In this report, the design process a compliant path translation mechanism is detailed. During the design process, it was found that no compliant mechanism existed that could provide a translation from a reversible reciprocating path to a path describing an area. The process that was taken to arrive at the compliant mechanism which was able to perform this translation is described. During this research, a novel compliant mechanism translating a reversible reciprocating path to an area describing path has been modelled, produced and experimented on.

**Index Terms**—Compliant mechanism, Path generator, Reciprocating motion, Intermittent motion, Hysteresis

## I. INTRODUCTION

**I**NTERMITTENT motion mechanisms are mechanisms which produce non-continuous motion. This motion is periodic, and will be zero for a non-instant amount of time. This motion consists of two distinct periods: dwell and motion. During dwell, the output is still with respect to the input, and during motion, the output moves with the input [1]. There are two types of intermittent motion: Oscillating dwell motion and indexed motion. For oscillating dwell motion, the start and end locations are the same each cycle. With an indexed motion, the end-effector is advanced along a DOF with a set distance at the end of each cycle [2]. A daily example of a machine which contains mechanisms generating this type of motion is the wristwatch. Watches contain a clockwork which is able to turn energy stored in a torsion spring into time regulated movement of the hands on the dial [3]. The escapement regulates this conversion of energy to timed motion. But a watch can also contain other types of intermittent motion mechanisms, such as the mechanism behind date wheels. These mechanisms typically consist of around ten parts which engage to produce the desired motion [4]. These parts wear down as a result of mechanical interaction and have to be maintained to function properly [1]. This maintenance can range from oiling the mechanism to replacing worn parts [5]. Additionally, the friction between parts incur energy loss on the mechanism. As a result, a watch could run out of energy faster than intended because the mechanism is energy-inefficient.

Apart from watches, many other devices also depend on intermittent motion such as: sewing machines, projectors, packing machines, presses, etc. [6]–[8]. In these devices, intermittent motion is a key component to the behaviour of the machine, generating the movement necessary for the machine to perform its task. Traditionally intermittent motion is generated using mechanisms containing higher kinematic pairs such as

gears, cams, or Geneva mechanisms. However, these types of mechanisms have several undesirable side effects [1]:

- Wear
- Friction
- Play
- Impacts
- High part count

During the last two decades, researchers have begun to investigate linkages for their performance in the generation of intermittent motion [9]. Linkages are able to solve or mitigate some of the aforementioned side effects, such as impacts and wear. as an effect, linkages have the advantage that they are able to operate at higher speeds, as well as requiring less maintenance. But the synthesis of linkages is comparatively more difficult, due to the sensitivity of the mechanism to small variations in geometry [10]. Additionally, when a linkage is scaled down, the production, assembly, and maintenance of the mechanism becomes increasingly challenging [11], [12].

To overcome these issues, one could synthesise a compliant mechanism. In contrast with traditional mechanisms, compliant mechanisms are ideally not affected by friction. Furthermore, they can function without wear and fully compliant mechanisms do not require assembly, resulting in a reduced need for maintenance. These advantages stem from the basic function of compliant mechanisms, namely that movement generated by a compliant mechanism is the result of deflection of members rather than a mechanical interaction between components [11], [13].

As such it would be favourable to design a compliant mechanism that could replicate the behaviour of an intermittent motion mechanism. In this report, the design of such a mechanism is attempted. This design is tackled in a few steps, first a design process is set up in section II. Then in the following sections III to V the development of a PRB and Ansys APDL model is explained. After which the production of a case study is presented in section VI, after which the experimentation is explained in section VII. Finally data processing, results, discussion, and conclusion are shown in sections VIII to XI.

## II. DESIGN PROCESS

Based on the literature project, the following design question was posed: How can angular motion be transmitted periodically between two axes using a planar compliant mechanism?

To solve the problems observed in traditional mechanisms, a compliant mechanism has been designed. This report describes

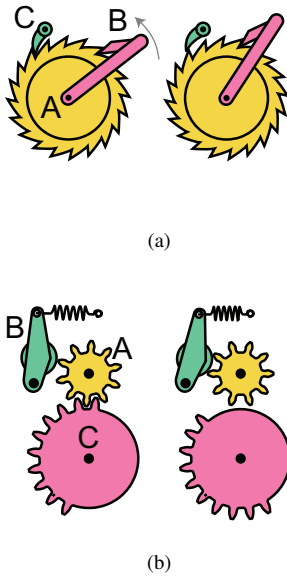


Fig. 1. Two figures showing examples of intermittent motion mechanisms, a) shows a ratchet, and b) shows a mutilated gear with holding pawl. The mechanism parts are coloured based on their respective function, pink parts are the input of the mechanism, yellow parts are the outputs, and green parts provide locking to the output.

the process that was followed to produce the compliant mechanism. Initially, the objective was to design a compliant replacement for a ratchet, however during the design process this objective was replaced with designing a compliant path generation mechanism. A general ratchet might look as shown in fig. 1.

In the literature, no comparable mechanism was found in fully compliant form. As was concluded, for some applications such as small scale mechanisms, compliant mechanisms provide improvements in various areas. To fill this gap, design research was started. To generate a design, the design process should be tackled in an organised manner. To do this the problem was first identified. Then the objective was divided into functions. For each of these functions, multiple solutions would then be conceived, which would then be combined using a morphological chart to generate concepts. These concepts should then be evaluated on performance, and from this the best concept can be selected.

**A. Problem**

First, the boundary conditions of the design objective were defined. In fig. 2 a schematic drawing of the design problem is shown. The ratcheting mechanism has been simplified to two axles with a mutilated gear attached on one side, and a normal gear existing on the other axle. The eventual mechanism should exist between the input and output and should perform two functions.

**B. Functions**

To perform the behaviour that is required from a ratchet, the following functions were identified:

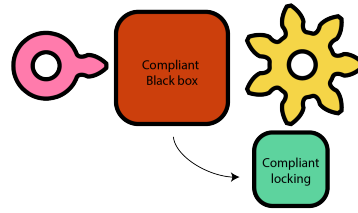


Fig. 2. A figure showing an abstract overview of the system as defined for the assignment.

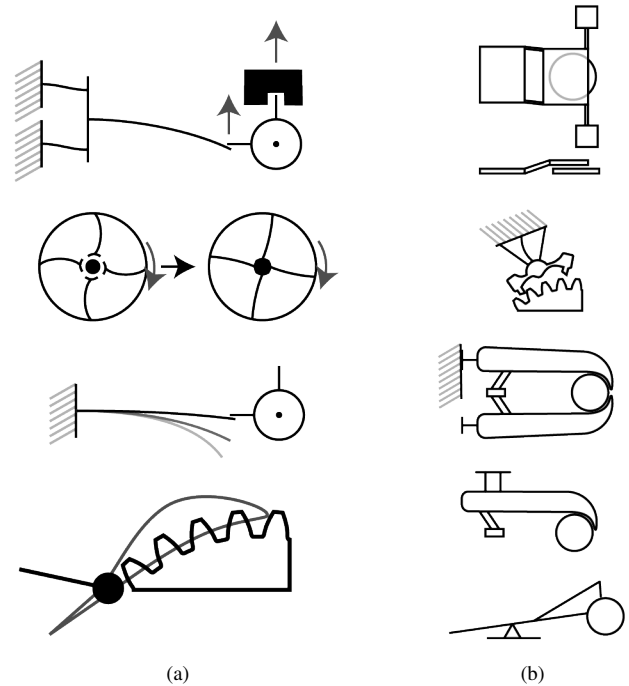


Fig. 3. Two figures showing the solutions developed for the two defined functions. a) shows the solutions developed for actuation, from top to bottom it shows: preload actuation, clamp actuation, dynamic actuation and follow actuation. b) shows the solutions developed for locking, from top to bottom it shows: LEM disk brake locking, compliant escapement locking, claws gripping from the side, claws gripping from the rear, and the actuation attached pawl.

- Periodic actuation
- Locking

The actuation means that the mechanism should be able to displace the output based on a intermittently rotating input. The output should be moved with an accurate and predictable distance.

The locking is necessary to ensure the output stays at its index whenever the mechanism is not actuated.

**C. Function solutions**

To generate a matrix of morphological chart, a set of solutions has to be generated for the functions. These solutions are presented in fig. 3.

1) *Actuation:* The first function for which solutions are being developed is the actuation of the mechanism. The

displacement should be performed such that an accurate amount of displacement is obtained at each iteration.

*a) Preload:* The first solution for the actuation is a preload mechanism. The idea is that the end-effector of this mechanism is manoeuvred around the desired tooth of the output gear. After which it is set free, where it will rest on this tooth providing pressure in the direction of movement. This movement is constricted by the locking mechanism, and when this locking mechanism is removed, the output gear moves over one position. After this movement, the compliant mechanism has been restored to its initial configuration, and the output has been displaced with one position. Consequently the brake is restored to its position, holding the output in place.

This design would have the benefit of negating impacts to the output, while still ensuring that the mechanism switches over in a short amount of time. A disadvantage of this method is the path generation that is necessary to move the end-effector of the linkage around the tooth of the gear. This path is made more difficult by the fact that the input is essentially an oscillation. Which would mean that the mechanism needs to ensure that the forward stroke is different than the return stroke.

*b) Clamp:* This mechanism would function by placing a concentric ring around the output axle. This ring should contain several arms which are forced to move inward when the mechanism is actuated (similar to an aperture mechanism). These arms then grip the axle and move it for the duration of actuation of the outside ring. The arms could also be mounted such that the surface that interacts with the output is force to move relative to the outer ring itself to further accelerate motion. This should be a mechanism that can be designed requiring minimal deflection from its members, as the hands of the clamp could be placed at a minimal distance from the output axis before deformation.

*c) Dynamic:* This mechanism would require a similar motion profile to that of the preload mechanism. However, instead of preloading the output by providing pressure on a tooth, the mechanism would move the output gear by providing velocity directly. A big disadvantage of this mechanism is that upon the interaction with the output, an impact is generated by the end-effector of the compliant mechanism coming into contact with the still output. Furthermore, this design still requires a similar motion path to the preload mechanism, as it has to be able to move around a gear tooth before it can be set up for the next actuation.

*d) Push or pull follow:* This mechanism would interface with the teeth of the output gear. And gently move them along to the next desired position. This would be based on actuating the end-effector along a path as shown in figure fig. 3a. This path is necessary because it is desired to only interact with the output gear upon the desired actuation moment. In contrast to the dynamic mechanism, this mechanism would not incur an impact on the system, but rather would produce a smooth velocity curve.

*2) Locking:* Between each actuation, the output should be locked to ensure that the mechanism does not slip back while the actuation is not engaged. Ideally, locking has a monolithic mechanical connection to the actuation of the mechanism and exists in the same plane.

*a) LEM Brake:* This solution is inspired by the text on LEMs in [11], combined with disk brakes which can be found in everyday vehicles such as cars and motorcycles. This mechanism would be produced in plane and placed on the output gear with a preload. This preload ensures that the output gear is held. Then when the actuation mechanism engages with the gear, the LEM is deformed such that it relieves the pressure from the gear allowing it to be moved by the actuation.

*b) Escapement type brake:* This locking would be reminiscent of a traditional escapement, however in compliant form utilising a bistable element so that an external mechanism must switch over the escapement to allow the output to move. By utilising a bistable element, the escapement would form a mechanical connection to the output gear. Every time the actuation is activated, it will push the bistable escapement over to its next position while moving the output gear. This produces locking between the movements of the gear.

*c) Claws gripping gear from the side or the back:* Similar to the LEM disk brake, the claws would work by using a preload to hold the output gear. The difference between these mechanisms is the axis in which the gear is held. Furthermore, this solution would allow for an actuation mechanism to exist within it, as well as existing in only one plane.

*d) A pawl attached to the actuation mechanism:* For this solution, the actuation mechanism first has to be developed. The idea for this solution is to place a holding mechanism directly on the actuation mechanism, or make the actuation such that it is always engaged with the output gear. Then, when the actuation is started, the holding mechanism will disengage from the gear allowing it to be moved.

#### D. Developing the solutions

When the solutions for the design problem had been defined, these solutions could be worked out further into actual designs. When observing the solutions, one can see that some are worked out in concept further than others. Since designing the kinematics of linkages is relatively difficult, the decision was made to start there.

*1) Linkage:* To perform the motions shown in fig. 3a, it is necessary to generate a path that is capable of moving around the teeth of a geared wheel.

The first challenge that this posed, is that the motion required on the output side has the inverse curvature of the input motion. To solve this problem, inspiration was taken from locomotion mechanisms to generate the necessary path to move around the gear teeth.

Using the website *motiongen*, in combination with inspiration obtained from papers on locomotion mechanisms as well as the instantaneous centre method. The linkage shown in fig. 4a was devised.

This four-bar mechanism is able to move a gear by interacting with one of its teeth. However, it would also push the gear back to the starting position, because it follows the same path on the forward stroke as the return stroke.

#### E. General problem

During the development of solutions for the actuation of the mechanism it was observed that most of the actuation solutions

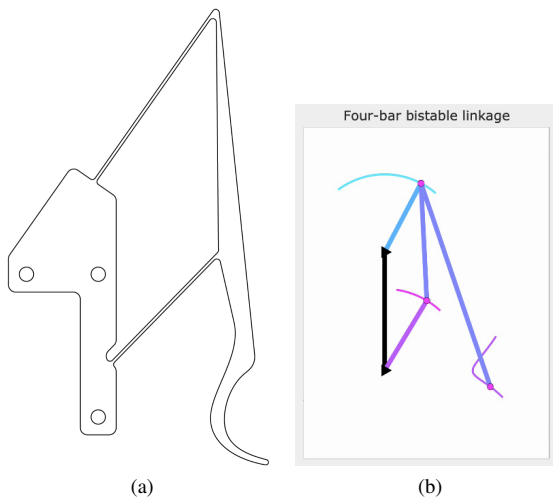


Fig. 4. Two figures showing both the developed compliant four-bar mechanism a) and its PRBM counterpart with the path drawn by its end-effector b).

that were considered required the synthesis of a path that describes an area. This path is shown in fig. 3a, and although it is one of the solutions, it is also the general path that is required for the preload and momentum based solutions.

The path shown is not in itself a difficult path to synthesise, there are linkages which allow a designer to obtain such a path. However, the difficulty is that the mechanism should translate reversible reciprocating motion, to area describing motion.

This general problem lead to a new design cycle. The first goal was to obtain a mechanism which is able to perform the general required motion. After which an attempt is made at solving the problem of converting non-full cycle to full cycle motion.

#### F. Hypothesis

To produce the required path shape using a compliant mechanism, a new hypothesis was set up inspired by a paper found during the literature research.

1) *Inspiration:* During the literature research, an interesting report was found where the authors reported an effect which was undesired for their research[14]. The paths shown in fig. 5 are created by two end-effectors, the path of one end-effector has been highlighted. And as one can see each of these end-effectors follows a fully enclosed path during each actuation of the mechanism.

The authors explained this behaviour of the mechanism as a result of material creep. This means that the mechanism will retain part of the imposed deformation while external load is reduced. As a result the path on the backstroke is different to the path on the forward stroke.

A few attempts were made to recreate this effect utilising a 3d printed PETG model, these attempts failed. Although the mechanisms did display a slight difference between strokes, this was deemed too small for the intended application. Furthermore if the mechanism would be produced in microscale, the eventual mechanism should be made from silicon or metal. Silicon and metal exhibit no material viscosity, meaning that designing a mechanism that would work based on this effect would not

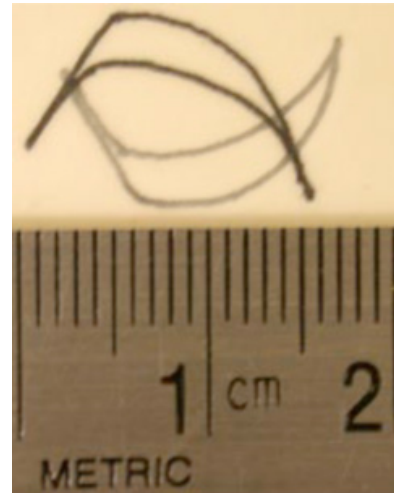


Fig. 5. A picture showing the path generated by the linearly actuated compliant mechanism developed by Mankame et al. adapted from [14, fig. 8]

work for many applications. However, these tests did provide the inspiration to make an attempt at increasing the effect of hysteresis, and producing the required motion path that way.

2) *How to generate hysteresis:* Hysteresis is defined as history dependent behaviour, many types of hysteresis are due to a transfer or loss of energy. Hysteresis is generally something that designers try to avoid, this is because it can lead to difficult control as a result of unpredictability. However, in this case hysteresis might be made to work in favour of the intended behaviour. There are several mechanisms which generate hysteresis such as:

- Dampers (force/location)
- Friction (force/location)
- Play (location/location)
- Ferromagnetic hysteresis (Magnetic field/magnetic permeability)
- Bistability (force/location)
- Creep (force/location)

From this list only bistability is an interesting option for this project. Because the goal was to synthesise a compliant mechanism, the first three are not valid candidates as these require solid body interactions, creep had already been ruled out, and magnetic hysteresis was outside of the scope of this research.

3) *How does a bistable element introduce hysteresis?:* Bistable mechanisms are mechanisms that have two stable positions. To switch between these positions, the mechanism requires energy to be put in. As one can see in fig. 6, when such a mechanism is actuated using force as an input, there is a certain range over the force-axis where three valid intersections exist at different displacements. As a result, when the input force exceeds the maximum or the minimum peaks, the mechanism will displace over to the next valid position

4) *Where to place a bistable element?:* To gain a different motion path on the return stroke compared to the forward stroke, the bistable element needs to be included such that an interaction occurs between the four-bar and the bistable element. This requires two properties:

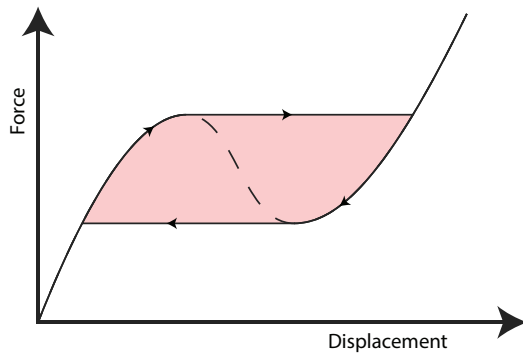


Fig. 6. A figure showing the force-displacement behaviour of a general snap-through bistable mechanism.

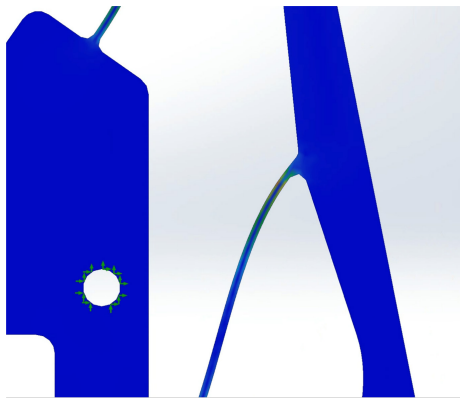


Fig. 7. A picture showing the flexure in the location of interest when it is deformed.

- 1) The bistable element can change the kinematics of the four-bar.
- 2) The bistable element can exchange energy with the four-bar.

In simulation the four-bar mechanism shown in fig. 4a deforms as shown in fig. 7. This mechanism was also 3D printed, and from visual observation, this simulation does provide an accurate representation of how the four-bar behaves. From the shape of the flexure shown in fig. 7, it was hypothesised that replacing the attachment point of this flexure with a rotary bistable element would provide the required hysteresis to produce the motion shown in fig. 8. If a bistable element is placed in this position such that it would relax the flexure after switching position, this would straighten out the flexure slightly. Thus increasing its length slightly, with a result that the end-effector would move away from the 'normal' motion path. And as a result of bistability, the bistable element will not switch back at the same location as its initial switchover thus switching back later.

5) *What mechanisms exist that generate hysteresis?:* Before reviewing relevant literature, an attempt was made to design a compliant bistable mechanism which would have one degree of freedom. The mechanism that resulted from this design is shown in fig. 9. It was hypothesised that this design would produce bistable behaviour as the flexures are tilted slightly off the radial lines. When actuated counterclockwise in the case

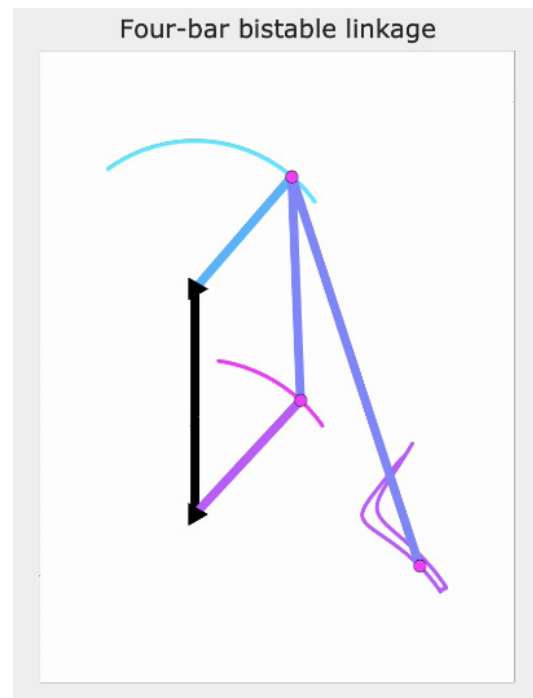


Fig. 8. A figure showing the hypothesised path produced by a four-bar mechanism when inducing hysteresis by incorporating the bistable element in joint three, resulting in a lengthening of link D when the bistable element switches over.

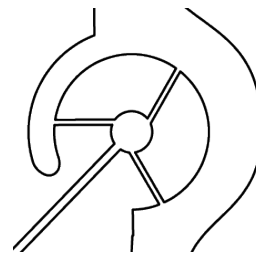


Fig. 9. A picture of the first design of a rotary bistable element.

of fig. 9, a compressive force would build in the flexures until they buckle and force over the central axis to the next stable position.

This mechanism quickly proved not to be ideal, simulations indicated that it did not behave as a bistable mechanism. And a 3D printed prototype of the mechanism confirmed this and showed that the part quickly fails upon actuation. This is due to the high stresses that build up in the connections of the flexures to the central axis of the mechanism. To reduce the time spent designing bistable mechanisms, the decision was made to evaluate what solutions already exist.

The mechanisms shown in fig. 10 were found in relevant literature. To decide which of the mechanisms shown in fig. 10 are ideal for their intended application, a comparison table was made: table I. The bistable mechanism ideally has one degree of freedom. This ensures that the bistable mechanism can realistically be modelled and incorporated into a larger model. Furthermore, its complexity needed to be relatively low. The complexity was judged on the relative feature size of

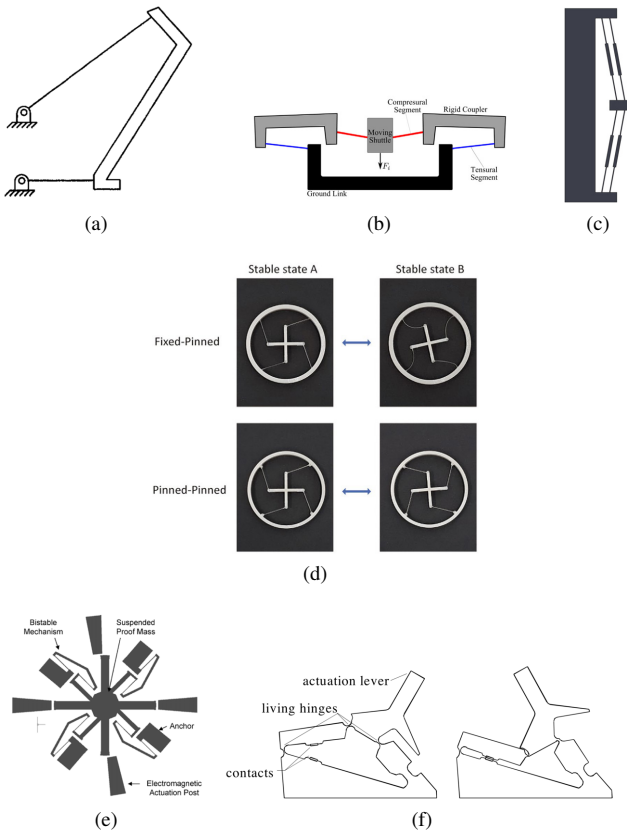


Fig. 10. Six figures showing the considered bistable mechanisms. [15]–[20]

TABLE I

COMPARISON TABLE FOR THE CONSIDERED BISTABLE MECHANISMS FOR THE DESIGN. THE LETTERS CORRESPOND WITH THE MECHANISMS IN FIG. 10. A PLUS DENOTES A POSITIVE ASPECT AND A MINUS DENOTES A NEGATIVE ASPECT.

	Fully Compliant	DOF	Complexity
a)	-	1	+
b)	+	2	-
c)	+	2	+
d)	-	1	+
e)	+	1	-
f)	+	1	+

the smallest features, and the amount of these small features necessary. Because ideally the final design can be 3D printed, the size of the entire mechanism is determined by its smallest feature, as this can not be smaller than 0.4 mm across its smallest axis. Lastly, the bistable mechanism could not contain rigid axles, as this voids the preference of a final design being fully compliant. Based on the comparison table, the decision was made to continue with the bistable switch as designed by Howell shown in fig. 10f. An added benefit of the mechanism from Howell is the fact that its input can be made to displace as well as rotate, which means that more length is added to link D.

### G. Final design

Based on the presented hypothesis, and the chosen bistable element, and four-bar mechanism, a mathematical model was

developed. This model is presented at the end of section V, here an explanation is also provided for the change made in the configuration of the four-bar mechanism with respect to the four-bar presented in section II-D1. From this modelling process, a general four-bar mechanism was obtained shown in fig. 11a. This model has not been designed as a finished model or prototype, rather as a proof of concept. To increase the likelihood that eventual prototypes would not be produced unless there was a reasonable belief that the prototype would work, the final configuration has been designed with the help of the models that are elaborated on further in sections IV and V. As mentioned before, the mechanism was ideally easy to produce using a 3D printer. Therefore the minimum feature size was limited to 0.4mm. This meant that the design of the bistable element is a case of balancing priorities. Regarding that the living hinges as Howell describes them in his book [21] need to be as compliant as possible. This makes the living hinges a thickness of 0.4 mm. The problem however was that the hinges could not be too long relative to the dimensions of the bistable element, otherwise the assumptions of PRBM do not hold anymore. But on the other side, when the stiffness of the living hinges increases, the stiffness of the 'stiff' hinge also has to increase in order to ensure bistability. However, when this flexure gets too stiff, the bar that is attached to it also has to get stiffer, which in turn would mean that the relative size of the mechanism had to increase. Since using plastic and with the available fabrication methods, no configuration would be ideal, the design parameters that are shown in table II were chosen to be those with least compromises.

TABLE II

PARAMETERS OF THE FINAL MECHANISM DESIGN. THE VARIABLE NAMES CAN BE REFERENCED FROM FIGS. 16 AND 20, AND AN F IN SUBSCRIPT DENOTES FLEXURE VARIABLES.

Segment	Length/angle	Width	Segment	Length/angle	Width
$l_A$	132 mm	20 mm	$l_{bA}$	54 mm	5 mm
$l_B$	864 mm	20 mm	$l_{bB}$	31 mm	5 mm
$l_C$	160 mm	20 mm	$l_{bC}$	26 mm	5 mm
$l_D$	80 mm	20 mm	$l_{bD}$	10 mm	5 mm
$l_{f1}$	4 mm	1.2 mm	$l_{bf1}$	1.4 mm	0.4 mm
$l_{f2}$	4 mm	1.2 mm	$l_{bf2}$	1.4 mm	0.4 mm
$l_{f3}$	4 mm	1.2 mm	$l_{bf3}$	1.4 mm	0.4 mm
$l_{f4}$	4 mm	1.2 mm	$l_{bf4}$	1 mm	1.6 mm
$\theta_{B0}$	95 °		$\gamma_{B0}$	18.56 °	

TABLE III

MATERIAL PARAMETERS AND THICKNESS OF THE PLANAR MECHANISM

	Value	Unit
Material	PETG	
Young's modulus	1607	MPa
Thickness $d_p$	5	mm



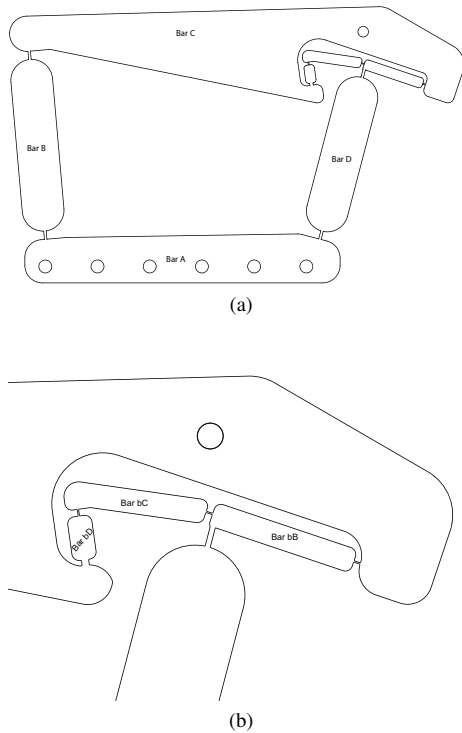


Fig. 11. A figure showing the outline of the mechanism that is analysed in this paper. a) shows the full mechanism and b) shows the bistable element in its final location. The circle hole that exists above the bistable mechanism is the point of interest which also exists in the PRBM and FEM models.

III. BISTABLE MODEL

To validate that the concept of integrating a bistable mechanism into an axle of a four-bar mechanism would work, it would be necessary to develop a model. This allows one to get a deeper understanding of the functioning of a system, and as a result develop it more effectively. As discussed in section II-E, the bistable mechanism that would be considered is the bistable switch shown in fig. 13a.

During the first few attempts, the paper relating to the design of this mechanism had not been found yet, and rigid body model of the mechanism was incorrectly identified as shown in figure fig. 13b. For the functional model of the compliant bistable element, the relevant paper and book were found and incorporated.

From the initial results of modelling in APDL and small 3D printed prototypes, it was expected that a snap-back bistable mechanism would be required for the production of full cycle motion from the four-bar mechanism. This assumption also meant that to model a snap-back mechanism, a multiple DOF model would be required as a 1 DOF mechanism such as a four-bar mechanism can not encapsulate this behaviour. However during the development of the four-bar mechanism models, the conclusion was drawn that the relevant behaviour of the four-bar mechanism was in the force-displacement graph. And this behaviour does not require snap-back to produce hysteresis. As shown in fig. 12. For a forced-displacement model, snap-back is required to generate hysteresis, however for a force actuated system snap through is enough to produce hysteresis.

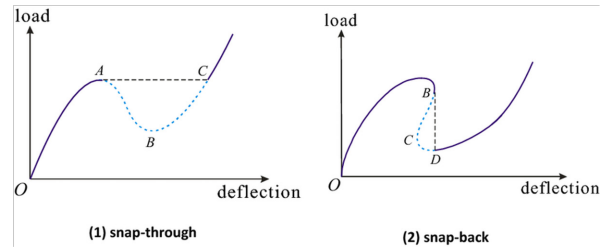


Fig. 12. Two figures showing snap-through vs snap-back figure from [22]

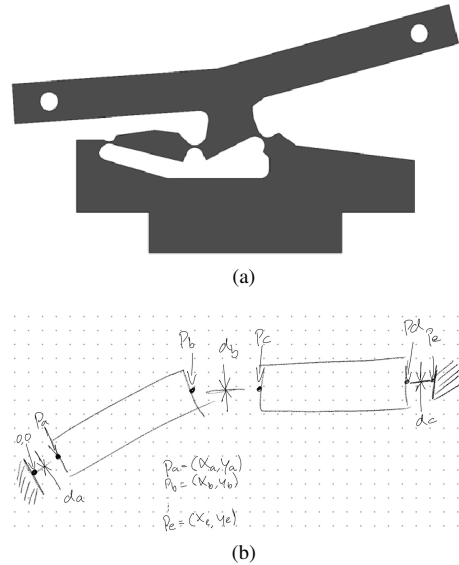


Fig. 13. Two figures showing the bistable switch as designed by Larry Howell a), and the parametrical PRBM representation used for the first attempts at the model b).

Regarding the interaction between the four-bar mechanism and the bistable element, it was concluded that the four-bar mechanism only exerts force on the bistable element rather than providing a forced displacement. From this observation, the conclusion was drawn that a four-bar mechanism would be able to provide the necessary behaviour. And with this information, the bistable element was fully adjusted in section III-C to fit this conclusion. This also made it possible to model the interaction fully in Matlab rather than depending on APDL simulations for the behaviour of the bistable element.

A. Model attempts six bar

As mentioned previously, these attempts were based on a fundamentally incorrect assumption. The compliant hinges in fig. 13a had been identified as long flexures which would be approximated in PRBM as a beam with two axes. This assumption had been made due to the fact that only three flexures were present, and this was incorrectly identified as a three-bar linkage. Additionally, the length of the flexures was the same, so it was not possible to assume any one of them should be modelled using more or less DOF than the others. These two assumptions lead to the representation shown in fig. 13b.

The model attempts were all based on the same assumption, namely that for each timestep the mechanism would exist in

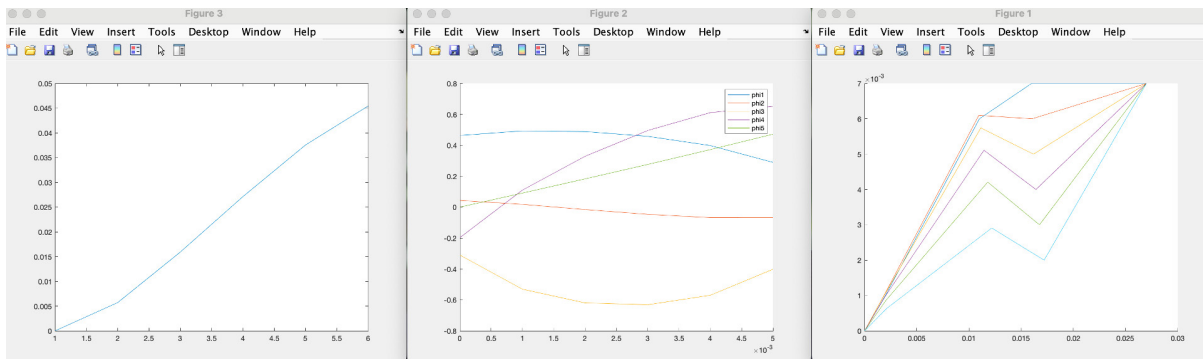


Fig. 14. Three figures showing the results for the bistable element with right axle reduced to a single axle. The left figure shows the total energy in the system, the middle figure shows the energy in each axle, and the right figure shows the shape of the bar mechanism for a few timesteps.

the lowest energy state that was attainable from the previous timestep. To find this lowest energy state, the kinematics and energy equations of the mechanism were written such that they could be used as input for a minimisation algorithm. This minimisation algorithm would then search for the set of variables that provided the lowest energy state available.

From fig. 13b one can see that the approximation of the system was a 6 bar mechanism with three DOF. Of these three DOF, one DOF would be actuated, namely the y displacement of point four or  $P_c$  as denoted in this figure. This leaves 2 DOF to determine based on the energy of the system.

Initially an attempt was made to solve this by minimising the energy function of the system defined as:

$$\sum E = \sum \frac{1}{2} * k_i * d\gamma_i^2 \quad (1)$$

With the vector loop equation as the constraint.

However this did not work, the optimisation algorithm used in Matlab returned errors that no optimum could be found satisfying the constraints. It is expected that this might be due to the constraints being too rigid which resulted in the error.

In the next attempt, the decision was made to solve each time step by consecutively running optimisation algorithms to find the minimum. This would work by using the same energy equation, and optimising the angle of the left flexure with a fixed angle of the right flexure. After which the angle of the right flexure would be optimised using the found optimum from the previous optimisation. This would be alternated until the difference between each iteration is below a predefined threshold. This however also proved not to work.

### B. Model attempts five bar

When no solution for the six bar mechanism could be found, attempts were shifted to an approximation using a five bar mechanism. This approximation does contain the problem that one of the axles would need to be removed, which presents the problem that this axle needed to be selected such that all assumptions are still applied consistently.

For the first attempt at a five bar mechanism, the right flexure in fig. 13b was reduced to a single axle. This axle was chosen with the reasoning that the bar attached to the axle would approximate a circular profile with a reasonable

accuracy. However, this does introduce an inconsistency, since this reasoning also holds true for the left flexure. With one DOF removed, the system proved more solvable and the first results were obtained.

In this attempt, the five bar mechanism was optimised for the angle of the left flexure, the angle of the left bar and for the angle of the middle flexure. However all these methods did not provide the results expected when compared with the APDL model.

Looking at the simulations obtained from APDL like fig. 17, the observation was made that the flexures on the extremes exhibit flexure behaviour that can be described using one axle. However, the central flexure takes on various shapes during the actuation of the mechanism. From this the conclusion was drawn that the central flexure might lack DOFs to accurately model the behaviour found in the APDL model.

As the reader can see from figs. 14 and 15, the models behave very similarly. The physics of this iteration were tackled the same as with the previous iteration.

1) *Conclusion:* After all the attempts made to model the bistable element and comparing to the APDL results of these iterations, the conclusion was drawn that PRBM did not leave enough DOF in the middle flexure to accurately model its buckling, and adding too many DOFs would negate the benefits of using Matlab to model the system. In APDL, it was found that the flexure would form an S-shape, which snaps through to an arc as shown in fig. 17. No method was conceived to develop a model of this behaviour without introducing additional variables. After these attempts, the decision was made to use APDL data of the bistable element to further continue the Matlab model of the full mechanism.

### C. Final bistable model

Because implementing results obtained from APDL did not prove to be accurate or effective. Or when it did become accurate, the model became too complex, as well as resulting in a slow model. The decision was made to have another attempt to model the bistable element using PRBM. In essence the bistable element did not change, however this time the the new bistable mechanism is based on the requirements Howell provides in his book in the chapter on bistable mechanisms [21].



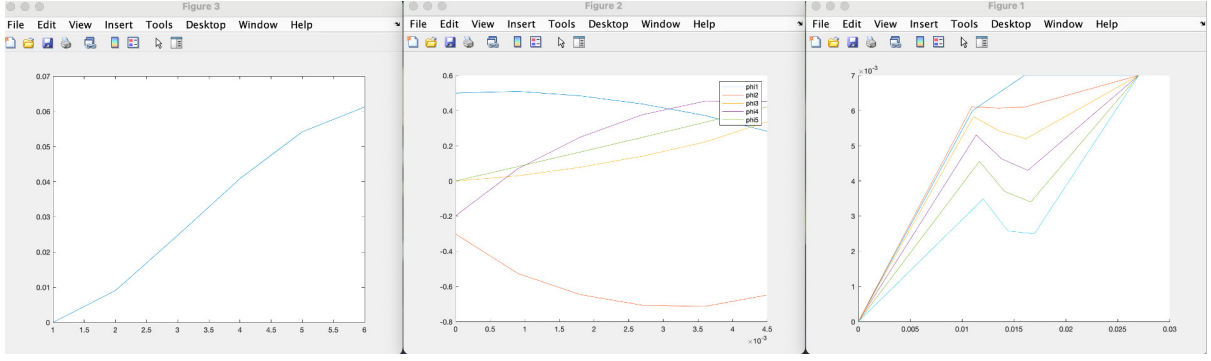


Fig. 15. Three figures showing the results for the bistable element with the left and right axle reduced to a single axle, and the middle flexure increased to three axles. The left figure shows the total energy in the system, the middle figure shows the energy in each axle, and the right figure shows the shape of the bar mechanism for a few timesteps.

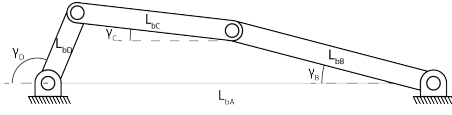


Fig. 16. A figure showing a schematic representation of the bistable mechanism with with the angles and distances as defined.

1) *Kinematics*: The kinematics of a four-bar mechanism are well known, the calculations used in this paper are based on the paper by Tang [23]. The author of that makes use of the Freudenstein equation to solve their system and visualise it in Matlab. The calculations used by Tang are adapted for the coordinate system used in this paper as shown in fig. 16.

From this representation the vector loop equations can be set up:

$$L_{bB}\cos[\gamma_B] + L_{bC}\cos[\gamma_C] - L_{bD}\cos[\gamma_D] - L_{bA} = 0 \quad (2)$$

$$L_{bB}\sin[\gamma_B] + L_{bC}\sin[\gamma_C] - L_{bD}\sin[\gamma_D] = 0 \quad (3)$$

These vector loop equations can be described using the Freudenstein equation.

$$K_1(\gamma_B)\sin[\gamma_D] + K_2(\gamma_B)\cos[\gamma_D] + K_3(\gamma_B) = 0 \quad (4)$$

With variables  $k_i(\gamma_B)$

$$K_1(\gamma_B) = -2L_{bB}L_{bD}\sin[\gamma_B] \quad (5)$$

$$K_2(\gamma_B) = 2L_{bD}(L_{bA} - \cos[\gamma_B]) \quad (6)$$

$$K_3(\gamma_B) = L_{bA}^2 + L_{bD}^2 + L_{bB}^2 - 2L_{bA}L_{bB}\cos[\gamma_B] \quad (7)$$

This equation can be solved to obtain  $\gamma_D(\gamma_B)$  as a function of  $\gamma_B$ , and  $\gamma_C(\gamma_B, \gamma_D)$  as a function of  $\gamma_B$  and  $\gamma_D$ .

$$\gamma_D(\gamma_B) = 2 * \operatorname{atan2}\left(-2k_1 \pm \sqrt{4(k_1^2 + k_3^2 - k_2^2)}, 2(k_3 + k_2)\right) \quad (8)$$

$$\gamma_C(\gamma_B, \gamma_D) = \operatorname{atan2}(L_{bD}\sin[\gamma_D] - L_{bB}\sin[\gamma_B], L_{bA} + L_{bD}\cos[\gamma_D] - L_{bB}\cos[\gamma_B]) \quad (9)$$

From the kinematics, the displacement  $d_y$  of axle three relative to its initial position was also obtained as follows:

$$d_y(\gamma_B) = L_B\sin[\gamma_B] - (L_B\sin[\gamma_{B0}]) \quad (10)$$

2) *Stiffness*: For the PRBM, the absolute rotation of each of the axles needs to be calculated as follows:

$$\alpha_1 = (\gamma_B - \gamma_{B0}) \quad (11)$$

$$\alpha_2 = (\gamma_B - \gamma_{B0}) - (\gamma_C - \gamma_{C0}) \quad (12)$$

$$\alpha_3 = (\gamma_C - \gamma_{C0}) - (\gamma_D - \gamma_{D0}) \quad (13)$$

$$\alpha_4 = (\gamma_D - \gamma_{D0}) \quad (14)$$

This axle rotation can be used to calculate the resulting torque provided by the flexures.

$$T_i = -\frac{E_i * I_i}{l_i} * \alpha_i \quad (15)$$

The reaction moment of the mechanism as a function of displacement, is described by the following formula:

$$M_{rB} = -T_1 - T_2 - (T_2 + T_3) * h_{32} + \quad (16)$$

$$(T_3 + T_4) * h_{42} \quad (17)$$

With  $h_{32}$  and  $h_{42}$  defined as:

$$h_{32} = \frac{L_{bB}\sin[\gamma_D - \gamma_B]}{L_{bC}\sin[\gamma_C - \gamma_D]} \quad (18)$$

$$h_{42} = \frac{L_{bB}\sin[\gamma_C - \gamma_B]}{L_{bD}\sin[\gamma_C - \gamma_D]} \quad (19)$$

Due to the design limitations using a 3D printer, the stiffness ratio between link D and flexure four of the bistable element is too low to disregard the bar compliance. Initially, the effect of this small difference in compliance was not taken into account. However after obtaining the results from APDL it became clear that it would be necessary to correct for the difference

in stiffness resulting from not regarding link D as infinitely stiff. To retain the mechanism as a four-bar mechanism, this compliance was accounted for by correcting the stiffness of this axis [24], and adjusting axle position by referencing APDL results.

$$\frac{1}{T_4} = \frac{1}{T_{f4}} + \frac{1}{T_{b4}} \quad (20)$$

#### D. Ansys APDL

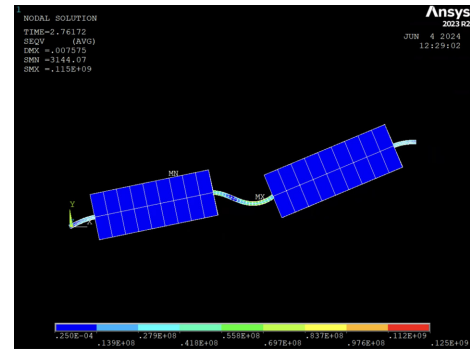
While working on the model of the bistable element in PRBM, Ansys APDL was used to verify whether the assumed configuration of the models should actually produce bistable behaviour. And whenever results were obtained from PRBM, Ansys was used to verify whether the results obtained agreed with FEM. When the bistable element did not solve in PRBM, results from Ansys were also used to provide the PRBM model of the entire system with the data on the behaviour of the bistable element.

1) *Initial Bistable Element*: The bistable element was first implemented into Ansys APDL to validate the results obtained from the PRBM analysis. The choice was made to perform this validation using Ansys APDL, because this program generally provides accurate results for the system. So when the two models would agree, this meant that they likely provide an accurate prediction of the system behaviour. When the validation would be complete, Matlab could be used to perform parameter sweeps on the bistable element to find the best configuration. During the first iterations, the approximation of the bistable element shown in fig. 13b was used in Ansys APDL. This resulted in the model that is shown in its deformed state in fig. 17. This model of the bistable element was characterised by the fact that it produces snap-back behaviour. This behaviour was quite difficult to simulate, as it produced bad convergence numbers for the timesteps at which it occurred. That meant that many configurations of model and solver settings produced no results, as the solver could not converge the solution. From this model the initial force, moment, y-displacement, and angular rotation data was obtained.

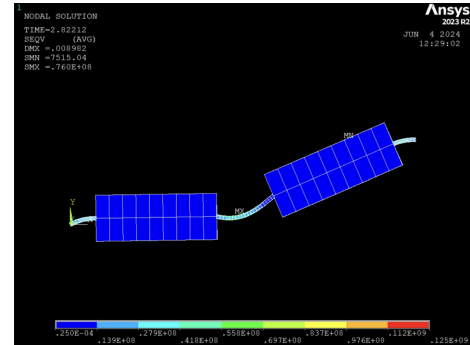
2) *Bistable Parameter sweep*: Before the Bistable element was redefined as in section III-C, a Matlab script was developed which could sweep the parameters of the bistable element in APDL. This way an ideal variant of the bistable element could be found for interaction with the four-bar mechanism. The criteria for the bistable element are as follows:

- Force peak magnitude
- Ratio between force peaks
- Displacement between stable points

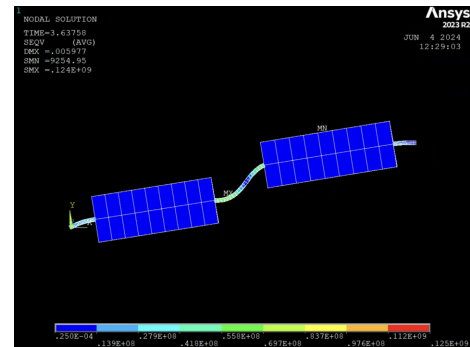
To fully define the start configuration of the bistable element when defined as in fig. 13b, a total of sixteen variables is required. Seven of these variables were defined beforehand leaving nine remaining variables. For these variables a starting configuration was defined. Using this starting configuration, the locations of points one to six can be calculated. With these locations the bistable element can be modelled in APDL. Then using the thicknesses of each of the bar the bistable element can be meshed in APDL. By varying one of these nine variables on each run, slight variations of the bistable element



(a)



(b)



(c)

Fig. 17. Three figures obtained from Ansys APDL that show the snap-back behaviour of the old approximation of the model. a) shows the mechanism as it is being actuated downwards just before snap, b) shows the mechanism just after snap, and c) shows the mechanism after snap being actuated upwards.

could be simulated to select the best configuration within the searching range around the initial configuration. From there the same solver was run as for the other variations of the bistable element, from which all necessary data can be obtained. From this optimisation, a configuration was found that was found to be ideal. However, this model of the bistable element became irrelevant with the modelling iteration described in section III-C.

3) *Final Bistable Element*: The final bistable element has also been modelled in APDL. To obtain a configuration that would be possible to 3D print, and that would comply with the assumptions of the PRBM. The parameters of the final bistable element were chosen by hand. The moment-angle relationship knowledge obtained from section III-D2 was used to get the

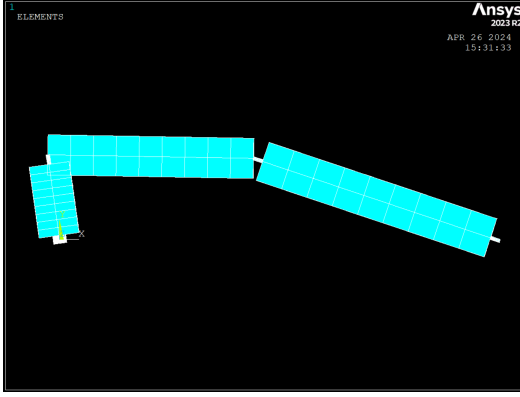


Fig. 18. A picture showing the final bistable element as modelled in APDL

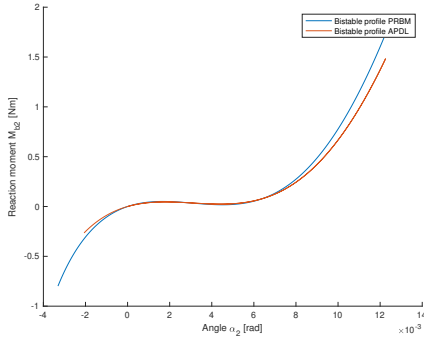


Fig. 19. A graph showing the moment-angle relationship obtained from both the PRBM and APDL model.

ideal configuration.

The model developed in APDL is shown in fig. 18. One can see that compared to the old model shown in fig. 17, the new mechanism makes use of thinner and shorter flexures which could be modelled in PRBM using a single hinge per flexure.

The element is described using beams that are modelled using beam188 elements, with an isotropic material with a Young's modulus of  $1607[MPa]$  and a Poisson's ratio of  $0.38[-]$ . The solver is set to non linear geometry, and the mechanism is actuated by forcing a rotation on link B. This rotation is from  $0[rad]$  to  $0.425[rad]$  and then returns to  $0.075[rad]$  on the return stroke. This results in the figure shown in section III-D3

#### IV. FOUR BAR MODEL

In PRBM the compliant four-bar mechanism is approximated as a four-bar linkage. Modelling each of the flexures as a one DOF pivot with an internal torsional spring constant.

##### A. Kinematics

The kinematics of the four-bar mechanism are the same as those of the bistable element, for clarity a different set of variables will be used to describe the four-bar mechanism. These variables are shown in fig. 20.

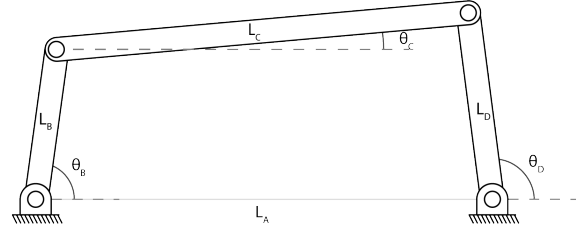


Fig. 20. A figure showing the four-bar mechanism with its variables defined.

From this definition, the following loop equations can be obtained for the four-bar mechanism. Because the calculations are the same as for the bistable element, only the loop equations and the final equations for  $\theta_D$  and  $\theta_C$  are shown.

$$l_B \cos[\theta_B] + l_C \cos[\theta_C] - l_D \cos[\theta_D] - l_A = 0 \quad (21)$$

$$l_B \sin[\theta_B] + l_C \sin[\theta_C] - l_D \sin[\theta_D] = 0 \quad (22)$$

$$\theta_D(\theta_B) = 2 * \text{atan2}(-2k_1 \pm \sqrt{4(k_1^2 + k_3^2 - k_2^2)}, 2(k_3 + k_2)) \quad (23)$$

$$\theta_C(\theta_B, \theta_D) = \text{atan2}(l_D \sin[\theta_D] - l_B \sin[\theta_B], l_A + l_D \cos[\theta_D] - l_B \cos[\theta_B]) \quad (24)$$

##### B. Stiffness

Next the stiffness of the flexures in the compliant four-bar mechanism are calculated using the following formula.

$$T_i = -k_i * \phi_i \quad (25)$$

$$T_i = -\frac{EI_i}{l_i} * \phi_i \quad (26)$$

Where  $\phi$  is defined as:

$$\phi_1 = \theta_B - \theta_{B0} \quad (27)$$

$$\phi_2 = (\theta_B - \theta_{B0}) - (\theta_C - \theta_{C0}) \quad (28)$$

$$\phi_3 = (\theta_C - \theta_{C0}) - (\theta_D - \theta_{D0}) \quad (29)$$

$$\phi_4 = (\theta_D - \theta_{D0}) \quad (30)$$

## V. COMBINED MODEL

The entire system was simulated by combining the calculations of the four-bar mechanism and the bistable element. This process consisted of a few iterations, akin to the model of the bistable element. Each iteration contained some mistakes which were attempted to be solved in the next iteration. The first model consists of a model that models the interaction between the bistable element and the four-bar mechanism as being force based, this model still utilised the APDL data for the bistable element. This did not give the desired results, so for the next iteration, the decision was made to switch to a moment estimated model. This again did not provide the desired results, and the conclusion was drawn that the chosen bistable element was affected almost equally by both effects. On the last two iterations, the force and moment were taken into account. On the second to last iteration, still an APDL model is used, however this model did not function anymore because the model did not behave as expected anymore due to the complexity of obtaining the moment balance. Lastly, the functioning model is presented that is fully based on PRBM data, but that can also incorporate APDL and experimental data for the bistable element.

### A. Force-Estimated

In section III several attempts at the analytical estimation of the bistable element are described. On this iteration of the PRBM model of the entire system, the analytical model of the bistable had not been solved. Instead, APDL was used to characterise the behaviour of the bistable element as in section III-D2. The bistable element that was modelled is shown in fig. 21. This model was dependent on the following assumptions:

- The displacement of the relevant point on the bistable element is relatively small in the x axis.
- The force exerted on the bistable element is always perfectly parallel to the y axis.
- The moment exerted on the bistable element through flexure three is irrelevant for the behaviour of the bistable element.
- The behaviour of the bistable element can be simplified as a lengthening and shortening of link D.

1) *Simplifying the force-displacement characteristics:* Because this model was based on an applied force, the decision was made to simplify the force-displacement characteristics of the bistable element as shown in fig. 22. This was done to ensure that only one intersection would exist over the entire range of bistable element displacement. To ensure that a hysteresis loop could still be produced, two profiles were created, the behaviour of the bistable element on the forward path, and the behaviour of the bistable element on the return path. The data available to the model would switch once the deformation of the bistable element had exceeded 4.5mm. This way, when the mechanism switches over on the forward stroke, the mechanism behaviour would immediately switch over to the profile of the backward path. This ensured that the model could not infinitely cycle between the two points on the graph.

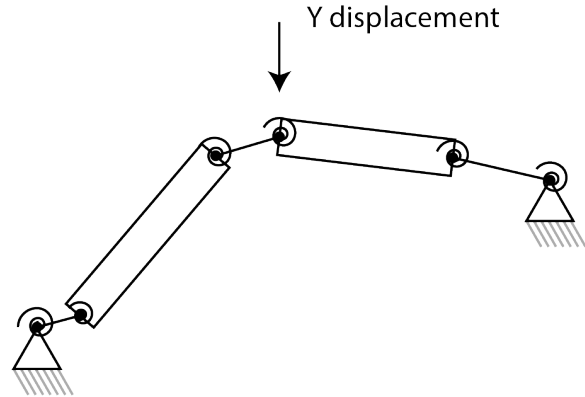


Fig. 21. A figure showing the bistable element as it is modelled in the force estimated model.

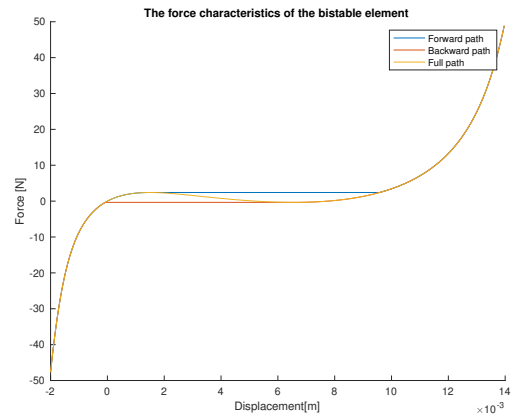


Fig. 22. A graph showing the force-displacement characteristics of the bistable element. the figure shows both the simplification and the original path obtained from simulation.

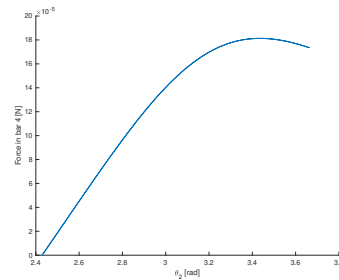


Fig. 23. A plot showing the force in link D as a function of actuation angle  $\theta_B$ . For the configuration shown in fig. 4a.

In fig. 23 one can see that the peak of the force in link D exists before the maximum actuation angle is reached. Because the input will be oscillating, this means that the force graph of link D will include a dip in its peak. As a result it is not possible to tune the bistable element such that it will switch over beyond  $\theta_B = 3.45[rad]$ , as the peak force has already been met. This dip is due to the geometry of the mechanism, which has angle  $\phi_3$  decrease beyond  $\theta_B = 3.45[rad]$ . This results in a net decrease of force in link D. As such, the decision was made to choose a different four-bar mechanism configuration from this point on, the configuration shown in fig. 4a was changed to the configuration shown in fig. 11a.

2) *Force in link D*: The following paragraph explains the method initially used to calculate the force in link D. At a later stage, the conclusion was drawn that this method was incorrect, because it did not take the effect of internal forces in the link into account correctly. This force model is used for the first three iterations for the combined model, and is corrected in the final model with a new force in link calculation.

Continuing on the assumption from the PRBM: approximating the flexures as single axles, the force in link D can be calculated.

To calculate the force in link D, the four-bar mechanism is reduced to a three-bar mechanism. On which calculations can be performed statically per time step. This is based on the assumption that  $\theta_B$  is the actuated variable. Which means that the location of axle two is given. Thus, only the moments generated by the axles two up to and including four are relevant for the force in link D.

In order to calculate this force, the free body diagrams of links C and D were set up as shown in section V-A2.

For these free body diagrams one can derive the balance equations to calculate the unknown force. The assumption was made that apart from a moment, the axles can only transmit force in the axial direction of the beams. This means that for the moment balance, only the moments and the force supplied by the other beam is relevant.

For the moment with respect to the constrained axles, only the force exerted perpendicular to the link is relevant. To calculate this, a new angle  $\Omega$  is defined as shown in fig. 24a.

From fig. 24a one can see that the angle can be constructed as follows:

$$\Omega = \theta_D - (\theta_C + \frac{\pi}{2}) \quad (31)$$

Using eq. (31), the moment balance around axle 2 can be derived:

$$\begin{aligned} \sum M_{z2} &= -M_2 + M_3 + F_D * \cos(\Omega) * l_C \\ \sum M_{z2} &= -M_2 + M_3 + F_D * \cos((\theta_C + \frac{\pi}{2}) - \theta_D) * l_C \end{aligned} \quad (32)$$

Solving this for  $F_D$  one obtains:

$$F_D = \frac{-M_2 + M_3}{\cos((\theta_C + \frac{\pi}{2}) - \theta_D) * l_C} \quad (33)$$

A similar operation is then performed for the moment around axle four. For this axle, the force in link C is relevant to

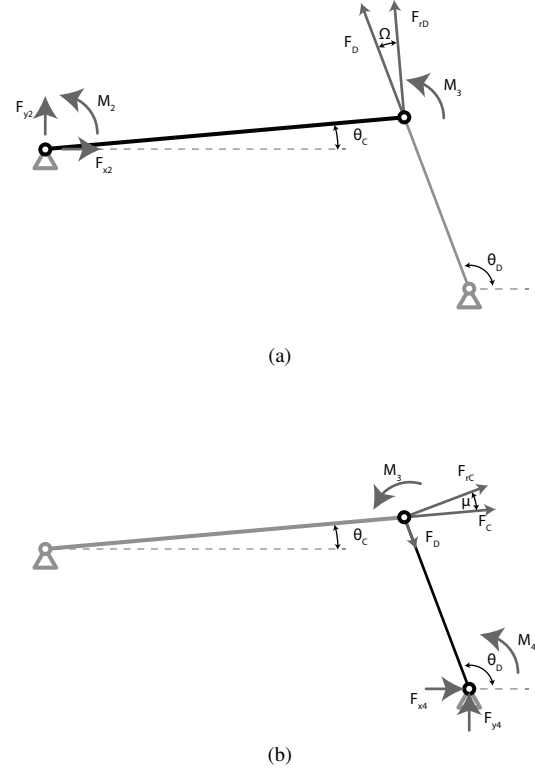


Fig. 24. Two figures showing the free body diagrams used for links C a) and D b). The assumption was made that apart from a moment, the axles can only carry over force in the axial direction of the beams.

calculate this moment. The force in link C provides a force which contains a component in the axial direction of link D. The relevant angle for this is constructed angle  $\mu$ .

$$\mu = (\theta_D - \frac{\pi}{2}) - \theta_C \quad (34)$$

$$\sum M_{z4} = -M_3 - M_4 - F_3 * \cos(\mu) * l_D = 0 \quad (35)$$

$$\sum M_{z4} = -M_3 - M_4 - F_3 * \cos((\theta_D - \frac{\pi}{2}) - \theta_C) * l_D = 0 \quad (36)$$

$$F_3 = \frac{F_D}{\sin(\mu)} \quad (37)$$

$$F_3 = \frac{F_D}{\sin((\theta_D - \frac{\pi}{2}) - \theta_C)} \quad (38)$$

Substituting eq. (38) into eq. (36) gives:

$$F_D * \frac{\cos((\theta_D - \frac{\pi}{2}) - \theta_C) * l_D}{\sin((\theta_D - \frac{\pi}{2}) - \theta_C)} = -M_3 - M_4 \quad (39)$$

Solving for  $F_D$  one obtains:

$$F_D = (-M_3 - M_4) \frac{\sin((\theta_D - \frac{\pi}{2}) - \theta_C)}{\cos((\theta_D - \frac{\pi}{2}) - \theta_C) * l_D} \quad (40)$$

Combining eqs. (33) and (40) the full equation for the effect of the axial moments on the internal force of link D can be constructed:

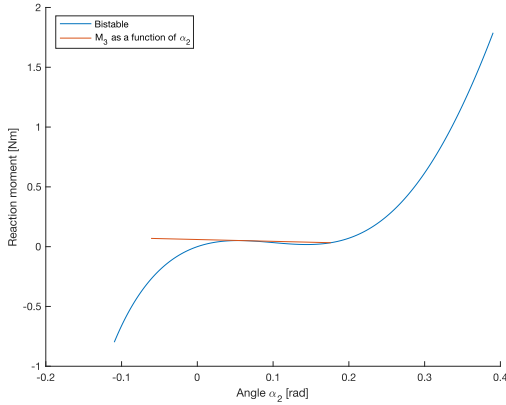


Fig. 25. A plot showing the characteristic moment-angle behaviour of a bistable element, with the moment in axle three plotted as a line.

$$F_D = \frac{-M_2 + M_3}{\cos((\theta_C + \frac{\pi}{2}) - \theta_D) * l_C} + \frac{(-M_3 - M_4) \sin((\theta_D - \frac{\pi}{2}) - \theta_C)}{\cos((\theta_D - \frac{\pi}{2}) - \theta_C) * l_D} \quad (41)$$

3) *Lengthening of link D*: To model the lengthening of link D, the information of the APDL simulation of the bistable element was incorporated into the calculations. This meant that the vertical displacement of the bistable element  $dy_{b2}$  was added to the starting length of link D  $L_{D0}$ .

$$l_D = L_{D0} + dy_{b2} \quad (42)$$

### B. Moment-Estimated

Because the estimation of the mechanism behaviour through the use of the force in link D did not provide accurate enough results. The decision was made to look into how the model would behave when the moment in axle three was used as the significant transmission of force.

#### 1) Angle change due to deflection:

The moment in axle three was now taken as the relevant force on the bistable element. As a result, the effects of the displacement of the bistable element became relevant for the estimation of the resulting moment. This meant that the moment-displacement graph could not be simplified. This is because there is a relationship between the moment in axle three and the displacement of the bistable mechanism. This relationship means that when evaluating the moment balance at each timestep the effect of this displacement has to be taken into account. To solve this, the balance is obtained by iteration. First, a new displacement is estimated based on the displacement of the previous timestep multiplied by 1.05. Second, the moment is calculated based on the information of the previous timestep with the new  $\theta_B$ . Third, using this estimated displacement an intersection with the moment-displacement graph is calculated from which a moment is obtained. Fourth, the convergence is calculated by dividing the difference between the moment provided by the axle, and the moment that is obtained from

the intersection. Fifth, this convergence is divided by ten and then added to the displacement estimation.

As long as the absolute convergence is larger than  $10^{-6}$  steps three to five are repeated until this convergence criterion is met.

This model provided a better prediction of the size of the cycled area, however the location of the forward crossover was incorrect. The conclusion was that the behaviour of the mechanism could not accurately be predicted with either the force-displacement or the moment-displacement. As such, the decision was made to attempt to combine these methods not relying on the assumption that either one of them could be neglected for modelling.

### C. Combined version 1

Incorporating the effect of both the moment and the force required characterising the effects of both forces on the bistable element. The moment-displacement graph will look different under the effect of an applied force. This means that to obtain a displacement as a result of a combination of force and moment, a sweep was performed in APDL. This resulted in two surfaces, a moment-force-angle and a moment-force-displacement surface for the bistable element. To obtain the equilibrium configuration, the moment and force values from the four-bar mechanism were used to obtain the angle  $\gamma_B$  and displacement  $d_y$  of the bistable element. Using these new values for  $\gamma_B$   $d_y$ , the four-bar mechanism was calculated again, resulting in a new combination of moment and force, which is consequently used to obtain new values for  $\gamma_B$   $d_y$ . This is repeated until the difference between two iterations got lower than  $1e-6$ .

This method resulted in a model that was computationally heavier than simulating the system in APDL, and did not provide a working model. The interactions between the four-bar mechanism and the surface projections of the bistable element behaviour based on APDL data proved not to work. The decision was then made to reevaluate the chosen definition of the bistable element with aid from the compliant mechanisms book by Howell [21].

### D. Final combined version

After a lot of work trying to fit the APDL data to a combined model, the decision was made to give the bistable element one last modelling attempt. The relevant mechanism was found in Compliant Mechanisms[21]. And it was hypothesised that the snap-through exhibited by the first model was not vital for the functioning of the full mechanism. This meant, a 'more simple' bistable mechanism that has the same force-displacement behaviour on the forward stroke as well as on the return stroke would suffice. The explanation of the resulting model is shown in section III-C.

1) *Force in beam*: The sum of moment exerted on the bistable element is calculated using the torque and force in hinge three. The internal force is a result of the four-bar mechanism stiffness, and is found per time step using static equations.



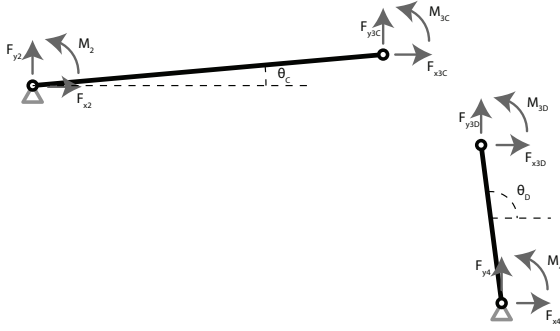


Fig. 26. A figure showing the free body diagram of links C and D for an arbitrary configuration.

From the free body diagram, the force and moment balances can be determined for links C and D.

The balances for link C are:

$$\sum Fx_C = Fx_2 + Fx_{3C} = 0 \quad (43)$$

$$\sum Fy_C = Fy_2 + Fy_{3C} = 0 \quad (44)$$

$$\sum M_{2C} = M_2 + M_{3C} + l_C[Fy_{3C}\cos[\theta_C] - Fx_{3C}\sin[\theta_C]] = 0 \quad (45)$$

$$\sum M_{s3C} = M_2 + M_{3C} + l_C[Fx_2\sin[\theta_C] - Fy_2\cos[\theta_C]] = 0 \quad (46)$$

The balances for link D are:

$$\sum Fx_D = Fx_4 + Fx_{3D} = 0 \quad (47)$$

$$\sum Fy_D = Fy_4 + Fy_{3D} = 0 \quad (48)$$

$$\sum M_{4D} = M_4 + M_{3D} + l_D[Fy_{3D}\cos[\theta_D] - Fx_{3D}\sin[\theta_D]] = 0 \quad (49)$$

$$\sum M_{s3D} = M_4 + M_{3D} + l_D[Fx_4\sin[\theta_D] - Fy_4\cos[\theta_D]] = 0 \quad (50)$$

The force and moment balance in joint three of the four-bar mechanism is then:

$$\sum Fx_3 = Fx_{3C} + Fx_{3D} = 0 \quad (51)$$

$$\sum Fy_3 = Fy_{3C} + Fy_{3D} = 0 \quad (52)$$

$$\sum M_3 = M_{3C} + M_{3D} = 0 \quad (53)$$

These equations are solved for  $Fx_3$  and  $Fy_3$  to obtain the internal forces of link D at the location of joint three.

$$Fx_3(\gamma_B) = -\frac{L_C[M_3 + M_4]\cos[\theta_C] + L_D[M_2 - M_3]\cos[\theta_D]}{l_C l_D \sin[\theta_C - \theta_D]} \quad (54)$$

$$Fy_3(\gamma_B) = -\frac{L_C[M_3 + M_4]\sin[\theta_C] + L_D[M_2 - M_3]\sin[\theta_D]}{l_C l_D \sin[\theta_C - \theta_D]} \quad (55)$$

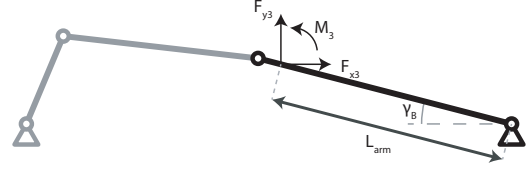


Fig. 27. A schematic representation of the force and moment exerted on link B of the bistable mechanism by the four-bar mechanism.

Because deformation of bistable element change the configuration of the four-bar mechanism, all moments and angles in eqs. (54) and (55) are functions of  $\gamma_B$  at each timestep.

2) *Matlab Implementation:* The complete mechanism is modelled by combining the data of the bistable mechanism with the data of the compliant four-bar mechanism. Since developing a fully analytical solution of the entire mechanism is outside of the scope of this paper. The choice was made to solve the system numerically.

To simulate the behaviour of combining the bistable element and the compliant four-bar mechanism. The force and moment in axle three of the four-bar mechanism were used to approximate effective change in length of link D. To do this, the moment-displacement behaviour of the bistable element is determined using eq. (17). This produces the graph shown in fig. 25.

To determine the interaction between the bistable element and the four-bar mechanism. Three further assumptions are made, namely that:

- The displacement of the bistable mechanism in y direction can be directly translated to a change in length of link D of the four-bar mechanism.
- The displacement of the bistable mechanism in x direction is small enough to not take into account with respect to the behaviour of the entire system.
- The force generated in link C can be approximated as a moment around axle two of the bistable element.

a) *Force-Moment axle three:* The interaction between the two four-bar mechanisms is modelled using a moment balance at the attachment point to find the deflection of the bistable element. This is the attachment point of link D of the four-bar mechanism to link B of the bistable element. The forces exerted by the four-bar mechanism are shown in fig. 27. From this deflection of the bistable element, the change in length  $d_y$  of link D  $l_D$  can be calculated as shown in eq. (10).

For each timestep of the simulation, an angle  $\theta_B$  is set. Using this set angle, the moment exerted by the four-bar mechanism can be calculated as a function of  $\gamma_B$ . By obtaining the internal forces as a function of  $\gamma_B$ , the effect of the changing kinematics is accounted for in the model. Equation (57) describes the moment that the four-bar mechanism applies on the bistable element.

$$M_{4B}(\gamma_B) = M_3(\gamma_B) - \quad (56)$$

$$(Fx_3(\gamma_B)\sin[\gamma_B] + Fy_3(\gamma_B)\cos[\gamma_B])L_{arm} \quad (57)$$

This exerted moment is then balanced with the reaction moment of the bistable mechanism obtained using eq. (17).

$$M_{Bi}(\gamma_B) = M_{AB}(\gamma_B) \quad (58)$$

At the intersections between  $M_{AB}(\gamma_B)$  and  $M_{Bi}(\gamma_B)$ , the four-bar mechanism and the bistable element are in balance. Given that both  $M_{AB}(\gamma_B)$  and  $M_{Bi}(\gamma_B)$  can be calculated using eqs. (17) and (57), their intersection can be found at each timestep. However, between a certain range of moments, three intersections may be found between the graphs of  $M_{AB}(\gamma_B)$  and  $M_{Bi}(\gamma_B)$ , of which only one is valid with respect to the previous timestep. To ensure that only the correct intersection is found, the intersection is searched for within a range of  $\gamma_B$ . When no intersection is found within the range, the range is increased until an intersection is found. Whenever multiple intersections are found, the range is decreased. This process is shown in fig. 29. From this intersection angle  $\gamma_B$  and the corresponding change in length  $dl_D$  is found for the current value of  $\theta_B$ .

*b) four-bar mechanism bistable element interaction:* Now the moment-displacement graph of the bistable element and the moment exerted on the bistable element by the four-bar mechanism is known. The interaction between the mechanisms can be determined. To do that, the simulation is divided into timesteps, where for each timestep the intersection is found between  $M_{in}$  as a function of  $\alpha_2$  for a given  $\theta_B$  and  $M_{b2}$  of the bistable mechanism. This look as shown in fig. 28, which is performed for each time step.

Three iterations of a time step may look as shown in fig. 29. From the PRBM the graph in fig. 30 is obtained.

*c) Sensitivity of the mechanism:* During modelling, the observation was made that the behaviour of the mechanism was quite sensitive to changes of the mechanism stiffness. This scale of this effect was determined by performing a sensitivity test. The sensitivity was determined by varying the stiffness of flexures with factors  $f_{AB}$  and  $f_{Bi}$  for the four-bar mechanism and the bistable element respectively. The resulting plots are shown in figs. 32 and 33.

This relative stiffness was obtained by increasing or decreasing the thickness of all flexures in the four-bar mechanism and bistable element separately. The thickness was determined as follows:

$$k_i = \frac{Ed_p d_{fi}^3}{12 * l_i} \quad (59)$$

where

$$d_{fi} = \sqrt[3]{f_s d_f} \quad (60)$$

Before changing the bistable model to incorporate the compliance of link D, the effect of the different stiffnesses of the two elements was constant for each ratio  $frac{f_{bi} f_{AB}}$ . This looked as shown in fig. 32, as one can see the behaviour of the full mechanism scales quite cleanly when the bistable element is estimated more simply. The reason this happens is that the thickness of link D of the bistable element was not scaled with the same factor. This meant that the stiffness of the bistable element does not scale cleanly when the compliance of this

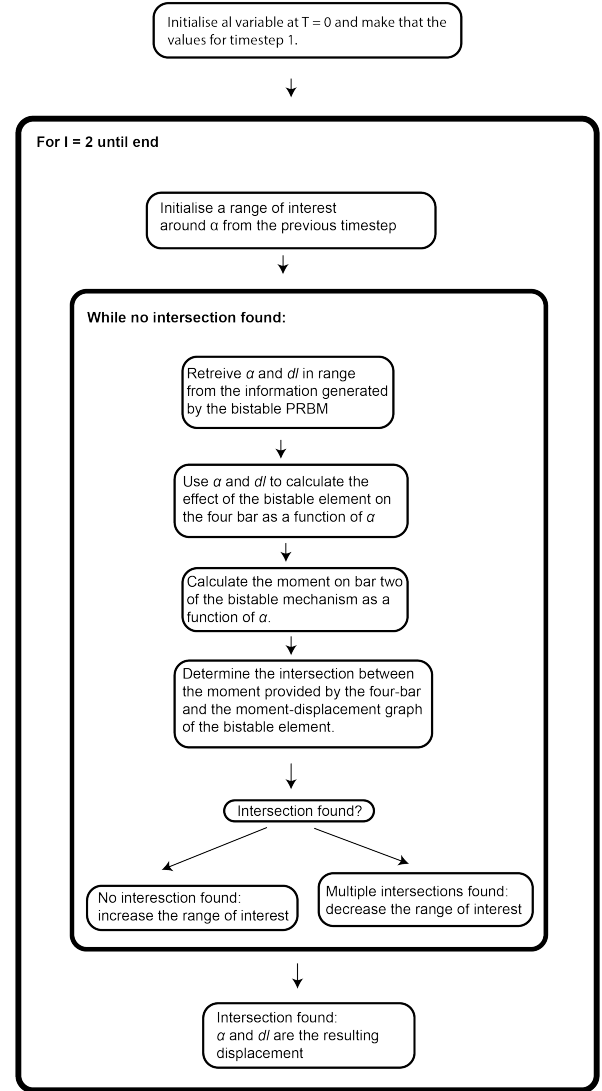


Fig. 28. The flowchart of the interaction between the bistable mechanism and the four-bar mechanism in the numerical model.

link is taken into account. The effect of this on the behaviour of the bistable element is shown in fig. 31.

From fig. 33 it is visible that the ratio between the four-bar mechanism and the bistable element has an effect on the crossover moment of the mechanism. The effect of the relative stiffness becomes greater as the stiffness of the bistable element is lower. This indicates that for a robust design it would be optimal to stick with a stiffer configuration. Generally, the range between the crossovers increases with a decreasing four-bar mechanism stiffness.

*3) APDL:* To validate the obtained results from the combined model, Ansys APDL was used. The full mechanism is actuated with a forced rotation of link B. Resulting in the moment-displacement graph shown in fig. 35a and the location-location graph shown in fig. 35b.

The compliant mechanism is described using beams that are



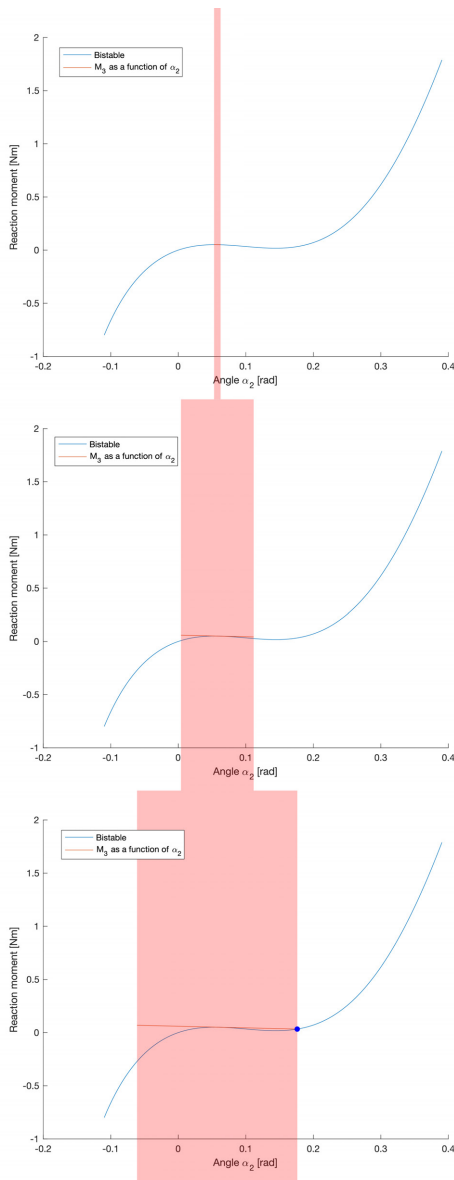


Fig. 29. A plot showing the intersection data obtained from the model from the timestep of the first crossover. The graph shows how the algorithm searches for an intersection by gradually increasing the range of interest shown in red. Until it finds an intersection between the two lines at the blue dot. The red area represents the range of interest at each timestep, the blue line shows  $M_{bi}(\alpha_2)$  and the orange line shows  $M_{4B}(\alpha_2)$ .

modelled using beam188 elements, with an isotropic material with a Young's modulus of  $1607[MPa]$  and a Poisson's ratio of  $0.38[-]$ . The solver is set to non linear geometry, and the mechanism is actuated by forcing a rotation on link B. This rotation is from  $0[rad]$  to  $0.425[rad]$  and then returns to  $0.075[rad]$  on the return stroke. This results in the figure shown in section III-D3

## VI. PRODUCTION

For experimentation, the prototypes were produced using a 3D printer. Two 3D printers were available: Prusa Mk3S and the bambulabs x1 Carbon. From these two the bambulabs printer produced the highest quality and most repeatable prints.

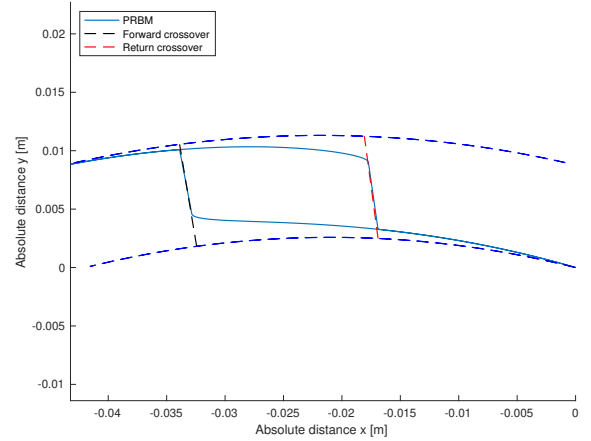


Fig. 30. A figure showing the path predicted by the PRBM. The blue lines indicate the paths between which the mechanism switches during operation, the black line indicates the crossover line on the forward stroke, and the red line indicates the crossover line on the return stroke.

The material that was used was polymatter PETG. PETG was chosen as the most ideal material for the production of compliant mechanisms because it is not very brittle or too stiff like ABS or PLA, but it still is able to bear loads in contrast to TPU.

The printer settings were adjusted to attempt the highest tolerances. Normally the bambulabs printer prints with a print speed of  $300\text{ mm/s}$  for PETG prints. however on the inspection of the first set of samples, it was noticed that this meant that the print head tended to cut corners in the parts with a high amount of detail. These effects of the printer were limited by utilising a lower printing speed, the important settings that were changed were as follows:

- 1) All print speeds to a maximum of  $150\text{ mm/s}$
- 2) outer wall speed to  $50\text{ mm/s}$
- 3) all line widths set to  $0.39$
- 4) Wall construction outer wall first and then inner wall.

After printing the samples were numbered and assessed on production accuracy using a vhx keyence 7000 digital microscope. This produced dimensional measurements of the samples to an accuracy of  $10\mu m$ . The results from these measurements are available in tables IV and V. As one can see, the mean error of the flexures is roughly  $130[\mu m]$  with a standard deviation of roughly  $70[\mu m]$

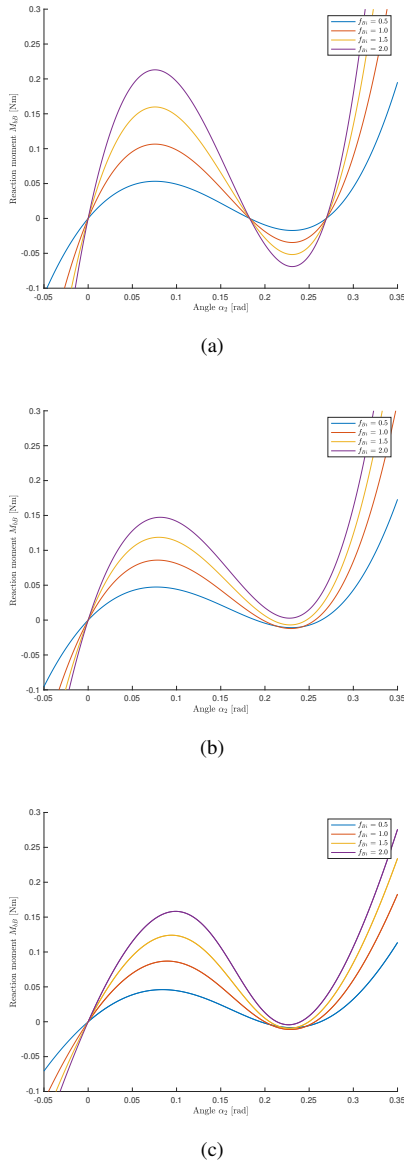


Fig. 31. Three figures showing the effect of changing the thickness  $d_b f_i$  of the flexures with factor  $f_{Bi}$  on the moment-angle relationship of the bistable element. a) shows how the behaviour changes for the model that does not include the correction in eq. (20), b) shows how the behaviour changes for the corrected model, and c) shows the prediction made by the Ansys APDL model.

## VII. EXPERIMENT

To validate the models generated in Matlab and APDL, three experiments were defined: The first experiment validates whether the path drawn by the full mechanism is similar to the predictions made by the models; The second experiment measures the Force-Displacement curve of the bistable element; And the third evaluates the force-displacement curve of the full mechanism. With this data it is possible to review the results obtained from both models and the real life data, and evaluate whether the models are an accurate predictor.

To verify that the designed mechanism would work as predicted when produced. Three experiments had to be carried out, the motion path of the point of interest defined for the

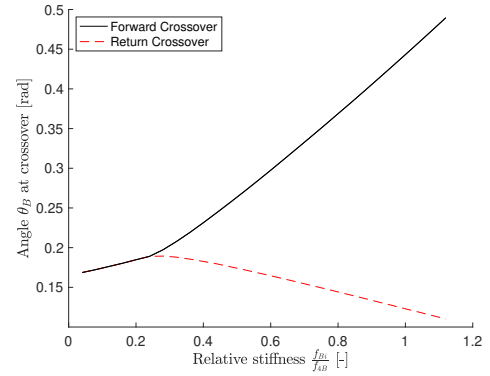


Fig. 32. A plot showing the effect of the stiffness ratio between the bistable element and the four-bar mechanism for the "simple" bistable model.

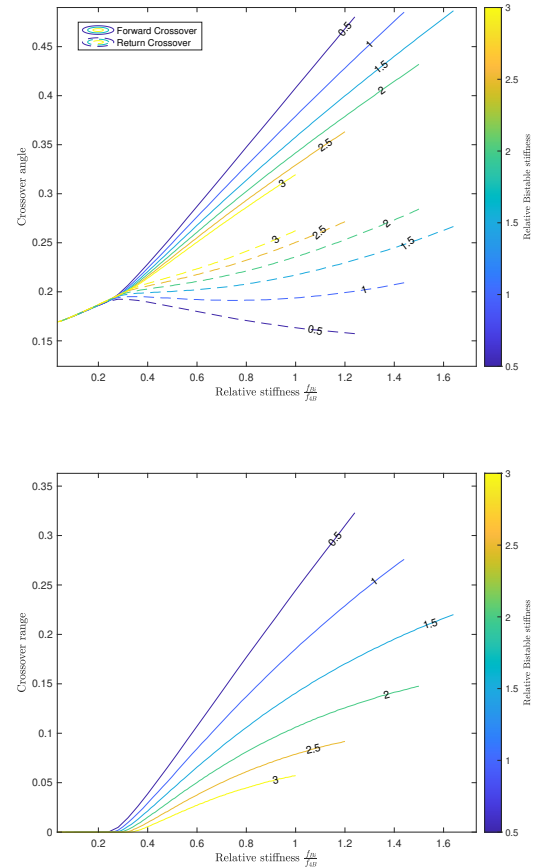


Fig. 33. Two graphs showing the effect of changing the flexure stiffnesses of the bistable and four-bar mechanism parts of the mechanism on the predicted crossover angles of the full mechanism. The x axis denotes the relative stiffness of the bistable element divided by the relative stiffness of the four-bar mechanism compared to the normal configuration. Because the force-displacement graph of the bistable element does not scale linearly this graph does not reduce to one line for each crossover. a) Shows the crossover angle on the forward stroke (solid line) and the crossover angle on the return stroke (dotted line). b) Shows the range between these crossovers as a function of relative stiffness.

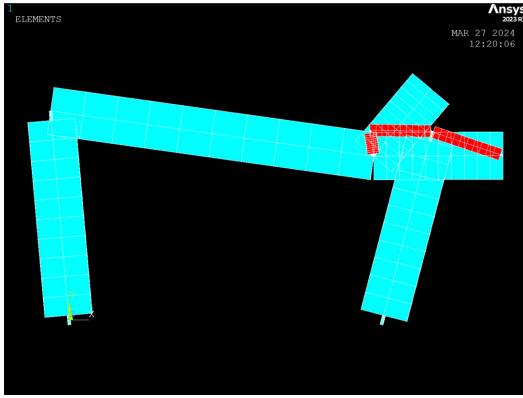


Fig. 34. A figure showing the model of the four-bar mechanism in APDL, the blue bars are the four-bar mechanism, and the red bars are the bistable element connected to the four-bar mechanism.

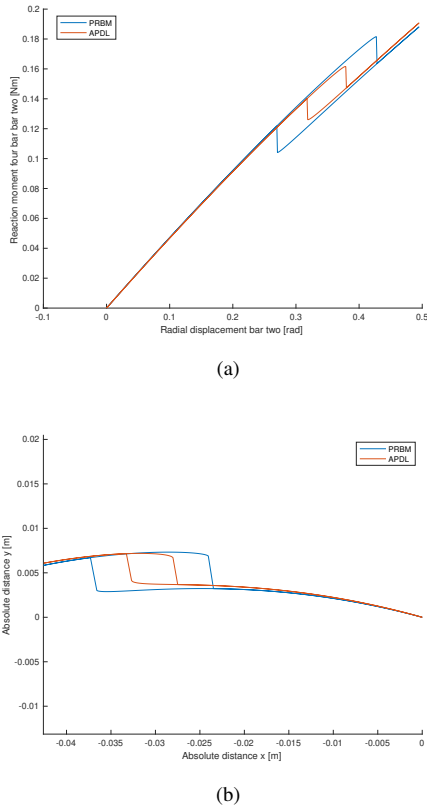


Fig. 35. Two graphs comparing the results obtained from the PRBM and the APDL models. a) shows the moment-angle relationship of the entire mechanism, and b) shows the location-location relationship of the entire mechanism.

APDL and PRBM should be tested, and the force-displacement graphs of the model and bistable element should be verified.

#### A. Motion path

1) *Method:* After the 3D-printed sample is taken out of the printer, it is moved to the test bed ensuring the mechanism is deformed as little as possible. The compliant mechanism is then fastened to a Thorlabs breadboard using the holes included in the base of the mechanism. Underneath the compliant mechanism, a sheet of A4 paper is fastened using the same

TABLE IV  
MEASURED DIMENSIONS OF THE FLEXURE WIDTHS AND LENGTHS OF THE BISTABLE ELEMENT GIVEN IN [ $\mu\text{m}$ ]

Sample	$f1_1$	$f2l_2$	$f3l_3$	$f4l_4$	$f1d_1$	$f2d_2$	$f3d_3$	$f4d_4$
1	1254	1245	1340	903	600	671	505	1746
2	1249	1308	1345	881	606	649	494	1747
3	1299	1214	1337	910	599	614	500	1747
4	1234	1345	1325	1007	567	629	501	1730
5	1444	1431	1441	882	453	506	557	1787
6	1391	1292	1335	905	448	474	461	1622
7	1426	1438	1404	860	478	468	558	1792
8	1379	1440	1408	901	467	488	568	1734
Control	1200	1200	1200	1000	400	400	400	1600
Mean	1320	1324	1348	916.6	513.1	544.3	504.9	1723
Mean error	134.5	139.1	166.9	-93.88	127.3	162.4	118	138.1
Standard Deviation	85.09	89.55	43.8	44.03	71.78	86.05	38.22	52.21

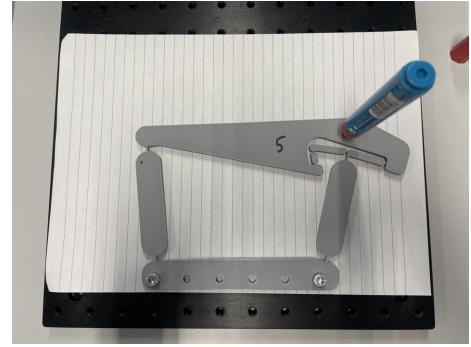


Fig. 36. A Picture showing the motion path experiment setup.

bolts as shown in fig. 36. Then, a ball-point pen is mounted in the hole located at the point of interest. This pen is dragged over the paper by the compliant mechanism during the stroke. The stroke is actuated by hand from rest until the bistable element switches over to the different path. Then it is pulled a bit further, after which the mechanism is moved back to its starting position or until the bistable element switches back. Then one cycle is complete. In total two cycles are completed for each experiment.

#### B. Force-Displacement

1) *Method:* The samples were printed using a bambulabs x1 carbon at 150 mm/s with wall speed of 75mm/s to ensure the single thickness flexures are printed as accurately as possible. The material used was polymaker PETG in grey, this material was selected as the best material available.

After printing the samples were numbered and assessed on production accuracy using a digital measurement microscope.

Next, the sample is mounted to a thorlabs breadboard such that it is not in contact with any surface. A second thorlabs breadboard with a PI linear stage with a plutek sb200 44 N force sensor is attached to the previous breadboard.

Then a wire (0.3mm copper) was attached to the load cell using a bolt. As it was predicted that the bistable element would produce a negative force over the course of its path, this wire is run over a pulley, and at the end a mass is added that has a weight greater than the largest predicted negative force.

to this wire a small clamp was added after which the force measurement of the load cell was zeroed. Then, the sample is

TABLE V  
MEASURED DIMENSIONS OF THE FLEXURE WIDTHS AND LENGTHS OF THE FULL COMPLIANT MECHANISM, ALL VALUES WITH SUBSCRIPT B INDICATE MEASUREMENTS FOR THE BISTABLE ELEMENT GIVEN IN  $[\mu\text{m}]$

sample	$fl_1$	$fl_2$	$fl_3$	$fl_4$	$fd_1$	$fd_2$	$fd_3$	$fd_4$	$fl_{1b}$	$fl_{2b}$	$fl_{3b}$	$fl_{4b}$	$fd_{1b}$	$fd_{2b}$	$fd_{3b}$	$fd_{4b}$
1	3912	3977	3932	3978	1214	1230	1220	1225	1249	1245	1368	1045	478	532	472	1701
2	3984	4024	3908	4043	1246	1250	1192	1220	1304	1305	1364	957	471	496	465	1703
3	3927	3869	3851	4015	1297	1323	1262	1248	1402	1390	1372	958	451	455	455	1651
4	4001	4038	3883	4039	1278	1287	1235	1233	1446	1311	1352	949	443	432	449	1636
5	3976	4010	3873	4043	1269	1277	1244	1231	1427	1343	1317	951	453	474	439	1625
Control	4000	4000	4000	4000	1200	1200	1200	1200	1200	1200	1200	1000	400	400	400	1600
Mean	3960	3984	3889	4024	1261	1273	1231	1231	1366	1319	1355	972	459.2	477.8	456	1663
Mean error	-40	-16.4	-110.6	23.6	60.8	73.4	30.6	31.4	165.6	118.8	154.6	-28	59.2	77.8	56	63.2
Standard Deviation	38.43	67.94	31.41	28.03	31.95	35.67	26.4	10.6	85.07	53.27	22.31	40.99	14.67	38.41	13	36.61

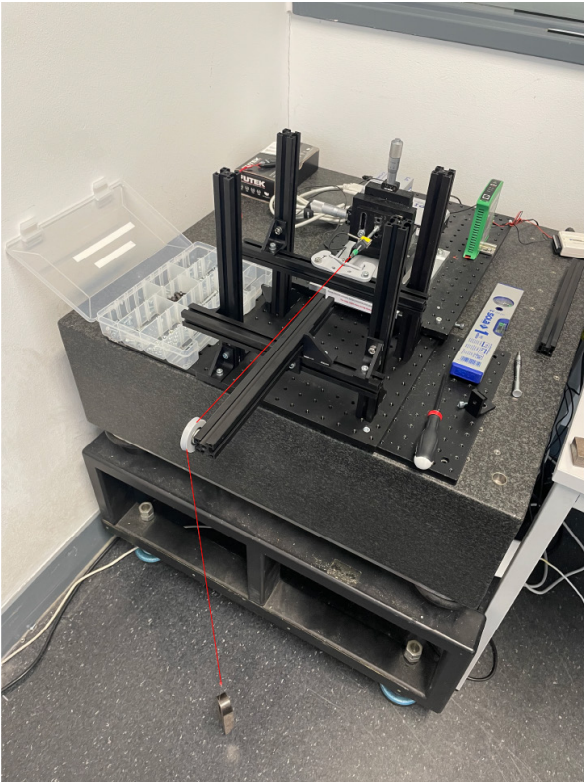


Fig. 37. A picture of the overview of the force-displacement experiment.

slid over the small clamp. To which it is then attached using a small bolt.

Because during the attachment of the compliant mechanism to the wire, the compliant mechanism is most likely preloaded. The next step is to move the linear stage to a point where the load cell again reads 0 N.

Next, the location of the stage is zeroed, and the sample is displaced. In the case of the bistable mechanism displacement is 1mm in the negative direction and 9mm in the positive direction, and in the case of the four bar mechanism displacement is 25 mm in the positive direction.

The last step is repeated until five cycles have been completed.

## VIII. DATA PROCESSING

When the experiment was completed, the data obtained had to be processed for visualisation, and implementation into the Matlab model.

In fig. 39a the data obtained from one of the force-distance experiments is shown. Although the general behaviour of the system is apparent from the graphing of the raw data, the data had to be processed to be compared to the data obtained from the models. Furthermore, to incorporate the data into the PRBM model itself, the data had to be cleaned up to ensure that the intersection algorithm could analyse the system.

### A. Force-Distance to Moment-Angle

First, the force-distance data that was obtained from the experiment had to be translated into a moment-angle relationship. This translation is based on a set of geometric relationships that allow the exerted moment and displaced angle  $\alpha_2$  to be estimated based on the force measured.

This geometry was based on three key-points which form a triangle for each timestep namely: the attachment point of the wire to the force sensor, the location of hinge one of either the bistable or four bar mechanism, and the attachment point of the wire to link B. The starting point of the attachment point to the load cell was taken as  $(0,0)$ , from where the displacement of the force cell was taken as a pure y-displacement. And assuming that the wire was perfectly parallel to the y axis at  $t = 0$ . From here, the  $(X,Y)$  coordinates of hinge two relative to the starting position of the load cell is calculated as follows:

$$P_x = l_w \cos[\epsilon_0] + l_{arm} \cos[\gamma_{B0}] \quad (61)$$

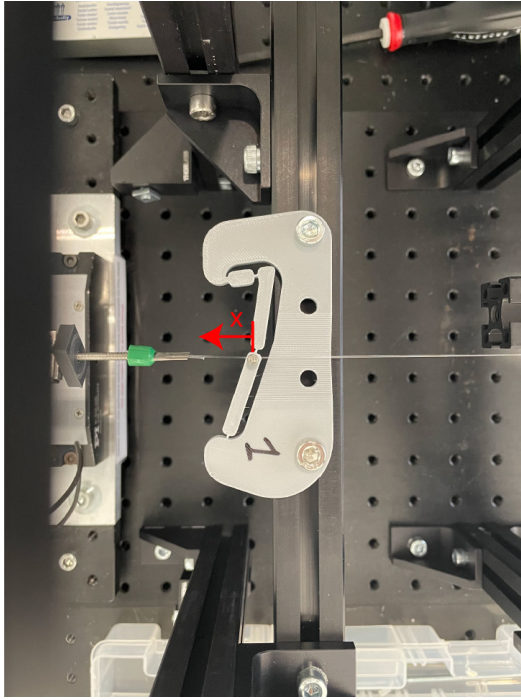
$$P_y = l_w \sin[\epsilon_0] - l_{arm} \sin[\gamma_{B0}] \quad (62)$$

From which the imaginary line segment BC can be calculated for each measurement point  $dy(t)$ :

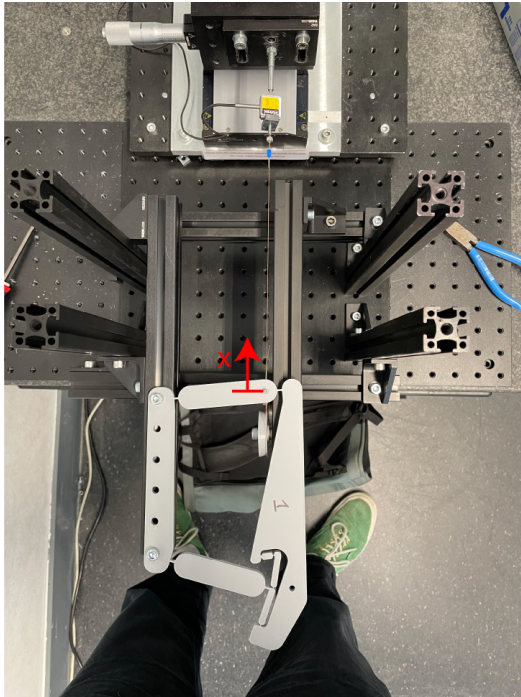
$$l_t(t) = \sqrt{P_x^2 + (P_y - dy(t))^2} \quad (63)$$

Which enables the cosine rule to be used to calculate the internal angles of the triangle, and the angle of hinge two.



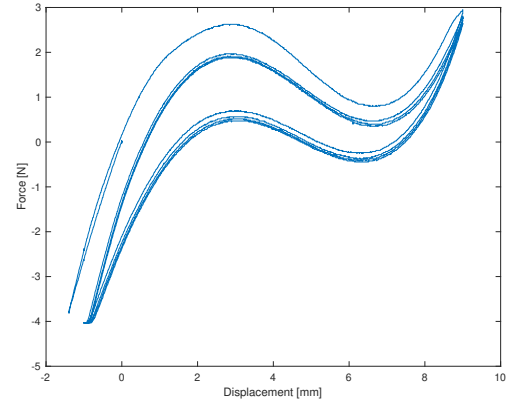


(a)

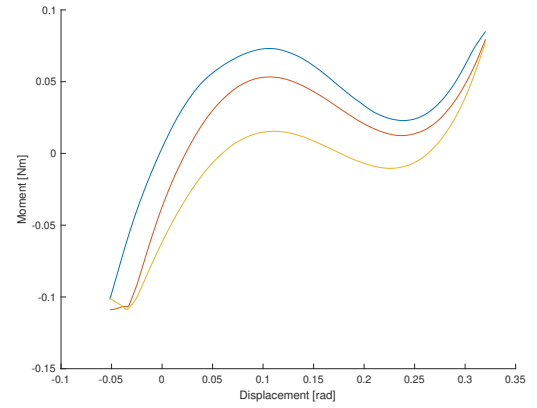


(b)

Fig. 38. Two pictures showing closeups of the bistable element (a) and the four bar mechanism (b) mounted in the testing setup. The red arrow indicates the positive pulling direction.



(a)



(b)

Fig. 39. Two plots showing the raw and processed results from the first force-distance experiment of bistable element sample five. a) shows the raw unprocessed data and b) shows the data after processing. In b) the blue line is the first forward stroke, the orange line is the forward stroke of cycles 2-N and the yellow line is the return stroke of cycles 1-N.

$$\alpha(t) = \text{acos}\left[\frac{l_w^2 + l_{arm}^2 - l_t(t)^2}{2l_{arm}l_w}\right] \quad (64)$$

$$\beta(t) = \text{acos}\left[\frac{P_x}{l_t(t)}\right] \quad (65)$$

$$\theta_B(t) = \text{acos}\left[\frac{l_{arm}^2 + l_t(t)^2 - l_w^2}{2l_t(t)l_{arm}}\right] - \beta; \quad (66)$$

Using these angles, it is possible to calculate the moment resulting from the geometry of the system. The angles can be used to calculate the effective force applied to the four bar mechanism as a result of the force measured by the load cell. The assumption here is that the load cell strictly measures the force in its y direction. From here the assumption is made that the deflection of the wire from vertical can be neglected  $\epsilon \approx \frac{\pi}{2} [\text{rad}]$ .

The effective force  $F_{EM}$  on link B is obtained by multiplying the measured force  $F_m$  with the sine of  $\alpha$ .

$$F_{EM} = F_m * \sin[\alpha] \quad (67)$$

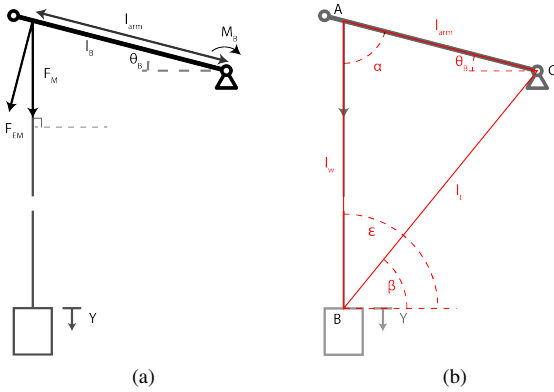


Fig. 40. Two diagrams showing an overview of the relevant angles, forces and moments for the conversion of Force-Distance to Moment-Angle. a) shows the relevant forces and moments, and b) shows the trigonometry used to obtain the relevant angles.

This effective force is then used to calculate the reaction moment.

$$M_B = l_{arm} * F_{EM} \quad (68)$$

### B. Data smoothing and interpolation

Using the previous calculations, the moment-displacement behaviour of the system can be obtained. Next, to ensure the experiment results can be implemented into the existing model, the data had to be smoothed. For this it was relevant to distinguish the different parts of the measurements. Namely the first forward stroke, the return strokes 1-N and the forward strokes 2-N. These strokes had to be extrapolated from the data because smoothing the entire dataset would result in one line. This one line does not represent the measured behaviour accurately and thus would make it impossible to use. The data was separated into three datasets by numerically differentiating the displacement measurement data, and taking all positive values as forward strokes, and all negative values as return strokes. To separate the first return stroke a second derivative was taken to find the index of the end of the first forward stroke. This is possible because the acceleration peaks at the start and end of each stroke. Next, the data points of the first forward stroke, the forward strokes 2-N and the return strokes 1-N were sorted by location. By doing this the data was transformed from a strict force-distance plot to a scatterplot of the force-distance relationship for each stroke. These three plots could then be smoothed using the smooth function in Matlab with the settings [25]:

- 1) span = 5%
- 2) method = rlowess

Using 'rloess' means that the function attempts to fit a 1st order polynomial to determine the location of the current data point. The 1st order polynomial is obtained from 5 percent of the total data set around each of the data points. This way, the effect of the discrete stepping that was observed in the measured data is removed without losing too much fidelity in the data.

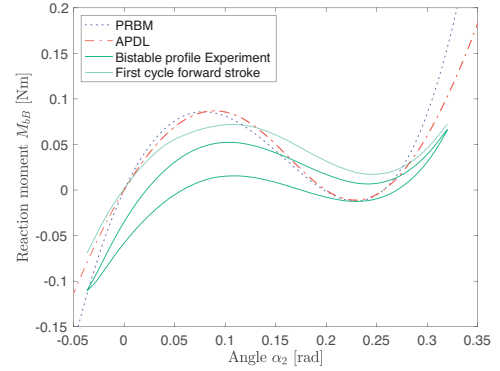


Fig. 41. A plot showing the force-displacement profile of the bistable mechanism. The green lines show the measured results, and the blue dotted and orange dot dashed lines show the results from PRBM and APDL respectively. The first forward stroke of the bistable element is less saturated.

The function smooth smoothes the datapoints for each point. In this specific set of data that means that some distance datapoints will contain multiple force information points, which after smoothing are the same. Although this is no problem for visualisation, this is less than ideal for the implementation into the model. To finalise the data processing, all duplicate datapoints are removed, and the data is interpolated to space the datapoints out equally over the measured distance.

This processing produces the lines that are shown in fig. 39b.

## IX. RESULTS

### A. Moment-Displacement Results

The results obtained from the moment-displacement experiments indicate that the predictions from PRBM and Ansys APDL correspond with the measured results. In fig. 42 one can observe that the models give a good prediction of the compliant mechanism stiffness. However regarding the bistable element the measurements correspond less with the predictions from the models. The expectation is that this is due to the production technique and material properties of PETG. Furthermore, a hysteresis loop was measured for the bistable element. Interestingly, this enhances the behaviour of the mechanism, because the crossover angle on the return stroke would happen later relative to the forward stroke than when no hysteresis is present. As a result the area that is described by the output of the mechanism is larger.

TABLE VI  
THE CROSSOVER ANGLE  $\theta_B$  PREDICTION ERROR OF THE PRBM AS A PERCENTAGE OF THE SWEEPED ANGLE  $\theta_B = 0.49[rad]$ .

	PRBM Cyc 1	PRBM Forward	PRBM Return
EXP1	3.84	12.21	4.31
EXP2	7.92	17.85	6.23
EXP3	13.7	16.47	8.71

### B. Path Results

From fig. 43 it is visible that the prediction made by the PRBM model made in Matlab agrees with the tested compliant

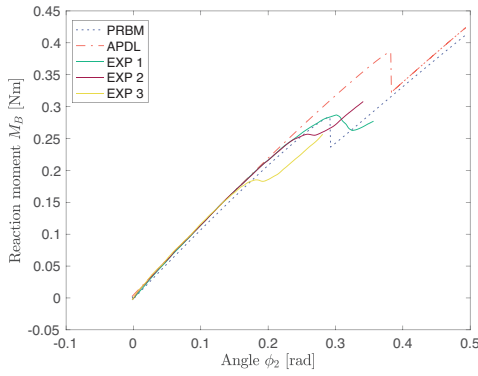


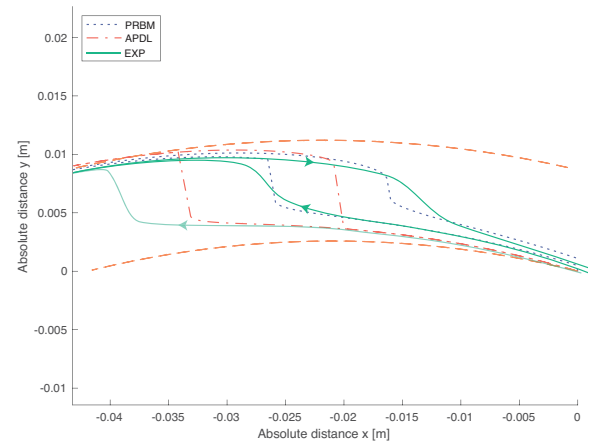
Fig. 42. A plot showing the results from the force-displacement experiments of the four-bar mechanism compared to the predictions from both the PRBM and the APDL models. The solid lines show the measured results, and the blue dotted and orange dot dashed lines show the results from PRBM and APDL respectively.

TABLE VII  
THE CROSSOVER ANGLE  $\theta_B$  ERROR AS A PERCENTAGE OF THE SWEEPED ANGLE  $\theta_B = 0.49[\text{rad}]$  AS PREDICTED BY THE PRBM WITH EXPERIMENT DATA IMPLEMENTED.

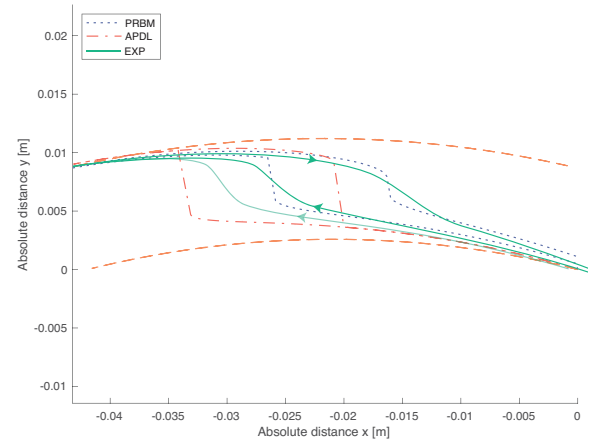
	EXP Bi Cyc 1	EXP Bi Forward	EXP Bi Return
EXP1	5.74	3.25	2.37
EXP2	6.02	2.39	4.29
EXP3	15.6	1.01	6.77

mechanism mechanism behaviour. In previous sections it was found that the stiffness of the bistable mechanism is determinative for the switchover angle of the full mechanism. In fig. 43 the two predictions obtained from PRBM are included to show to what degree the experiment results agree with the model prediction.

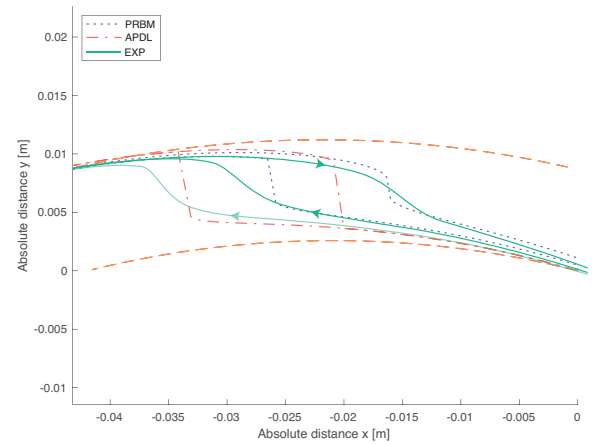
In the motion experiment results in fig. 43 one can see that the prototypes actuated earlier than predicted by the models on the forward stroke and tended to actuate later than predicted on the return stroke. This can be explained when looking at the measured force-displacement graph of the bistable element in fig. 41. In this graph one can see that the first peak of the bistable element on the forward stroke is less stiff than predicted, and on the return stroke the peak is stiffer than predicted. Combining this with fig. 33, this does provide an explanation for the difference between the model and the physical model. This is further supported by the results of the model when incorporating the experimental data into the PRBM. This can be seen in table VII, which shows the prediction error of the model with the experiment data incorporated. When comparing this to the prediction error of the fully PRBM model shown in table VI, one can see that including the experimental data does improve the model prediction. The percentages in table VI are taken as percentage of the actuation distance of the model, which is 0,49 rad. However, the prediction of the forward stroke suffers from this change. It is expected that this might be due to production variations, as one can see from fig. 43 the variation in crossover angle  $\theta_B$  of this first stroke is quite high between the samples. Whereas, the variation in crossover angle  $\theta_B$  for the latter forward and return strokes is



(a)



(b)



(c)

Fig. 43. Three plots showing the results of the path experiment. The dotted blue and dot-dashed orange lines represent the PRBM and Ansys APDL models respectively. The solid green lines show the measured paths, from each experiment the forward stroke of cycle one is shown in a less saturated green. a) shows the results for path experiment 1, b) shows the results for path experiment 2 and c) shows the results for path experiment 3.

lower.

From the experiments it is found that the forward crossover angle changes significantly after the first cycle. On this first cycle, the stiffness of the mechanism seems to follow

predictions relatively well. But from the second cycle it seems like the relative stiffness of the bistable element becomes significantly smaller. This corresponds with the measurement shown in fig. 41.

From the obtained results the observation may be made that the mechanism does exhibit the expected behaviour, however the crossover angles do not match predictions. The expectation is that this difference might be due to a set of variables:

- 1) Production irregularities
- 2) Creep in the material
- 3) Viscosity of the material

From fig. 33, the conclusion was drawn that the mechanism is sensitive to a variation of relative stiffness between the bistable element and the four bar mechanism. As such, a lack of accuracy in the production of the mechanism might result in a prediction error. To validate whether the difference observed is due to modelling methods or production methods two further experiments are performed. The force displacement of both the bistable element isolated, and the full compliant mechanism.

## X. DISCUSSION

The development of a compliant mechanism that translates motion between two axes intermittently has not been successfully developed. This was not accomplished due to the design challenge posed by the requirement set of the theoretical mechanism. Instead, during the development, the conclusion was drawn that a compliant mechanism that was able to translate a reversible reciprocating path to a path emulating a full cycle path would be necessary as a first step to the aforementioned intermittent motion mechanism. This type of compliant mechanism was too found not to exist and as such would need to be designed. As such, a four-bar mechanism which translates a reciprocating path into a history dependent area describing path has been successfully designed, modelled and tested. The results from the experiments indicate that the mechanism works and behaves as expected, and that the models developed in Matlab and APDL are reasonable predictors of real world behaviour.

The design process was set up as a standard design process, making use of a problem statement, functions, function solutions and a resulting design. Due to the nature of the problem statement, it was found during the development of function solutions that the required mechanisms to develop the necessary actuation mechanisms within the context of the problem statement did not exist. This was because the input was taken to be a reversible oscillation, and the required output would behave similar to a full-cycle locomotion mechanism. To solve this a new sub-design process was set up for the development of a compliant mechanism that could perform this translation. Because this new design problem was set up, the greater design problem was not solved with an ideal mechanism so this is something that can be researched further.

The two models that have been developed show good agreement. However, they do not fully agree with one another on the crossover angle  $\theta_B$ . This is likely due to a difference in freedom that the APDL model allows for in relation to the

PRBM. The PRBM is quite rigid in its kinematics because the joints and links can not deform or move, whereas the APDL model represents a physical model more accurately. The flexures are capable of taking on more complex shapes, and the links are able to bend. Where exactly the discrepancy originates is unknown, however it is expected to be correlated with the aforementioned rigidity of the PRBM.

On the other hand the PRBM model is significantly faster than the APDL model. Currently it has been implemented in Matlab, and it is able to calculate the behaviour of the system in a time-frame around 0.9 seconds for one run with 1000 timesteps. This is significantly faster than the APDL simulation which requires 3 seconds for a run with 200 timesteps.

The results from the experiments do not fully align with the predictions from the models. This is likely due to production and material issues. Regarding the difference in samples and the models, based on the optical measurements presented in tables IV and V the expectation was that the mechanisms would behave stiffer than the predictions. However, this was not the case in the measurements. This difference in stiffness expectation and reality is likely due to the production imperfections resulting from 3D printing. Things that might affect the difference to expected stiffness are things such as the layering of the prototype, the models are based on an isotropic material assumption.

Aside from production problems, the method of production itself determined the geometry of the system, limiting the design to a sub-optimal system. This problem mainly presents itself in the design of the bistable element, which is designed such that it can be 3D printed, but that it also can be modelled using the assumptions of PRBM. This last requirement could not be fully fulfilled, as the stiffness of bar four was too low compared with the stiffness of axle four. As a result, additional relations were added to adjust for the effect of the stiffness of bar four. Ideally this would not be necessary, for instance by using a different production method which is able to either produce larger parts with the same minimum feature size, or to produce parts with a smaller minimum feature size. This would allow a designer to more optimally design a bistable element, which can be modelled using PRBM. Another option is to only model the mechanism using APDL or another FEM analysis tool, as that would increase the possibilities in bistable element design. Additionally the produced prototypes could most likely be improved by replacing the flexures with metal leaf flexures, and by changing the production method to one with stiffer material for the links.

Concerning the experiments, it is expected that the motion path experiment could be improved in accuracy. Currently, the mechanism has to deal with the dragging force of the pen over the paper and this might have an impact on the motion path that is drawn versus the motion path that might be drawn when the mechanism is free to move, such as in the models. Furthermore, the mechanism was actuated by hand, this means that the speed of the actuation is not known as well as the force or consistency of actuation. All of this might be improved by measuring this data again using the setup that was also used for the force-displacement experiment. When one records the mechanism from above with a camera, software could be



used to visually track the displacement of the POI, from which a motion path can be drawn. This would further reduce the amount of unknown variables. However, to do this accurately, the specific characteristics of the utilised camera should be known to correct for things such as lens distortion and the effect of perspective. And the effect of gravity may need to be accounted for in the behaviour, although this probably will not affect the mechanism greatly.

During experimentation, some problems did occur. Firstly, during the first set of attempts to measure the force-displacement behaviour of the bistable element, the only wire that was available for measure was fishing wire. This kind of wire was not stiff enough to perform the necessary experiments with. To solve this, the fishing wire was initially replaced using 0.2 mm copper wire, this wire was stiff enough in tension and compliant enough in bending to obtain good measurements of the mechanism. This type of wire did pose some challenges, it was quite difficult to clamp such that the wire did not slip without cutting the wire. This problem was solved by a bootlace to clamp the wire using a distributed clamping force over the length of this bootlace. The bootlace was cut to length to ensure it did not extend beyond the link width. However, when testing the four-bar mechanism, this wire was not stiff enough in tension which meant that again the wire had to be replaced. This time the choice was made for a 0.3 mm copper wire, this copper wire was determined to be sufficiently stiff for both mechanisms, and this was utilised to perform the experiments.

As a result the force-distance experiments could also be improved. Some pull tests were performed on the wires, and at around 10 N the wire seems to yield. Although 10 N was never reached, the measurement of the four-bar mechanism did meet a maximum force of 9 N, which is close to the yield strength. But the material that was used was the only material available. For future testing, it is recommended to utilise a different wire material and thickness to measure the system or similar systems. The challenge is to find a wire that has low bending stiffness, and does not plastically deform around the pulley that is used for the system. But that the wire is still stiff enough to carry the force exerted without plastically deforming itself.

Additionally, in the experiments the load that was put on the bistable element and the four-bar mechanism was not purely a pulling force. This was a result of how the wire was clamped to the mechanisms. Namely, a hole was extruded through link two of both mechanisms. Although this hole was parallel to the pulling direction at the  $t = 0$ , when the mechanism starts deforming it starts to force a kink in the pulling wire. This might incur a moment on the relevant link. This problem could be alleviated by attaching the pulling wire to an axis that is mounted perpendicularly through link two, this way one can ensure that the only transferred load is a force. The choice was made not to do this, as it was desired to load the samples in-plane rather than from another plane. This could be solved by attaching two wires to both sides of the link, however these wires would then need to be attached such that they carry the same load. In the end the decision was made to mount the wire through the link.

Based on the observations made during this research the

following research topics are recommended:

- 1) Designing modelling and testing the mechanism using a different fabrication method.
- 2) Researching the effect of four-bar mechanism configuration on the effectiveness of the design.
- 3) Researching the effect of implementing different bistable elements.
- 4) Investigate the effect of load on the end-effector of the mechanism.

During the research of this thesis a lot was learned. This mainly showed in the adeptness at finding information, and searching for this information before attempting to solve a problem myself.

The initial linkage would probably have had a more ideal design if more time had been spent researching linkage design before the linkage was designed. During the latter part of this research, multiple books had been found that provided useful knowledge on the design of linkages. These books had not been found earlier because only google scholar and worldcat had been used to find relevant publications. It was found out that a lot of relevant books could be found quicker by searching through the relevant section in the library.

During the modelling of the bistable element, due to tunnel vision, I had not looked for bistable mechanisms in Howell's compliant mechanisms. Partly due to not recognising the book in relevant literature on bistable mechanisms likely because many papers on compliant mechanisms cite it, and partly because I had set my mind on solving the system defined in the chapter on the bistable model. In review this modelling unnecessarily took a lot of time without bearing fruits with regards to the final model. I mainly gained a lot of knowledge on the functioning of Matlab and various methods to tackle my final model.

Aside from the bistable element, the interaction between the mechanisms also took a lot of trial and error. The effect of both the force and moment proved to be significant for the prediction of mechanism behaviour. This would have been easier to conclude if this had been investigated more methodically before starting on the development of the interaction models.

Experimentation went quite well, only the first three tested samples could not be taken as useful data as things went wrong during testing. Afterwards, the results obtained were clean and usable.

## XI. CONCLUSION

To conclude, the original objective of this design report has not been met. However, during the research performed to get to this objective, a new objective had been set. In this thesis, the design, modelling and analysis of a fully compliant path translation mechanism has been performed. The models that have been developed have a close agreement with each other as well as with the experimental results. And from this a novel compliant mechanism for the translation of a reversible reciprocating path to a path describing an area has been found. Additionally, the fundamental working principle may also be applicable in other compliant mechanisms.

## REFERENCES

- [1] J. H. 1. Bickford, *Mechanisms for intermittent motion*. English. New York: Industrial Press, 1972, Section: viii, 264 pages illustrations 26 cm, ISBN: 0-8311-1091-0.
- [2] K. J. Waldron, G. L. Kinzel, and S. K. Agrawal, *Kinematics, Dynamics, and Design of Machinery*, en. John Wiley & Sons, Apr. 2016, Google-Books-ID: vRqJCgAAQBAJ, ISBN: 978-1-118-93328-2.
- [3] B. Ciechanowski, *Mechanical Watch – Bartosz Ciechanowski*, en, Blog, May 2022. [Online]. Available: <https://ciechanow.ski/mechanical-watch/> (visited on 02/17/2023).
- [4] T. C. o. t. V. d. Joux, *The Theory of Horology*, en. Swiss Federation of Technical Colleges, 2015, Google-Books-ID: csNnzQEACAAJ, ISBN: 978-2-940025-49-7.
- [5] H. C. Kelly, *A Practical Course in Horology*, en. Manual arts Press, 1944.
- [6] V. Kharzhevskiy, M. Pashechko, O. Tatsenko, M. Marchenko, and P. Nosko, “The Synthesis of Dwell Mechanisms on the Basis of Straight-Line Linkages with Fivefold Interpolation Nodes,” English, *Advances in Science and Technology Research Journal*, vol. 15, no. 1, pp. 18–25, 2021, ISSN: 2299-8624. DOI: 10.12913/22998624/128817.
- [7] N. Sclater, *Mechanisms and mechanical devices source-book*, English, 5th ed. New York: McGraw-Hill Professional ; 2011, Section: 546 pages . : illustrations ; 29 cm, ISBN: 978-0-07-170442-7.
- [8] G. Figliolini and J. Angeles, “Synthesis of conjugate Geneva mechanisms with curved slots,” en, *Mechanism and Machine Theory*, vol. 37, no. 10, pp. 1043–1061, Oct. 2002, ISSN: 0094-114X. DOI: 10.1016/S0094-114X(02)00062-9. [Online]. Available: <https://www.sciencedirect.com/science/article/pii/S0094114X02000629> (visited on 06/06/2023).
- [9] V. Kharzhevskiy, “KINEMATIC SYNTHESIS OF LINKAGE MECHANISMS USING BURMESTER POINTS AT THE GIVEN DWELL DURATION OF THE OUTPUT LINK,” en, *Advances in Science and Technology Research Journal*, vol. 11, no. 2, pp. 139–145, Jun. 2017, ISSN: 2080-4075, 2299-8624. DOI: 10.12913/22998624/68465. [Online]. Available: <http://www.journalssystem.com/astrij/KINEMATIC-SYNTHESIS-OF-LINKAGE-MECHANISMS-USING-BURMESTER-POINTS-AT-THE-GIVEN-DWELL-DURATION-OF-THE-OUTPUT-LINK,68465,0,2.html> (visited on 04/20/2023).
- [10] B. Thomaszewski, S. Coros, D. Gauge, V. Megaro, E. Grinspun, and M. Gross, “Computational design of linkage-based characters,” en, *ACM Transactions on Graphics*, vol. 33, no. 4, pp. 1–9, Jul. 2014, ISSN: 0730-0301, 1557-7368. DOI: 10.1145/2601097.2601143. [Online]. Available: <https://dl.acm.org/doi/10.1145/2601097.2601143> (visited on 12/30/2023).
- [11] L. L. Howell, “Compliant Mechanisms,” en, in *21st Century Kinematics*, J. M. McCarthy, Ed., London: Springer London, 2013, pp. 189–216, ISBN: 978-1-4471-4509-7. DOI: 10.1007/978-1-4471-4510-3\_7. [Online]. Available: [http://link.springer.com/10.1007/978-1-4471-4510-3\\_7](http://link.springer.com/10.1007/978-1-4471-4510-3_7) (visited on 12/08/2022).
- [12] G. K. Ananthasuresh and S. Kota, “Designing compliant mechanisms,” English, *Mechanical Engineering*, vol. 117, no. 11, pp. 93–96, Nov. 1995, Place: New York Publisher: American Society of Mechanical Engineers. [Online]. Available: <https://www.proquest.com/magazines/designing-compliant-mechanisms/docview/2659864985/se-2?accountid=27026>.
- [13] N. Lobontiu, *Compliant mechanisms: design of flexure hinges*, en. Boca Raton: CRC Press, 2003, ISBN: 978-0-8493-1367-7.
- [14] N. D. Mankame and G. K. Ananthasuresh, “A Novel Compliant Mechanism for Converting Reciprocating Translation Into Enclosing Curved Paths,” en, *Journal of Mechanical Design*, vol. 126, no. 4, pp. 667–672, Jul. 2004, ISSN: 1050-0472, 1528-9001. DOI: 10.1115/1.1759360. [Online]. Available: <https://asmedigitalcollection.asme.org/mechanicaldesign/article/126/4/667/458721/A-Novel-Compliant-Mechanism-for-Converting> (visited on 12/23/2022).
- [15] B. D. Jensen, L. L. Howell, and L. G. Salmon, “Design of Two-Link, In-Plane, Bistable Compliant Micro-Mechanisms,” en, *Journal of Mechanical Design*, vol. 121, no. 3, pp. 416–423, Sep. 1999, ISSN: 1050-0472, 1528-9001. DOI: 10.1115/1.2829477. [Online]. Available: <https://asmedigitalcollection.asme.org/mechanicaldesign/article/121/3/416/417937/Design-of-TwoLink-InPlane-Bistable-Compliant> (visited on 12/12/2023).
- [16] Q. Han, K. Jin, G. Chen, and X. Shao, “A novel fully compliant tensural-compressural bistable mechanism,” en, *Sensors and Actuators A: Physical*, vol. 268, pp. 72–82, Dec. 2017, ISSN: 09244247. DOI: 10.1016/j.sna.2017.10.012. [Online]. Available: <https://linkinghub.elsevier.com/retrieve/pii/S0924424717307045> (visited on 12/12/2023).
- [17] S. A. Zirbel, K. A. Tolman, B. P. Trease, and L. L. Howell, “Bistable Mechanisms for Space Applications,” en, *PLOS ONE*, vol. 11, no. 12, M. S. Kellermayer, Ed., e0168218, Dec. 2016, ISSN: 1932-6203. DOI: 10.1371/journal.pone.0168218. [Online]. Available: <https://dx.plos.org/10.1371/journal.pone.0168218> (visited on 12/12/2023).
- [18] H. Y. Jeong, S.-C. An, I. C. Seo, E. Lee, S. Ha, N. Kim, and Y. C. Jun, “3D printing of twisting and rotational bistable structures with tuning elements,” en, *Scientific Reports*, vol. 9, no. 1, p. 324, Jan. 2019, Publisher: Nature Publishing Group, ISSN: 2045-2322. DOI: 10.1038/s41598-018-36936-6. [Online]. Available: <https://www.nature.com/articles/s41598-018-36936-6> (visited on 04/16/2024).
- [19] R. Luharuka and P. J. Hesketh, “Design of fully compliant, in-plane rotary, bistable micromechanisms for MEMS applications,” en, *Sensors and Actuators A: Physical*, vol. 134, no. 1, pp. 231–238, Feb. 2007, ISSN: 09244247. DOI: 10.1016/j.sna.2006.04.030. [Online].

- Available: <https://linkinghub.elsevier.com/retrieve/pii/S0924424706003116> (visited on 04/16/2024).
- [20] B. D. Jensen and L. L. Howell, "Identification of Compliant Pseudo-Rigid-Body Mechanism Configurations Resulting in Bistable Behavior," en, in *Volume 7B: 26th Biennial Mechanisms and Robotics Conference*, Baltimore, Maryland, USA: American Society of Mechanical Engineers, Sep. 2000, pp. 881–890, ISBN: 978-0-7918-3520-3. DOI: 10.1115/DETC2000/MECH-14147. [Online]. Available: <https://asmedigitalcollection.asme.org/IDETC-CIE/proceedings/IDETC-CIE2000/35203/881/1093841> (visited on 04/16/2024).
- [21] L. L. Howell, *Compliant Mechanisms*, en. John Wiley & Sons, Aug. 2001, Google-Books-ID: tiiSOuhsIfgC, ISBN: 978-0-471-38478-6.
- [22] P. Zhang and C. Yang, "A theoretical proof of the invalidity of dynamic relaxation arc-length method for snap-back problems," en, *Computational Mechanics*, vol. 69, no. 1, pp. 335–344, Jan. 2022, ISSN: 0178-7675, 1432-0924. DOI: 10.1007/s00466-021-02071-9. [Online]. Available: <https://link.springer.com/10.1007/s00466-021-02071-9> (visited on 05/08/2024).
- [23] C. P. Tang, "Lagrangian Dynamic Formulation of a Four-Bar Mechanism with Minimal Coordinates," en, Mar. 2006.
- [24] H. Soemers 1957-, *Design principles : for precision mechanisms*, English. [Plaats van uitgave niet vastgesteld]: Herman Soemers, 2017, Section: 276 pagina's : illustraties; tabellen ; 25 cm., ISBN: 978-90-365-3103-0.
- [25] *Smooth response data - MATLAB smooth - MathWorks Benelux*. [Online]. Available: <https://nl.mathworks.com/help/curvefit/smooth.html> (visited on 05/11/2024).

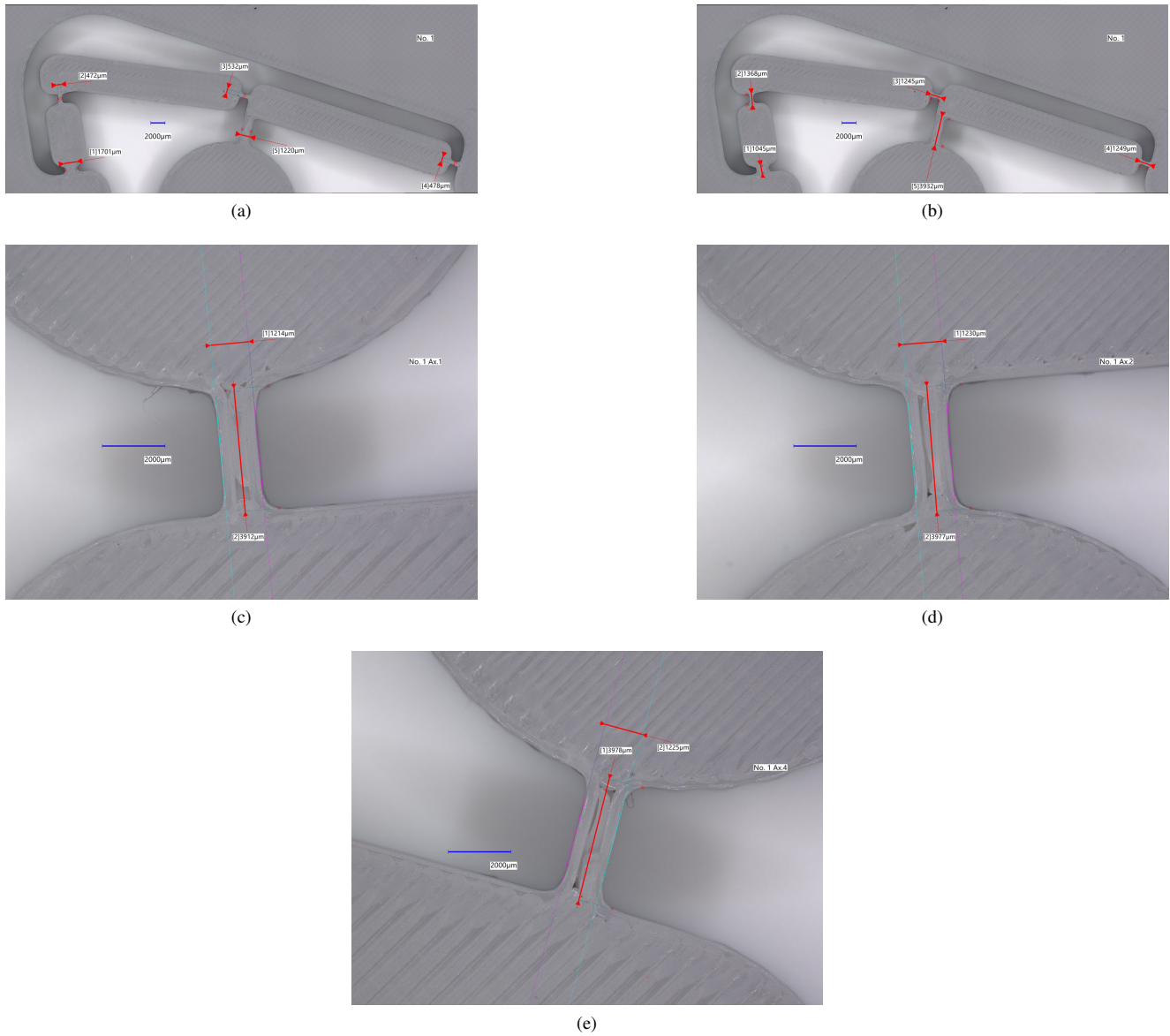


Fig. 44. Five figures showing the optical measurements made of compliant mechanism number 1.



Fig. 45. Measurements of bistable element sample number 1 made using an optical microscope

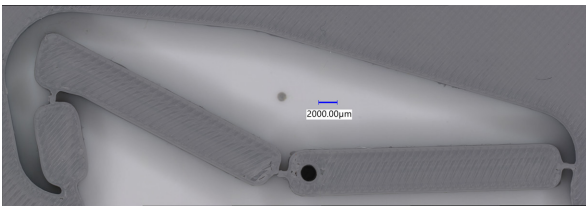


Fig. 46. Closeup of the bistable element showing failure in flexure three.

# A Review of Existing Intermittent Motion Mechanisms and Their Compliant Counterparts.

Michiel den Daas

**Abstract**—Intermittent motion mechanisms are prevalent mechanisms which provide motion in machines found in everyday life. Traditional intermittent motion mechanisms have been thoroughly developed, however with increasing knowledge in compliant mechanisms improvements might be found. To find areas for improvement, the landscape of intermittent motion was explored and categorised into six categories. These categories were then used to identify intermittent motion in compliant mechanisms. From this it was concluded that only three categories exist within compliant mechanisms. None of these three categories are solved in fully compliant form, as a result the solutions suffer from similar issues as the traditional mechanisms. As such, a need for further exploration and synthesis has been identified.

**Index Terms**—Intermittent motion, Dwell motion, Compliant mechanism, Ratchet, Function Generator

## I. INTRODUCTION

**I**NTERMITTENT motion mechanisms are mechanisms which produce non-continuous motion. This motion is periodic, and will be zero for a non-instant amount of time. This motion consists of two distinct periods: dwell and motion. During dwell, the output is still with respect to the input, and during motion the output moves with the input [1]. There are two types of intermittent motion: Oscillating dwell motion and Indexed motion. For oscillating dwell motion the start and end location are the same each cycle. With indexed motion, the end effector is advanced along a DOF with a set distance at the end of each cycle [2]. A daily example of a machine which contains mechanisms generating this type of motion is the wristwatch. Watches contain a clockwork which is able to turn energy stored in a torsion spring into time regulated movement of the hands on the dial [3]. The escapement regulates this conversion of energy to timed motion. But a watch can also contain other types of intermittent motion mechanisms, such as the mechanism behind date wheels. These mechanisms typically consist of around ten parts which engage to produce the desired motion [4]. These parts wear down as a result of mechanical interaction and have to be maintained to function properly [1]. This maintenance can range from oiling the mechanism to replacing worn parts [5]. Additionally, the friction between parts incur energy loss on the mechanism. As a result, a watch could run out of energy faster than intended because the mechanism is energy inefficient.

Apart from watches, many other devices also depend on intermittent motion such as: sewing machines, projectors, packing machines, presses, etc. [6]–[8]. In these devices, intermittent motion is a key component to the behaviour of the machine, generating the movement necessary for the machine to perform its task. Traditionally intermittent motion is generated using mechanisms containing higher kinematic pairs such as

gears, cams, or Geneva mechanisms. However these types of mechanisms have several undesirable side effects [1]:

- Wear
- Friction
- Play
- Impacts
- High part count

Over the last two decades, researchers have started researching linkages for their performance in the generation of intermittent motion [9]. Linkages are able to solve or mitigate some of the aforementioned side effects, such as impacts and wear. As an effect, linkages have the advantage that they are able to operate at higher speeds, as well as requiring less maintenance. But the synthesis of linkages is comparatively more difficult, due to the sensitivity of the mechanism to small variations in geometry [10]. Additionally when a linkage is scaled down, the production, assembly and maintenance of the mechanism becomes increasingly challenging [11], [12].

To overcome these issues, one could synthesise a compliant mechanism. In contrast with traditional mechanisms, compliant mechanisms are ideally not affected by friction. Furthermore, they can function without wear and fully compliant mechanisms do not require assembly, resulting in a reduced need for maintenance. These advantages stem from the basic function of compliant mechanisms, namely that the movement generated by a compliant mechanism is a result of deflection of members rather than a mechanical interaction between components [11], [13]. However no prior review on compliant mechanisms which produce intermittent motion has been found. Indicating that, the existence of compliant mechanisms emulating the behaviour of traditional intermittent motion mechanisms is not well documented. This highlights a need for further exploration in this area. To aid this exploration, the following research question has been defined:

What categories of intermittent motion mechanisms exist, and can these categories be used to identify compliant intermittent motion mechanisms?

In this article, the author will present an overview of the state of the art of intermittent motion mechanisms. To start, in the following sections the traditional mechanisms will be sorted into two categories of intermittent motion based on characteristics such as their construction, motion profile and mechanical behaviour. Following this these categories will be used to identify the found compliant intermittent motion mechanisms. From this, an overview of the state of the art of compliant intermittent motion is obtained, highlighting a gap in research. From this conclusions can be drawn and based on the obtained information, follow up research will be recommended.

## II. METHOD

The literature used in this paper was found through a combination of scopus and google scholar, search terms used to find relevant literature were: "compliant", "dwell motion", "intermittent motion", and "linkage-type". Books used were on loan from TU Delft library:

- Mechanisms and mechanical devices sourcebook by Neil Sclater [7]
- Mechanisms for intermittent motion by John H. Bickford [1]
- Classical and modern mechanisms for engineers and inventors by Preben W. Jensen [14]
- Theory of machines and mechanisms by John J. Uicker [15]
- Precision engineering: An evolutionary view by Chris Evans [16]
- Compliant mechanisms chapter by Larry Howell [11]
- A practical course in horology by Harold C. Kelly [5]

Further sources were obtained based on references contained in papers and books.

## III. MECHANICAL STATE OF THE ART

Intermittent motion is motion which has a periodic velocity, it starts and ends at a velocity of zero. This motion can take on two forms, either the position of the end effector is also periodic, or the end effector is allowed to travel infinitely along its DOF. The difference between these motions is illustrated in fig. 1. When the end effector is stationary, but the input continues movement, this is called a dwell. From this description, it follows that mechanisms which produce intermittent motion must allow the input to move while the output is constrained.

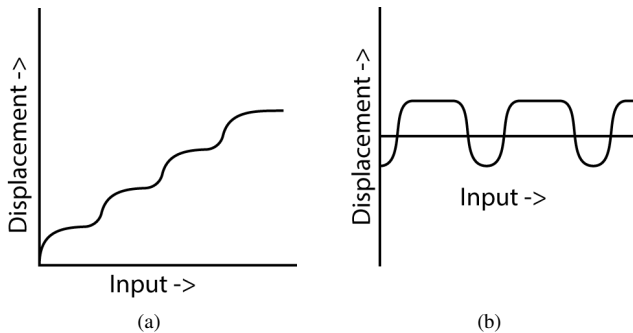


Fig. 1. Two different types of displacement profiles generated by intermittent motion mechanisms. (a) shows the motion profile produced by Indexing mechanisms and (b) shows the motion profile produced by a single-dwell oscillating dwell mechanism

Because new developments in traditional mechanisms are rare, the following chapter is mainly based on information compiled from books by: Bickford, Sclater, Jensen and Uicker [1], [7], [14], [15]. Based on the information obtained from these books, the following categories of intermittent motion mechanisms were identified:

- 1) Ratchets
- 2) Cams

- 3) Geneva mechanisms
- 4) Gears
- 5) Escapements
- 6) Linkages
- 7) Clutch and brake systems
- 8) Stepping motors

From this list clutch and brake systems, and stepping motors will not be taken into account. Clutch and brake systems, and stepping motors do not inherently produce intermittent motion. Instead, these mechanisms depend on control to produce the required motion.

One should note that a finished system might contain a combination of these categories to generate the intended motion curves. As mentioned before, intermittent motion can be categorised into two types. First, indexing mechanisms will be discussed and second oscillating dwell mechanisms will be discussed. This chapter will focus on the fundamentals of these mechanisms, this includes function, behaviour, wear, and energy losses.

Furthermore, for clarity the images of the mechanisms in the rest of the paper are coloured. The *input* of the mechanisms is made **pink**, the *output* is made **yellow**, and if a *locking* part or surface is present this is made **green**.

### A. Indexing mechanisms

In this report, an indexing mechanism is defined as follows: An indexing mechanism is an intermittent motion mechanism which provides an infinite motion along one axis, along this axis the mechanism can accurately position its end effector at certain indices [2]. At these indices, the output velocity is zero. In some mechanisms, the output is also locked in place by a locking mechanism, for instance in a geneva wheel. This behaviour results in a displacement graph which is stair-like (see fig. 1), and a velocity graph which oscillates around a point which is not zero.

1) *Ratchet and detent mechanisms*: Ratchets, shown in fig. 2, are one of the more common indexing mechanisms. An early use for ratchets was to obtain mechanical advantage, like pulling back the string of a crossbow. During the industrial revolution this changed, ratchets came into use to provide intermittent motion [1]. Generally ratchets are used to lock two axes relative to each-other. Furthermore, ratchets can ensure that torque/motion is only transferred in one direction and that a part can only travel a DOF in one direction. The amount of indices of a ratchet is dependent on a few factors:

- Ratchet wheel diameter and width
- Force requirements
- Production methods
- Material

Ratchets generally deal with harsh mechanical interactions, every time the pawl jumps over to the next index position this is paired with an impact. As a result, the mechanism might wear relatively quickly as a consequence of the impact forces which are applied to the wheel and pawl. To mitigate this wear a designer might consider balancing pawl spring stiffness, height of the ratchet teeth or teeth and pawl geometry.



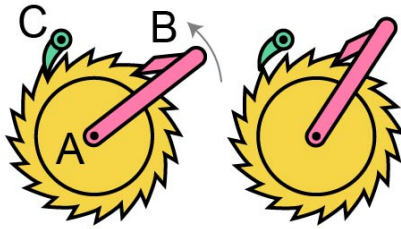


Fig. 2. A ratcheting mechanism (adapted from [7, Fig.22 p.10]). A. The ratchet wheel B. The driving pin C. The pawl.

However, these impacts will never reduce to zero without fundamentally changing the design of the ratchet, or adding parts to the existing mechanism. Additionally, these clicks are audible making the mechanism loud. Although silent ratchets do exist, for this type, the pawl is not constantly engaged with the wheel. As a result the output shaft could slip back. Aside from the impact wear, ratchets also suffer sliding wear between the indices. When the pawl is sliding over the toothed wheel, the sliding interaction creates friction and wears down both the wheel and the pawl. This friction also results in a loss of energy between the input and the output. Furthermore, the energy stored into the pawl spring is lost every time the mechanism clicks over. This is because the energy is not returned into the mechanism, but rather it is converted into sound heat and the deformation of material.

Ratchets typically consist of a toothed wheel and a sprung pawl. This toothed wheel can be connected to a mechanism, and the pawl to fixed ground. This pawl is mounted with respect to the toothed wheel in a way that the wheel collides with the pawl such that its movement is restricted. This allows the DOF on which the ratchet is placed to be indexed.

2) *Geneva Mechanisms*: Geneva or maltese cross mechanisms can be considered a midway between gears and cams. This type of mechanism provides indexing with between three and eighteen positions per rotation [1], [7]. This mechanism is a kind of dwell mechanism, this means that when the end effector is stationary, the input remains free to rotate. When a geneva mechanism is designed well, impacts can be minimized, and almost be removed. To do this, the designer has to ensure that the driver pin enters the slot of the geneva star when the velocity vector of the pin intersects the axis of rotation of the geneva star. Theoretically the driver pin will not impact the geneva star when this is done correctly, thus resulting in a smooth motion profile. The locking functionality of a geneva mechanism is based on sliding between surfaces. This can be seen in fig. 3 which shows the geneva wheel when it starts being engaged for movement. The mechanism is formed such that the output is locked by the input axis when it is not engaged for movement. This is done by the locking cam behind the engagement pin, this cam interfaces with the circular indents in the geneva star. This axis lock is a place where a lot of

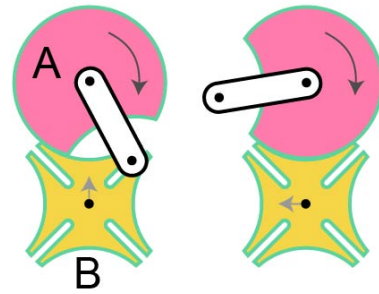


Fig. 3. A geneva wheel (adapted from [7, Fig.19 p.9]). A. The driving wheel B. The Geneva wheel.

friction can occur if torque is put on the output shaft. This friction can result in sliding wear and a loss of energy.

3) *Mutilated gears*: Gears are used to transmit torque or motion between two gears. Normally this happens with a constant input-output ratio. However, one could also design gears to transmit non-constant motion [17], [18]. There are two designs which can perform such motion: non-circular gears and mutilated gears. However, a system consisting purely of non-circular gears is not capable of producing intermittent motion, the angular speed of the output can only approach zero but will never be zero [19]. Mutilated gears are capable of producing intermittent motion in multiple ways, examples of this are shown in fig. 4.

All these solutions are capable of producing input-output behaviour similar to that of a Geneva mechanism. They generate motion whenever the teeth mesh. This results in impact forces at the interfacing of the gear teeth for each motion cycle. In each cycle, the first interaction between the input and the output gears produces a peak impact force. As well as these impact forces, friction is generated wherever two gears mesh. Also, similar to the Geneva mechanism, the gear shown in fig. 4b will experience more friction and wear when torque is exerted on the output axis.

4) *Escapements*: Similar to ratchets, escapements consist of a toothed wheel and a part designed to hold this toothed wheel. For escapements, this part is a pallet which is a specifically designed mechanical brake which regulates the rotation of the toothed wheel. In his book, Bickford describes two types of escapements: Clock escapements, and machine escapements [1, Ch. 11 & Ch. 12]). These mainly exist in the form of controlled escapements fig. 5a, runaway escapements fig. 5b and inverse escapements fig. 5c. The pallets of the escapements oscillate between positions to regulate the toothed wheel. This oscillation produces impacts between the wheel and the pallet. In the case of the runaway escapement, these impacts provide the necessary energy for the oscillation of the pallet. This means that the motion produced by the impact with one tooth rocks over the pallet to the next tooth. This slows down but does not stop the toothed wheel. This results in an inverse square relationship between the input torque and the rotation speed



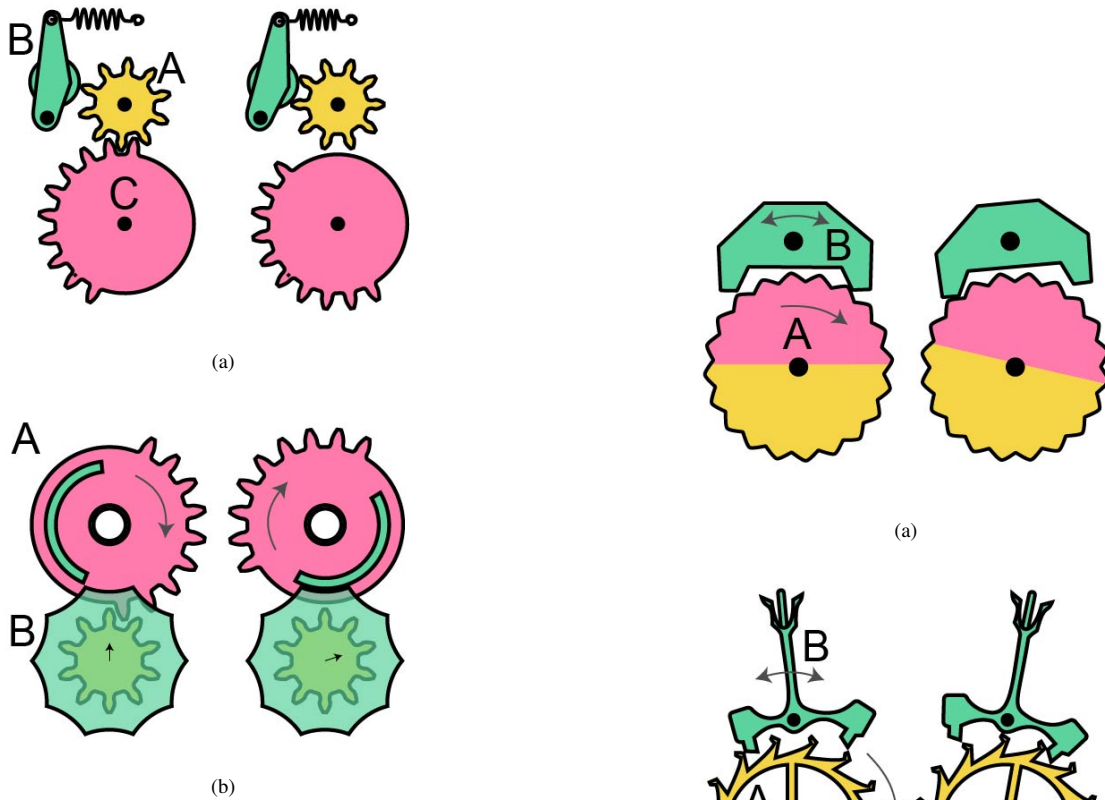


Fig. 4. Different types of mutilated gear which can transfer intermittent indexed motion. (a) shows a Mutilated gear with holding detent (adapted from [1, Fig. 10-11 p.143]). A. The driving gear B. The detent C. The driven gear. (b) shows a mutilated gear locked by a holding cam (adapted from [1, Fig. 10-10 p.143]). A. The driving gear with holding cam B. The driven gear with cam slot.

the escapement allows. In contrast, a controlled escapement uses the energy transferred from the toothed wheel to power the regulation mechanism. While the regulation mechanism is not meshing with the toothed wheel, the motion is completely stopped. In the case of a horological escapement, the torque put on the central axis provides the necessary energy to ensure the continuous oscillation of the regulation mass. This regulation mass is a weight attached to a spring which have been carefully configured to ensure a consistent frequency of oscillation. Theoretically, a controlled escapement has no relationship between input torque and the rotation speed of the output. For the inverse escapement, this is different again. For this type of escapement, the rotation of the wheel is governed by a pallet. However, this pallet does not operate on the energy provided by the input, but rather by an external input such as a solenoid.

The design of the escapement decides the amount of friction and the scale of impacts. This can be seen in fig. 5, this figure shows to kinds of escapement. The left image shows a runaway escapement, and the right image shows a clockwork escapement. A runaway may deal with higher impact loads than a controlled escapement. This results in more impact wear, whereas the controlled escapement experiences more sliding wear.

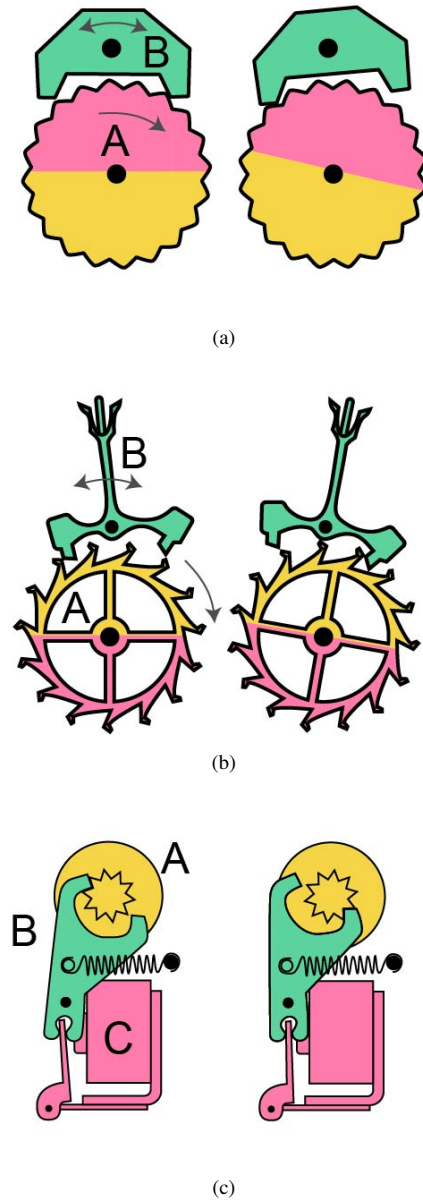


Fig. 5. Three types of escapements, a) shows a runaway or verge escapement(adapted from [1, Fig. 11-1 p.153]), b) shows a clockwork escapement developed for timekeeping (adapted from [1, Fig. 11-28 p.163]), c) shows an inverse escapement used as a counter system (adapted from [1, Fig. 12-38 p179]). In figures a) and b): A. Escapement wheel B. Pawl and in figure c) : A. Escapement wheel B. Pawl C. solenoid.

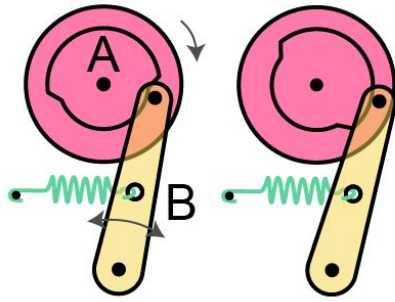


Fig. 6. Cam mechanism. A. Cam wheel B. Follower

### B. Oscillating dwell mechanisms

In this report an oscillating dwell mechanism is defined as follows: Oscillating dwell mechanisms are mechanisms of which the end effector oscillates between positions. At one or more of these positions the end effector velocity will be zero for a non-instantaneous time while the input remains in motion. These mechanisms provide an output oscillating within a limited range for an infinite input.

1) *Cams*: A common mechanism used to produce oscillating dwell motion is a cam follower mechanism, these can be used to provide a wide spectrum of motions. As shown in fig. 6, the overall construction cam systems is similar to a ratchet. However in function they are different. In a cam system, the output is the follower rather than the axle of the wheel. Another difference between cams and ratchet mechanisms is the fact that cams are used to provide a motion profile, while ratchets are used to index a mechanism and transfer torque or motion. Cams work with a shaped wheel (the cam) and a follower. This follower could be a ball bearing mounted to an arm for instance. In general, cams are rotated about an axis which means that the motion they provide is periodical and repeating once per cycle. As a result of the nature of a cam, the design process too is not too difficult. For this one could work by designing a displacement profile the follower should produce, after which this displacement profile is translated to a radial distance for each point of the cam profile. However this also means that the amount of detail added in the profile is proportional to cam diameter and engineering capabilities, which means that depending on the desired scale of the cam it might be difficult to obtain the desired motion profiles. Another thing to note is the fact that in design a cam might become an optimisation problem. This is because the follower might disengage from the cam depending on slope of the motion profile, the rotation speed of the cam and the stiffness of the follower spring. One could solve this by making the follower spring stiffer, however this could cause the friction forces to increase.

2) *Linkage Mechanisms*: Over the last two decades, development of linkage type intermittent motion mechanisms has increased. The intermittent motion produced by a purely

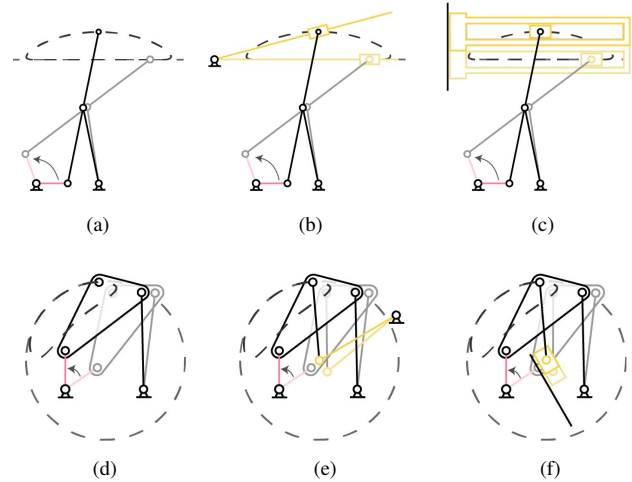


Fig. 7. Two types of linkage-type oscillating dwell mechanisms (adapted from [20, Fig. 1]). a) and d) show two types of four bar mechanisms, a) is a straight line generator and b) is a circle-arc approximator. Based on these mechanisms, intermittent motion can be generated, to do this a dyad is added to the linkage. b), c), e), and f) show examples of the resulting six-bar intermittent motion mechanisms. b) shows a linkage with a RPR dyad, c) shows a linkage with a RPP dyad, e) shows a linkage with a RRR dyad (stephenson III), f) Shows a linkage with a RRP dyad.

linkage based mechanism is limited to dwell motion. This motion is generally produced by linkages in one of two ways. The synthesis of linkage type dwell motion mechanisms was generalised by Kota et al. The methods Kota describes are based on either a mechanism tracing a part of a circle arc, or a mechanism that generates straight line motion [21], [22]. These mechanisms depend on an additional dyad to provide the dwell motion. This linkage is added such that the central joint of the dyad coincides with the centre of motion during the circular or the straight line part of motion. This two bar motion is connected as shown in figs. 7b, 7c, 7e and 7f. One of the links of this added dyad will be motionless when the four bar linkage produces this straight line or circular motion. Depending on what type of linkage the dwell mechanism is based, the required additional two-bar linkage is different. Namely in the case of straight line motion the two-bar linkage is either a RPR or a RPP dyad. In the case of the linkage based on a circle arc, the two-bar linkage is either a RRR or a RRP linkage .

Sanchez-Marin et al. follow up on this research, in this paper they perform a global search for high quality six-bar dwell linkages [20]. For this search, the linkages shown in fig. 7 were divided into the two aforementioned categories, straight line or circular motion, a dyad is then added to produce the output dwell. In order to perform the local search, an optimisation strategy was set up. The performance criteria were based on the relative dimensions of the mechanism and the quality/length of dwell produced relative to the input crank. For the global search, the researchers defined a genetic optimisation approach. This genetic optimisation was subject to the same performance criteria as the local optimisation.

Kharzhevskiy describes how dwell motion is used in industry to provide the necessary motion for certain operation such as laying thread in a raschel machine. Kharzhevskiy mentions

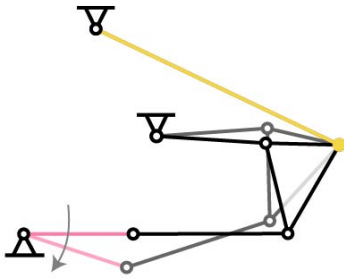


Fig. 8. The six bar dwell mechanism based on a Stephenson III linkage as described by Čavić et al. in [23].

the difference between traditional intermittent mechanisms, and linkages based on their kinematic interaction. Namely linkages contain lower kinematic pairs, whereas the aforementioned mechanisms contain higher kinematic pairs. For lower kinematic pairs the interaction between two rigid bodies is determined by a surface rather than a point or a line. As a result, the local stresses in the interaction sites are lower for lower kinematic pairs. Thus mechanisms based on lower kinematic pairs will suffer less wear than a higher kinematic pair [6], [9].

Čavić et al. [23] describe the synthesis of a linkage-type dwell mechanism based on a Stephenson III mechanism shown in fig. 8. This method is significantly different to the mechanisms described by [24] in the fact that the input is in the two-bar part of the mechanism, rather than the four-bar part. For synthesis, the Stephenson III linkage is considered in its extreme positions. These can be achieved when the angle between input links is either  $0^\circ$  or  $180^\circ$  [25], this is also known as a singularity point. To further aid synthesis the authors divided the linkage into three modules connected to the ground joints defined such that the output link will produce dwell. These modules were then synthesised apart from each other in order of solvability to generate a final linkage design.

For the analysis of linkage mechanisms, Figliolini et al. posit that the effects of jerk and jounce are overlooked when regarding the behaviour of a mechanism [26]. Although this is minded more in the design of cam and Geneva mechanisms. It can also provide vital information in the design of linkages. To mitigate this gap, Figliolini et al. characterised the kinematics of 6 bar dwell mechanisms analytically to analyse the jerk and jounce behaviour of these linkages.

Implementing differential evolution and the Geometric Centroid of Precision Positions (GCPP) technique, Shiakolas et al. present a method of synthesis of six-bar linkages for dwell motion [27]. To obtain the six-bar linkage, these methods of synthesis were combined. GCPP was used to provide an initial population for the evolution algorithm, after which the evolution algorithm was applied until convergence criteria were met.

To find existing straight line linkages, Baskar et al. used optimisation methods and a genetic algorithm to generate an atlas of all straight line four-bar mechanisms [28]. This atlas describes nine groups of four-bar mechanisms which are able

to produce this straight-line motion.

The generation of a four bar linkage based on a desired path output is described by Varedi-Koulai and Rezagholizadeh [29], this method uses a predetermined connecting rod. A main benefit of this method is that the coupler can be chosen by the user rather than being determined through the algorithm. The methods propose are either applied graphically or mathematically, and can return a mechanism for a path with or without prescribed timing.

A five-bar linkage based step mechanism has been synthesised by Corves et al. [30], producing indexing motion around a point. Since the five-bar linkage had two DOF for its end effector, the motion of the links is constrained by a geared connection between the two input links. As a result, the mechanism is able to produce stepped motion around a point. Considering the definition used in this paper, this mechanism is an indexing mechanism rather than a dwell mechanism. This is due to the fact that the linkage produces intermittent motion around a point, and thus can produce infinite travel along one DOF with a stepped profile.

The traditional mechanisms have existed for a while, as a result not that much fundamental development has happened in recent years. The narrative posed by Bickford, is similar to that in the book by Sclater. Even though the books are separated by almost forty years. In contrast linkages have had significant development during recent years, and are being researched due to their advantages over other traditional intermittent motion mechanisms.

#### IV. COMPLIANT STATE OF THE ART

Having categorised the state of the art of traditional intermittent mechanisms, the following step is to explore compliant intermittent motion. When the field of compliant intermittent motion has been surveyed, the compliant mechanisms can be identified based on the categories obtained with the traditional mechanisms. A table summarising the categories, and their characteristics can be found in section V. In appendix A, a figure can be found which shows the categories visually. This figure shows the aforementioned mechanisms, as well as compliant mechanisms (encircled with dark grey border) in the corresponding categories. This chapter will discuss the research performed into compliant intermittent motion mechanisms. Similar to section III, the mechanisms have been divided into indexing mechanisms and dwell mechanisms. With the further subdivision into the different categories of dwell and indexing mechanisms. However, within the body of literature pertaining to compliant intermittent motion, not all categories of intermittent motion mechanisms were identified. Namely, only ratchets, escapements and linkages have been found in compliant or partially compliant form.

##### A. Compliant indexing mechanisms

1) *Compliant ratchets*: Kennedy et al. developed a compliant ratcheting mechanism for military applications [31]. The main aim of this system was to provide reliable arming and safety

functions. The system performed within specifications, even surpassing them. The ratcheting is performed by a compliant double leaf linear stage with a leaf flexure extending to the ratchet wheel, with another flexure ensuring the ratchet wheel remains at an index between actuation. This system however still relies on traditional interactions between the driving pawl, the holding pawl and the ratchet. Furthermore, the driving pawl is a contact aided distributed compliant part. This part rubs against the pin which causes the pinch point visible in fig. 9. These are all non-ideal compared to what is possible with compliant mechanisms.

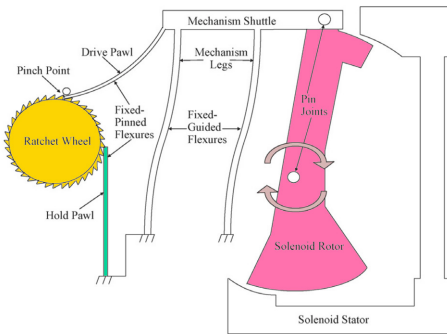


Fig. 9. CHEQR Compliant ratchet adapted from [31]

A multimaterial ratchet was developed by Sakhaei et al. This mechanism operates based on the flexibility of the tooth attachment [32]. The device replaces the spring in a ratchet-pawl mechanism with a semi compliant tooth. When meshed, these teeth can provide ratchet-like locking behaviour in linear mechanisms. Similar to the device developed by Kennedy et al., this multimaterial ratchet still contains friction interactions which are similar to traditional ratchets. However, this solution provides an improvement in part count, reducing necessary parts to two.

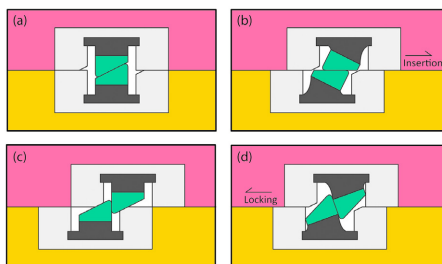


Fig. 10. Multimaterial ratchet adapted from [32]

In a different fashion, Hartmann synthesised a compliant part which can replace the pawl engaging with the ratchet wheel [33]. This compliant pawl operates based on an offset between two axes which attach to a solid ground, due to this offset, the pawl stores elastic potential energy upon displacement. This application is beneficial over normal pawl constructions due to the reduction in parts, this means that the mechanism is more suitable for small scales and will require less maintenance.

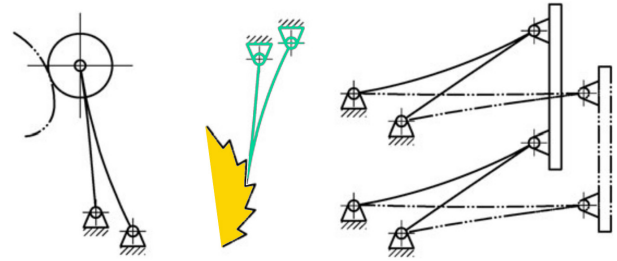


Fig. 11. Rocker arm ratchet adapted from [33]

Roach and Howell synthesised a compliant clutch design based on existing designs [34]. This was done by evaluating existing overrunning clutches based on whether they could be recreated using compliant parts. From this they determined ratchet based clutches were most appropriate to develop in compliant form. The resulting ratchet designs can be seen in fig. 21. One can observe that similar to aforementioned ratchets, the friction interactions present in traditional ratchets can still be found in these compliant clutches.

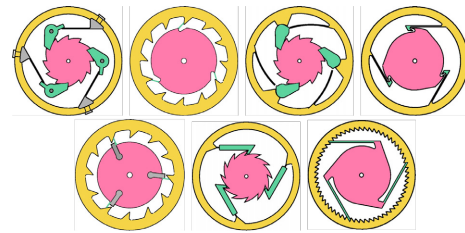


Fig. 12. Compliant clutches adapted from [34]

The patent by Minotti describes a few compliant mechanisms which are able to move along a ratcheted rail or a ratcheted wheel (provided the diameter of the wheel is large enough)[35]. To perform this actuation, the synthesised linkage is actuated by one DOF. The precise method of actuation is not described, however the author does present a fully compliant mechanism which is able to move along a ratcheted wheel or rail based on a one DOF input. The one downside of this mechanism, is that one of the locking teeth still relies on the aforementioned frictional interactions to engage with the toothed wheel.

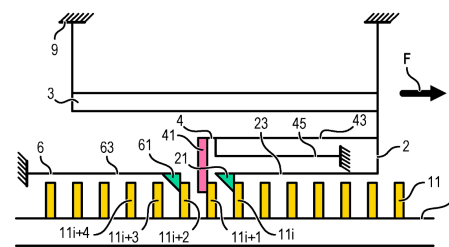


Fig. 13. Compliant ratchet adapted from [35]

Similarly in a patent by Burkhardt, a compliant MEMS driving system for a toothed wheel is described [36]. Compared with the ratcheting mechanism developed by Minotti, this mechanism has the advantage that the ratcheting action is not



driven by mechanical friction. Instead, the teeth are disengaged during actuation, after which the teeth are engaged again when the actuation cycle is stopped. To achieve this, the mechanism does not perform the movement as a result of its construction, rather as a combination of its inputs.

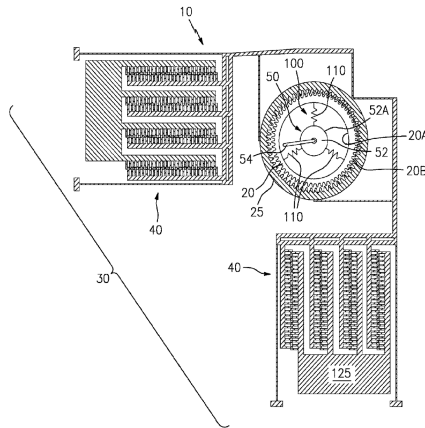


Fig. 14. 2DOF ratcheting mechanism adapted from [36]

Jensen also describes a compliant ratchet in his book [14, Fig. 15.17 p.467]. This ratchet is based on two leaf springs which aim to constrain the rotational movement of the central axis. This central axis is shaped like a square to ensure that the leaf springs are able to exert a moment around the central point of the axis, thus locking the axis in place.

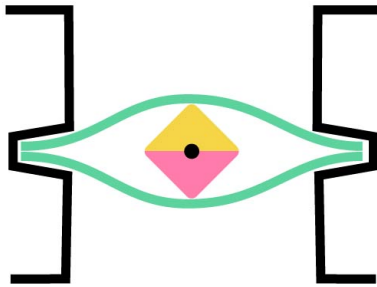


Fig. 15. Partially compliant ratchet proposed by Jensen in his book. [14]

2) *Compliant escapement*: In 2010, Gunten et al. developed a partially compliant escapement. This escapement was one of the first implementations of silicon in a watch mechanism [37]. The compliant part replaced the pallet fork assembly with one part, however the rest of the escapement was still traditional. Later Gunten et al. developed an oscillator which was fully compliant. Combining these two compliant meant that the amount of parts in the escapement could be reduced. However, its disadvantage was the fact that the oscillator was not planar, but rather made up of multiple cooperating layers, thus it required assembly [38]. In the same year, Semon et al. developed a fully compliant planar oscillator for a watch escapement [39]. This oscillator can resonate at fifteen Hz to

produce the required timed discharge of the watch mechanism. One disadvantage of this design was that the oscillator was the diameter of the entire watch face. The next year, Sybren et al. synthesised a different compliant escapement [40]. This escapement could be made the same size as a traditional oscillator. Furthermore, it was monolithic thus utilising the advantages compliant mechanisms.

## B. Compliant oscillating dwell mechanisms

1) *Compliant linkages*: Tekeş et al. studied the behaviour of parallel linear compliant guides [41]. This parallel arm guide was ideally controlled using an electromagnetic actuator which force-deflection history is known. However, for the experiment this actuator was replaced with a cam system. Through control their mechanism was able to perform dwell and indexing motion.

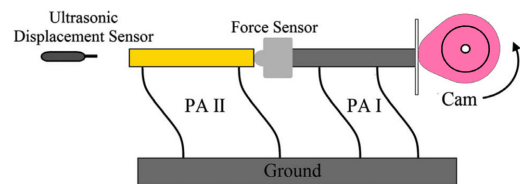


Fig. 17. Cam actuated compliant parallel linear guide setup. Adapted from [42, Fig.17]

Tekeş et al. describe the synthesis of a compliant double arm linear guide which interfaces with two gears through a bar mechanism. Using a comb drive to actuate the linear shuttle, this partially compliant intermittent motion mechanism can provide multiple dwell motion profiles based on a controlled input [41].

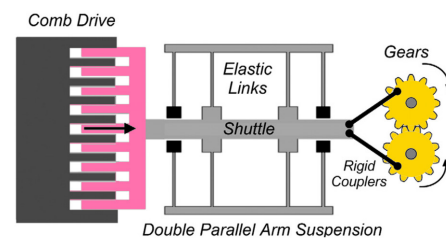
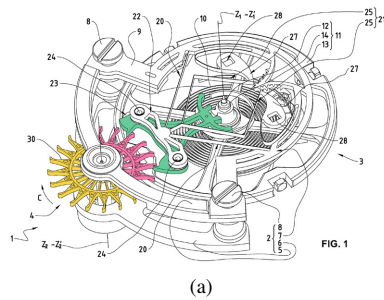
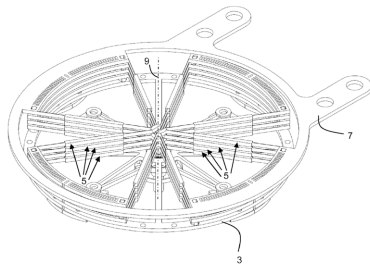


Fig. 18. Comb-drive actuated compliant double parallel arm mechanism. Adapted from [42, Fig.24]

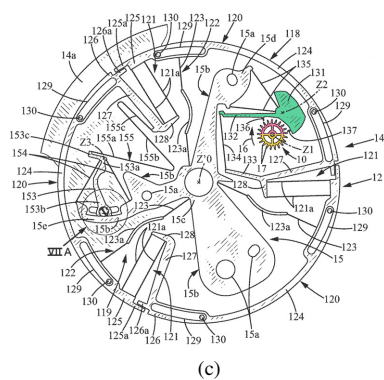
Sönmez synthesised an intermittent motion mechanism which is based on a buckling beam to provide intermittent motion [43]. The mechanism derived can be implemented at MEMS scale, and provides oscillating dwell motion with a single dwell. The dwell is created by the fact that the connecting rod is a flexible member, and the shuttle will only move once the critical buckling load of the buckling member is exceeded. Until then, the connecting member deforms, storing the energy. This means that the end effector is stationary until the buckling load is exceeded.



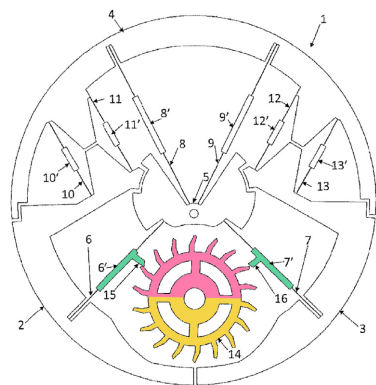
(a)



(b)



(c)



(d)

Fig. 16. Three types of compliant escapements developed during the last ten years: a) and b) show the escapement, and the accompanying oscillator developed by Gunten et al. [37], [38], c) shows the solution proposed by Semon et al. [39], and d) shows the latest development by Sybren et al. [40]

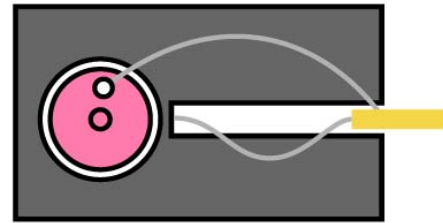


Fig. 19. A buckling intermittent motion MEMS linkage. Adapted from [43, Fig. 23]

In a later paper by Sönmez, the synthesis of a dwell mechanism based on a buckling arc is described [44]. For this mechanism the buckling member is replaced with an arc. As a result, the shuttle could be guided in linear direction by this arc, while the buckling characteristics of the previous design remain. Furthermore, this mechanism can provide a double dwell motion profile. This means, that this design requires one less mechanical interaction. Thus decreasing the amount of friction interactions, and decreasing the loss of energy due to damping.

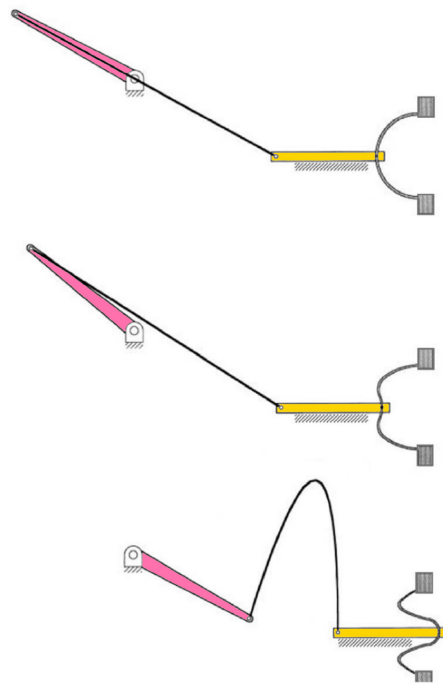


Fig. 20. A buckling intermittent motion mechanism, based on a buckling arc and connecting rod. Adapted from [44, Fig.3]

Sönmez et al. describe the synthesis of a compliant bistable mechanism in their paper [45]. To validate the design, a novel combination of PRBM and Elastica theory is used to assess the behaviour of the bistable elements. Tekeş et al. performed an experimental and simulation analysis on a similar bistable mechanism [46]. Showing the behaviour for a linear partially compliant mechanism. If this mechanism is made to be fully compliant, it could replace the buckling arc shown in fig. 20, allowing for the removal of one of the rigid joints. [46]

Later Tekeş describes the production and validation of a compliant translational dwell mechanism which obtains its behaviour through the buckling of members during motion [47], [48]. This mechanism is similar to the one synthesised by Sönmez. The author describes this mechanism as a partially compliant mechanism because of the rigid joints which are used to connect the buckling beams, and the linear stage which constrains the oscillating shuttle. From the experimental results, one can see that the obtained dwell is non-exact.

Based on the previously described research, it can be seen that the research pertaining to the field of compliant intermittent motion mechanisms is minimal. Furthermore, the solutions obtained from synthesis are still dependent on traditional mechanical interactions for their core function. This means that the proposed solutions do not benefit from the full advantages of a fully compliant system, such as a lack of friction for instance. In [43], Sönmez shows a MEMS partially compliant mechanism which approaches a monolithic design, however this still requires traditional revolute and prismatic joints.

## V. RESULTS

It was observed that apart from the book by Bickford, no review body focussed on intermittent motion could be found. This meant that no concrete, recent and encompassing categorisation of intermittent motion mechanisms was found. As such it was determined to be necessary to perform a categorisation. This categorisation resulted in the web shown in fig. 21. Generally, the mechanisms can be grouped into two overarching types namely: indexing and oscillating dwell mechanisms. Underneath these overarching types exist six categories. These categories are explained in section III, and are the main branches in fig. 21. Furthermore, two tables were generated which list the advantages and disadvantages of both traditional and compliant intermittent motion mechanisms. These tables, table I and II, are used to identify the areas where the traditional mechanisms can be improved, and whether compliant mechanisms already provide this improvement.

In traditional mechanisms the following challenges were found:

- 1) Impacts
- 2) Friction
- 3) Wear
- 4) High part count

These are challenges that can be mitigated using compliant mechanisms [11]. However, research into compliant intermittent motion generally lacks the solution to at least one of these problems. This hole in the state of the art shows in the following challenges for existing compliant intermittent motion mechanisms.

- 1) Friction interactions
- 2) Traditional rigid joints (prismatic and revolute)
- 3) Use of contact-aided friction based mechanisms

From this list the challenge which is solved least is that of friction. Even though a compliant mechanism could in theory run without friction, it is inherent to the design of the proposed solutions that some friction does play a role. This is a result of

the remaining rigid joint interactions present in the mechanisms, and the sliding interactions such as in the compliant ratchet by Kennedy et al. shown in fig. 9 [31].

It was observed that apart from ratchets, escapements, and linkage-type dwell mechanisms the design set of intermittent motion mechanisms remains largely unexplored. Furthermore, it is interesting to note that compliant ratchets are relatively similar to a traditional ratchet. The discussed ratcheting mechanisms are dependent on more traditional interactions, such as surface interactions.

In contrast, the developed linkage-type compliant dwell mechanisms would be impossible without utilising the characteristics of compliant mechanisms. For instance, in the mechanism by Sönmez [44] fig. 19, one can see that this mechanism is fully dependent on the buckling of beams, this would be impossible with a traditional linkage-type mechanism.

From the definition for indexing and oscillating dwell mechanisms, one can see that indexing mechanisms are impossible to be made fully compliant. This is as a result of the infinite travel along one DOF which is necessitated by the mechanism. In contrast, oscillating dwell mechanisms have a motion profile which suits itself better for compliant mechanisms. Oscillating dwell mechanisms oscillate around a position within a limited range of motion. Which is also possible in compliant mechanisms.

## VI. DISCUSSION

A literature survey into intermittent motion mechanisms has been performed. Based on what was found, this type of mechanism can be categorised into two encompassing types, namely: indexing mechanisms and oscillating dwell mechanisms. Indexing mechanisms provide movement along one DOF over an infinite range, the motion of the end effector is stopped and held at indices which are generally equally spaced. Oscillating dwell mechanisms on the other hand, provide an oscillating movement which contains a dwell period. Although all oscillating mechanisms will require movement along one DOF to be zero at some point during the cycle, these mechanisms only provide instantaneous dwell. Oscillating dwell mechanisms provide a non-instantaneous dwell at one or more positions of the input crank.

Under these two types of intermittent motion, a total of six categories of mechanism exist. Four indexing motion mechanisms, and two oscillating dwell mechanisms.

### 1) Indexing motion

- a) Ratchets
- b) Geneva mechanisms
- c) Mutilated gears
- d) Escapements

### 2) Oscillating dwell motion

- a) Cam mechanisms
- b) Linkage mechanisms



TABLE I  
TABLE SUMMARISING THE CHARACTERISTICS OF TRADITIONAL INTERMITTENT MOTION MECHANISMS.


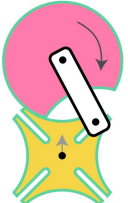
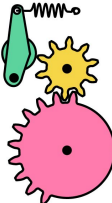
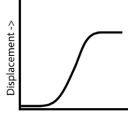
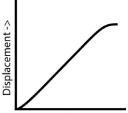
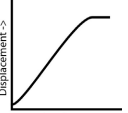
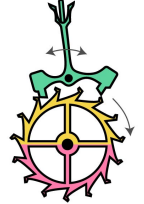
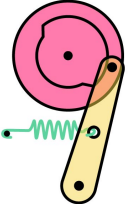
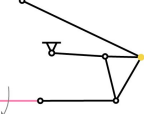

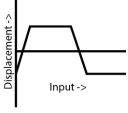
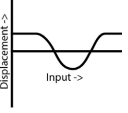


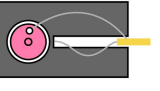
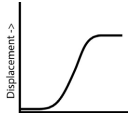
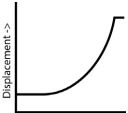
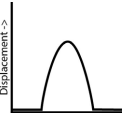
	Ratchets	Geneva mechanisms	Gears
Mechanism			
Motion Graph			
Advantages	Simple construction, can transmit high loads	Mild to no impacts, End effector locked during dwell	Easy synthesis, Exact dwell
Disadvantages	Harsh impacts, Frictional wear, Noisy	Only three-eighths indices, The locking surfaces experience stress when the output is under torque	Peak impact upon engagement
	Escapements	Cams	Linkages
Mechanism			
Motion Graph			
Advantages	Very precise timing	precise placement of output, no impacts	No impacts, High operation speeds
Disadvantages	Difficult synthesis and construction, behaviour dependent on input axis torque	Sliding wear, Mechanism behaviour is an optimisation of several variables	Difficult synthesis, Less precise, Difficult construction on small scales

TABLE II  
TABLE SUMMARISING THE CHARACTERISTICS OF COMPLIANT INTERMITTENT MOTION MECHANISMS.

	Ratchets	Escapements	Linkages
Mechanism			
Motion Graph			
Advantages	Less backlash, more predictable than	Less parts, Easier construction	Easy synthesis, Exact dwell
Disadvantages	Impacts, Frictional wear, Joints	Impacts	Peak impact upon engagement

In their traditional form all these mechanisms are found to suffer from the following problems:

- 1) *Impacts*
- 2) *Friction*
- 3) *Wear*
- 4) *High part count*
- 5) *Play*

These are problems that are known to be solvable by utilising the advantages of compliant mechanisms.

When regarding the body of research that can be found on compliant intermittent motion. It was revealed that from the six identified intermittent motion mechanism categories, only three have been made compliant. Two indexing mechanisms and two oscillating dwell mechanisms namely:

- 1) **Compliant indexing motion**
  - a) Ratchets
  - b) Escapements
- 2) **Compliant oscillating dwell motion**
  - a) Linkages

Between these three categories, differences in synthesis were observed.

Compliant ratchets are either similar in construction to the traditional method. Or they require two DOF to be controlled in order to perform the desired function. The compliant ratchets that were found still did not solve all the problems that have been identified in the traditional mechanisms. The main remaining problems are: Friction, impacts and a high part count. This is due to the high similarity to traditional ratcheting mechanisms. For example, the compliant pawl used in the mechanism proposed by Kennedy et al. [31] fig. 9 is constantly kept in contact with the ratchet wheel to ensure locking on indices. This problem is solved by Burkhardt et al. [36] fig. 14, however, the mechanism requires two DOF to perform this motion.

Compliant escapements have had a relatively big body of research in the form of patents. These patents outline the evolution of the compliant clockwork escapement. However, the escapement itself has not necessarily been innovated upon. Rather the focus was on a solution combining the regulating oscillator together with the escapement. This led to two integrated solutions by Semon et al. and Sybren et al. [39], [40]. However, these solutions still deal with mechanical friction and impacts at the ratchet wheel.

Compliant dwell linkages are unique in their characteristics, namely they rely on the qualities of compliant mechanisms to perform their motion. The linkage mechanisms developed by Sönmez and Tekeş utilise the buckling of their members to obtain the necessary dwell motion. This motion would not be possible with traditional bar mechanisms since in the modeling of bar mechanisms the assumption is always made that the bars of the mechanism do not bend. Although more of the qualities of compliant mechanisms are utilised by these solutions, the mechanisms still rely on the use of rigid rotary and prismatic joints. As a result these mechanisms too will suffer from similar problems as the traditional mechanisms.

From the obtained information, it can be reasoned that indexing mechanisms can not be made fully compliant. This

is because following from the definition of the indexing mechanism infinite motion along an axis is required. Regarding compliant mechanisms, an infinite motion along an axis is currently impossible to obtain. However, with some adjustments such as relaxing infinite motion, the mechanisms might be transformed into a design which offers similar performance in a monolithic part.

In contrast, oscillating dwell mechanisms can be made fully compliant. These mechanisms do not require infinite motion along one axis and could be controlled using an input that oscillates between two point without exceeding the motion range of a compliant mechanism.

On another note, when looking to compliant mechanisms for intermittent motion as a replacement for traditional mechanisms in existing device designs. Take a watch for instance, a fully compliant intermittent motion mechanism would be placed into the context of a traditional device. It is expected that on the input side a mechanical interaction is required to obtain a marriage of the mechanisms. This means that the mechanism can only be made such that friction is minimised at the interface between mechanisms rather than removed altogether. This is because the connection with the existing mechanism can not be made monolithic without redesigning the rest of the device. As such, the friction generated at the input and output of the compliant mechanism should be minimised as it can not be totally avoided. And one should look at the resulting lifetime of the mechanism on these interaction points, and compare this to the mechanism that is being replaced by the compliant mechanism.

Based on the literature review, the following research directions can be proposed.

- The development of fully compliant intermittent motion mechanisms
- The development of a mostly frictionless ratchet mechanism
- The viability of fully compliant intermittent motion

## VII. CONCLUSION

From the literature search, it was concluded that intermittent motion can be divided into two types. Namely indexing motion and oscillating dwell motion. These two types can then be further divided into six categories. These six categories are: Ratchets, Geneva mechanisms, mutilated gears, escapements, cam mechanisms and linkage mechanisms. These categories can be used to identify three categories of compliant intermittent motion mechanism, namely: Ratchets, escapements and linkages. None of the found solutions for these categories are made fully compliant. However, they do utilise the characteristics of compliant mechanisms. It was also found that the existing body of research pertaining to compliant intermittent motion is rather small. Roughly twenty papers and 10 patents were found, of which multiple referring to different steps of the same research. This shows that although mechanisms for intermittent motion have existed for a long time, new development options still present themselves.

## REFERENCES

- [1] J. H. 1. Bickford, *Mechanisms for intermittent motion*. English. New York: Industrial Press, 1972, Section: viii, 264 pages illustrations 26 cm, ISBN: 0-8311-1091-0.
- [2] K. J. Waldron, G. L. Kinzel, and S. K. Agrawal, *Kinematics, Dynamics, and Design of Machinery*, en. John Wiley & Sons, Apr. 2016, Google-Books-ID: vRqJCgAAQBAJ, ISBN: 978-1-118-93328-2.
- [3] B. Ciechanowski, *Mechanical Watch – Bartosz Ciechanowski*, en, Blog, May 2022. [Online]. Available: <https://ciechanow.ski/mechanical-watch/> (visited on 02/17/2023).
- [4] T. C. o. t. V. d. Joux, *The Theory of Horology*, en. Swiss Federation of Technical Colleges, 2015, Google-Books-ID: csNnzQEACAAJ, ISBN: 978-2-940025-49-7.
- [5] H. C. Kelly, *A Practical Course in Horology*, en. Manual arts Press, 1944.
- [6] V. Kharzhevskiy, M. Pashechko, O. Tatsenko, M. Marchenko, and P. Nosko, “The Synthesis of Dwell Mechanisms on the Basis of Straight-Line Linkages with Fivefold Interpolation Nodes,” English, *Advances in Science and Technology Research Journal*, vol. 15, no. 1, pp. 18–25, 2021, ISSN: 2299-8624. DOI: 10.12913/22998624/128817.
- [7] N. Sclater, *Mechanisms and mechanical devices source-book*, English, 5th ed. New York: McGraw-Hill Professional ; 2011, Section: 546 pages . : illustrations ; 29 cm, ISBN: 978-0-07-170442-7.
- [8] G. Figliolini and J. Angeles, “Synthesis of conjugate Geneva mechanisms with curved slots,” en, *Mechanism and Machine Theory*, vol. 37, no. 10, pp. 1043–1061, Oct. 2002, ISSN: 0094-114X. DOI: 10.1016/S0094-114X(02)00062-9. [Online]. Available: <https://www.sciencedirect.com/science/article/pii/S0094114X02000629> (visited on 06/06/2023).
- [9] V. Kharzhevskiy, “KINEMATIC SYNTHESIS OF LINKAGE MECHANISMS USING BURMESTER POINTS AT THE GIVEN DWELL DURATION OF THE OUTPUT LINK,” en, *Advances in Science and Technology Research Journal*, vol. 11, no. 2, pp. 139–145, Jun. 2017, ISSN: 2080-4075, 2299-8624. DOI: 10.12913/22998624/68465. [Online]. Available: <http://www.journalssystem.com/astrij/KINEMATIC-SYNTHESIS-OF-LINKAGE-MECHANISMS-USING-BURMESTER-POINTS-AT-THE-GIVEN-DWELL-DURATION-OF-THE-OUTPUT-LINK,68465,0,2.html> (visited on 04/20/2023).
- [10] B. Thomaszewski, S. Coros, D. Gauge, V. Megaro, E. Grinspun, and M. Gross, “Computational design of linkage-based characters,” en, *ACM Transactions on Graphics*, vol. 33, no. 4, pp. 1–9, Jul. 2014, ISSN: 0730-0301, 1557-7368. DOI: 10.1145/2601097.2601143. [Online]. Available: <https://dl.acm.org/doi/10.1145/2601097.2601143> (visited on 12/30/2023).
- [11] L. L. Howell, “Compliant Mechanisms,” en, in *21st Century Kinematics*, J. M. McCarthy, Ed., London: Springer London, 2013, pp. 189–216, ISBN: 978-1-4471-4509-7. DOI: 10.1007/978-1-4471-4510-3\_7. [Online]. Available: [http://link.springer.com/10.1007/978-1-4471-4510-3\\_7](http://link.springer.com/10.1007/978-1-4471-4510-3_7) (visited on 12/08/2022).
- [12] G. K. Ananthasuresh and S. Kota, “Designing compliant mechanisms,” English, *Mechanical Engineering*, vol. 117, no. 11, pp. 93–96, Nov. 1995, Place: New York Publisher: American Society of Mechanical Engineers. [Online]. Available: <https://www.proquest.com/magazines/designing-compliant-mechanisms/docview/2659864985/se-2?accountid=27026>.
- [13] N. Lobontiu, *Compliant mechanisms: design of flexure hinges*, en. Boca Raton: CRC Press, 2003, ISBN: 978-0-8493-1367-7.
- [14] P. W. Jensen, *Classical and modern mechanisms for engineers and inventors* (Mechanical engineering), English. New York: M. Dekker, 1991, Section: vi, 603 pages : illustrations ; 24 cm., ISBN: 978-0-8247-8527-7. [Online]. Available: <http://catdir.loc.gov/catdir/enhancements/fy0647/91019847-d.html> (visited on 03/06/2023).
- [15] J. J. Uicker, G. R. Pennock, and J. E. Shigley, *Theory of machines and mechanisms*, en, Fifth edition. New York: Oxford University Press, 2017, ISBN: 978-0-19-026448-2.
- [16] C. Evans, *Precision Engineering: An Evolutionary View*, en. Cranfield Press, 1989, Google-Books-ID: \_0RSAAAAMAAJ, ISBN: 978-1-871315-01-1.
- [17] F. Zheng, L. Hua, X. Han, B. Li, and D. Chen, “Synthesis of indexing mechanisms with non-circular gears,” en, *Mechanism and Machine Theory*, vol. 105, pp. 108–128, Nov. 2016, ISSN: 0094114X. DOI: 10.1016/j.mechmachtheory.2016.06.019. [Online]. Available: <https://linkinghub.elsevier.com/retrieve/pii/S0094114X16301240> (visited on 02/28/2023).
- [18] A. A. Prikhodko, A. I. Smelyagin, and A. D. Tsybin, “Kinematics of Planetary Mechanisms with Intermittent Motion,” en, *Procedia Engineering*, International Conference on Industrial Engineering, ICIE 2017, vol. 206, pp. 380–385, Jan. 2017, ISSN: 1877-7058. DOI: 10.1016/j.proeng.2017.10.489. [Online]. Available: <https://www.sciencedirect.com/science/article/pii/S187770581735172X> (visited on 02/28/2023).
- [19] G. Figliolini and J. Angeles, “The Synthesis of Elliptical Gears Generated by Shaper-Cutters,” en, *Journal of Mechanical Design*, vol. 125, no. 4, pp. 793–801, Dec. 2003, ISSN: 1050-0472, 1528-9001. DOI: 10.1115/1.1631573. [Online]. Available: <https://doi.org/10.1115/1.1631573> (visited on 06/06/2023).
- [20] F. Sanchez-Marin and V. Roda-Casanova, “An approach for the global search for top-quality six-bar dwell linkages,” en, *Mechanism and Machine Theory*, vol. 176, p. 104974, Oct. 2022, ISSN: 0094-114X. DOI: 10.1016/j.mechmachtheory.2022.104974. [Online]. Available: <https://www.sciencedirect.com/science/article/pii/S0094114X22002282> (visited on 03/16/2023).
- [21] S. Kota, A. G. Erdman, and D. R. Riley, “Development of Knowledge Base for Designing Linkage-Type Dwell Mechanisms: Part 2—Application,” en, *Journal of Mechanisms, Transmissions, and Automation in Design*,

- vol. 109, no. 3, pp. 316–321, Sep. 1987, ISSN: 0738-0666. DOI: 10.1115/1.3258796. [Online]. Available: <https://asmedigitalcollection.asme.org/mechanicaldesign/article/109/3/316/434339/Development-of-Knowledge-Base-for-Designing> (visited on 03/14/2023).
- [22] S. Kota, A. G. Erdman, and D. R. Riley, “Development of Knowledge Base for Designing Linkage-Type Dwell Mechanisms: Part I—Theory,” en, *Journal of Mechanisms, Transmissions, and Automation in Design*, vol. 109, no. 3, pp. 308–315, Sep. 1987, ISSN: 0738-0666. DOI: 10.1115/1.3258795. [Online]. Available: <https://asmedigitalcollection.asme.org/mechanicaldesign/article/109/3/308/434310/Development-of-Knowledge-Base-for-Designing> (visited on 03/14/2023).
- [23] M. Čavić, M. Penčić, M. Rackov, J. Dorić, and Z. Lu, “Graphical synthesis of 6-bar dwell linkage mechanism,” en, *FME Transactions*, vol. 47, no. 2, pp. 226–233, 2019, ISSN: 1451-2092, 2406-128X. DOI: 10.5937/fmet1902226C. [Online]. Available: <https://scindeks.ceon.rs/Article.aspx?artid=1451-20921902226C> (visited on 03/14/2023).
- [24] F. Sanchezmarin, “Global optimization in path synthesis based on design space reduction,” en, *Mechanism and Machine Theory*, vol. 38, no. 6, pp. 579–594, Jun. 2003, ISSN: 0094114X. DOI: 10.1016/S0094-114X(03)00010-7. [Online]. Available: <https://linkinghub.elsevier.com/retrieve/pii/S0094114X03000107> (visited on 01/09/2023).
- [25] M. Jagannath and S. Bandyopadhyay, “A new approach towards the synthesis of six-bar double dwell mechanisms,” Springer, 2009, pp. 209–216, ISBN: 3-642-01946-3.
- [26] G. Figliolini and C. Lanni, “Jerk and Jounce Relevance for the Kinematic Performance of Long-Dwell Mechanisms,” en, in *Advances in Mechanism and Machine Science*, T. Uhl, Ed., ser. Mechanisms and Machine Science, Cham: Springer International Publishing, 2019, pp. 219–228, ISBN: 978-3-030-20131-9. DOI: 10.1007/978-3-030-20131-9\_22.
- [27] P. S. Shiakolas, D. Koladiya, and J. Kebrle, “On the optimum synthesis of six-bar linkages using differential evolution and the geometric centroid of precision positions technique,” en, *Mechanism and Machine Theory*, vol. 40, no. 3, pp. 319–335, Mar. 2005, ISSN: 0094-114X. DOI: 10.1016/j.mechmachtheory.2004.07.005. [Online]. Available: <https://www.sciencedirect.com/science/article/pii/S0094114X04001260> (visited on 04/20/2023).
- [28] A. Baskar, M. Plecnik, and J. Hauenstein, “Finding Straight Line Generators Through the Approximate Synthesis of Symmetric Four-Bar Coupler Curves,” English, ISSN: 2511-1256, vol. 24 SPAR, 2022, pp. 277–285, ISBN: 978-3-031-08139-2. DOI: 10.1007/978-3-031-08140-8\_30.
- [29] S. Varedi-Koulai and H. Rezagholizadeh, “Synthesis of the four-bar linkage as path generation by choosing the shape of the connecting rod,” *Proceedings of the Institution of Mechanical Engineers, Part C: Journal of Mechanical Engineering Science*, vol. 234, no. 13, pp. 2643–2652, Jul. 2020, Publisher: IMECHE, ISSN: 0954-4062. DOI: 10.1177/0954406220908616. [Online]. Available: <https://doi.org/10.1177/0954406220908616> (visited on 12/06/2022).
- [30] B. Corves, G. Lonij, and M. Hüsing, “Kinematic Synthesis of a Step Mechanism Based on a Five Bar Linkage,” en, *Applied Mechanics and Materials*, vol. 162, pp. 1–10, Mar. 2012, ISSN: 1662-7482. DOI: 10.4028/www.scientific.net/AMM.162.1. [Online]. Available: <https://www.scientific.net/AMM.162.1> (visited on 03/16/2023).
- [31] J. A. Kennedy, L. L. Howell, and W. Greenwood, “Compliant high-precision E-quintet ratcheting (CHEQR) mechanism for safety and arming devices,” en, *Precision Engineering*, vol. 31, no. 1, pp. 13–21, Jan. 2007, ISSN: 01416359. DOI: 10.1016/j.precisioneng.2006.01.001. [Online]. Available: <https://linkinghub.elsevier.com/retrieve/pii/S0141635906000080> (visited on 01/09/2023).
- [32] A. H. Sakhaei, S. Kaijima, T. L. Lee, Y. Y. Tan, and M. L. Dunn, “Design and investigation of a multi-material compliant ratchet-like mechanism,” en, *Mechanism and Machine Theory*, vol. 121, pp. 184–197, Mar. 2018, ISSN: 0094114X. DOI: 10.1016/j.mechmachtheory.2017.10.017. [Online]. Available: <https://linkinghub.elsevier.com/retrieve/pii/S0094114X17307474> (visited on 01/17/2023).
- [33] L. Hartmann and L. Zentner, “A compliant mechanism as rocker arm with spring capability for precision engineering applications,” English, *Mechanisms and Machine Science*, vol. 30, pp. 1–7, 2015, ISBN: 9783319158617, ISSN: 2211-0984. DOI: 10.1007/978-3-319-15862-4\_1.
- [34] G. M. Roach and L. L. Howell, “Evaluation and Comparison of Alternative Compliant Overrunning Clutch Designs,” *Journal of Mechanical Design*, vol. 124, no. 3, pp. 485–491, Aug. 2002, ISSN: 1050-0472. DOI: 10.1115/1.1480414. [Online]. Available: <https://doi.org/10.1115/1.1480414> (visited on 01/20/2023).
- [35] P. Minotti, G. Bourbon, and P. L. Moal, “Indexation passive d’un élément mobile présentant des dents,” fr, EP2802852B1, Oct. 2017. [Online]. Available: [https://patents.google.com/patent/EP2802852B1/en?q=\(PASSIVE+INDEXING+OF+A+MOVABLE+ELEMENT+HAVING+TEETH\)&oq=PASSIVE+INDEXING+OF+A+MOVABLE+ELEMENT+HAVING+TEETH](https://patents.google.com/patent/EP2802852B1/en?q=(PASSIVE+INDEXING+OF+A+MOVABLE+ELEMENT+HAVING+TEETH)&oq=PASSIVE+INDEXING+OF+A+MOVABLE+ELEMENT+HAVING+TEETH) (visited on 03/28/2023).
- [36] W. Burkhardt, M. Subarew, H. Hellriegel, and H. Zachmann, “Bidirectional mems driving arrangements with a force absorbing system,” US20220171341A1, Jun. 2022. [Online]. Available: [https://patents.google.com/patent/US20220171341A1/en?q=\(BIDIRECTIONAL+MEMS+DRIVING+ARRANGEMENTS+WITH+A+FORCE+ABSORBING+SYSTEM\)&oq=BIDIRECTIONAL+MEMS+DRIVING+ARRANGEMENTS+WITH+A+FORCE+ABSORBING+SYSTEM](https://patents.google.com/patent/US20220171341A1/en?q=(BIDIRECTIONAL+MEMS+DRIVING+ARRANGEMENTS+WITH+A+FORCE+ABSORBING+SYSTEM)&oq=BIDIRECTIONAL+MEMS+DRIVING+ARRANGEMENTS+WITH+A+FORCE+ABSORBING+SYSTEM) (visited on 03/28/2023).
- [37] S. v. Gunten and Q. Gubler, “Mécanisme et procédé de réglage d une vitesse dans un mouvement horloger,” fr, EP3037894A1, Jun. 2016. [Online]. Available: [https://patents.google.com/patent/EP3037894A1/en?q=\(escape](https://patents.google.com/patent/EP3037894A1/en?q=(escape)

- ment)&assignee=ulyse+nardin&oq=ulyse+nardin+escapement&page=1 (visited on 05/24/2023).
- [38] S. v. Gunten, “Oscillateur mécanique,” fr, EP3637196A1, Apr. 2020. [Online]. Available: [https://patents.google.com/patent/EP3637196A1/en?q=\(oscillator\)&assignee=ulyse+nardin&oq=ulyse+nardin+oscillator&page=2](https://patents.google.com/patent/EP3637196A1/en?q=(oscillator)&assignee=ulyse+nardin&oq=ulyse+nardin+oscillator&page=2) (visited on 02/15/2023).
- [39] G. Semon, W. J. B. Ypma, S. L. Weeke, and N. Tolou, “Device for Timepiece, Clockwork Movement and Timepiece Comprising Such a Device,” en, US20200333746A1, Oct. 2020. [Online]. Available: <https://patents.google.com/patent/US20200333746A1/en?inventor=nima+tolou&assignee=lvmh&oq=lvmh+nima+tolou> (visited on 02/16/2023).
- [40] L. W. Sybren and P. L. Maarten, “A mechanical watch,” en, NL2024076B1, Jul. 2021. [Online]. Available: [https://patents.google.com/patent/NL2024076B1/en?q=\(oscillator\)&assignee=flexous&oq=flexous+oscillator](https://patents.google.com/patent/NL2024076B1/en?q=(oscillator)&assignee=flexous&oq=flexous+oscillator) (visited on 05/17/2023).
- [41] A. Tekeş, Ü. Sönmez, and B. A. Güvenç, “Trajectory Control of Compliant Parallel-Arm Mechanisms,” en, *Journal of Mechanical Design*, vol. 132, no. 1, p. 011006, Jan. 2010, ISSN: 1050-0472, 1528-9001. DOI: 10.1115/1.4000637. [Online]. Available: <https://asmigitalcollection.asme.org/mechanicaldesign/article/doi/10.1115/1.4000637/461942/Trajectory-Control-of-Compliant-ParallelArm> (visited on 03/16/2023).
- [42] A. Tekeş, Ü. Sönmez, and B. A. Güvenç, “Compliant folded beam suspension mechanism control for rotational dwell function generation using the state feedback linearization scheme,” en, *Mechanism and Machine Theory*, vol. 45, no. 12, pp. 1924–1941, Dec. 2010, ISSN: 0094-114X. DOI: 10.1016/j.mechmachtheory.2010.07.005. [Online]. Available: <https://www.sciencedirect.com/science/article/pii/S0094114X10001333> (visited on 03/16/2023).
- [43] Ü. Sönmez, “Synthesis methodology of a compliant exact long dwell mechanism using elastica theory,” en, *International Journal of Mechanics and Materials in Design*, vol. 3, no. 1, pp. 73–90, Mar. 2006, ISSN: 1573-8841. DOI: 10.1007/s10999-006-9014-y. [Online]. Available: <https://doi.org/10.1007/s10999-006-9014-y> (visited on 03/13/2023).
- [44] Ü. Sönmez, “Introduction to Compliant Long Dwell Mechanism Designs Using Buckling Beams and Arcs,” en, *Journal of Mechanical Design*, vol. 129, no. 8, pp. 831–843, Aug. 2007, ISSN: 1050-0472, 1528-9001. DOI: 10.1115/1.2735337. [Online]. Available: <https://asmigitalcollection.asme.org/mechanicaldesign/article/129/8/831/471699/Introduction-to-Compliant-Long-Dwell-Mechanism> (visited on 03/13/2023).
- [45] Ü. Sönmez and C. C. Tutum, “A Compliant Bistable Mechanism Design Incorporating Elastica Buckling Beam Theory and Pseudo-Rigid-Body Model,” *Journal of Mechanical Design*, vol. 130, no. 4, Feb. 2008, ISSN: 1050-0472. DOI: 10.1115/1.2839009. [Online]. Available: <https://doi.org/10.1115/1.2839009> (visited on 12/06/2022).
- [46] A. Tekes, H. Lin, and K. McFall, “Design, Analysis, Experimentation, and Control of a Partially Compliant Bistable Mechanism,” en, *Journal of Dynamic Systems, Measurement, and Control*, vol. 142, no. 1, p. 011008, Jan. 2020, ISSN: 0022-0434, 1528-9028. DOI: 10.1115/1.4045151. [Online]. Available: <https://asmigitalcollection.asme.org/dynamicsystems/article/doi/10.1115/1.4045151/1065460/Design-Analysis-Experimentation-and-Control-of-a> (visited on 03/13/2023).
- [47] A. Tekes, H. Lin, and K. McFall, “Design, modelling and experimentation of a novel compliant translational dwell mechanism,” en, *Journal of Mechanical Science and Technology*, vol. 33, no. 7, pp. 3137–3145, Jul. 2019, ISSN: 1976-3824. DOI: 10.1007/s12206-019-0609-2. [Online]. Available: <https://doi.org/10.1007/s12206-019-0609-2> (visited on 03/13/2023).
- [48] A. Tekes and H. Lin, “Compliant Translational Double Exact Dwell Mechanism,” en, in *Volume 4A: Dynamics, Vibration, and Control*, Pittsburgh, Pennsylvania, USA: American Society of Mechanical Engineers, Nov. 2018, V04AT06A009, ISBN: 978-0-7918-5203-3. DOI: 10.1115/IMECE2018-86073. [Online]. Available: <https://asmigitalcollection.asme.org/IMECE/proceedings/IMECE2018/52033/Pittsburgh,%20Pennsylvania,%20USA/289694> (visited on 03/16/2023).
- [49] R. Halicioglu, A. Jomartov, and M. Kuantova, “Optimum design and analysis of a novel planar eight-bar linkage mechanism,” en, *Mechanics Based Design of Structures and Machines*, pp. 1–22, Nov. 2021, ISSN: 1539-7734, 1539-7742. DOI: 10.1080/15397734.2021.1995410. [Online]. Available: <https://www.tandfonline.com/doi/full/10.1080/15397734.2021.1995410> (visited on 03/16/2023).

## APPENDIX

TABLE III  
COMPARISON TABLE OF THE RELEVANT COMPLIANT INTERMITTENT MOTION MECHANISMS.

	impacts	Friction	Joints	Not scalable	Part count
CHEQR Ratchet	x	x	x		3
Multimaterial ratchet	x	x		x	2
Compliant rocker ratchet	x	x	x	x	3
Compliant clutch	x	x			2
Minotti ratchet	x	x			2
Burkhardt ratchet					2
Jensen ratchet		x		x	2
Gunten Escapement 2014	x		x		6
Gunten Escapement 2020	x				3
Semon Escapement	x			x	2
Sybren Escapement	x				2
Parallel compliant guide		x	x		6
MEMS long dwell		x	x		2
Buckling arc long dwell		x	x		3
Double exact buckling dwell		x	x		5

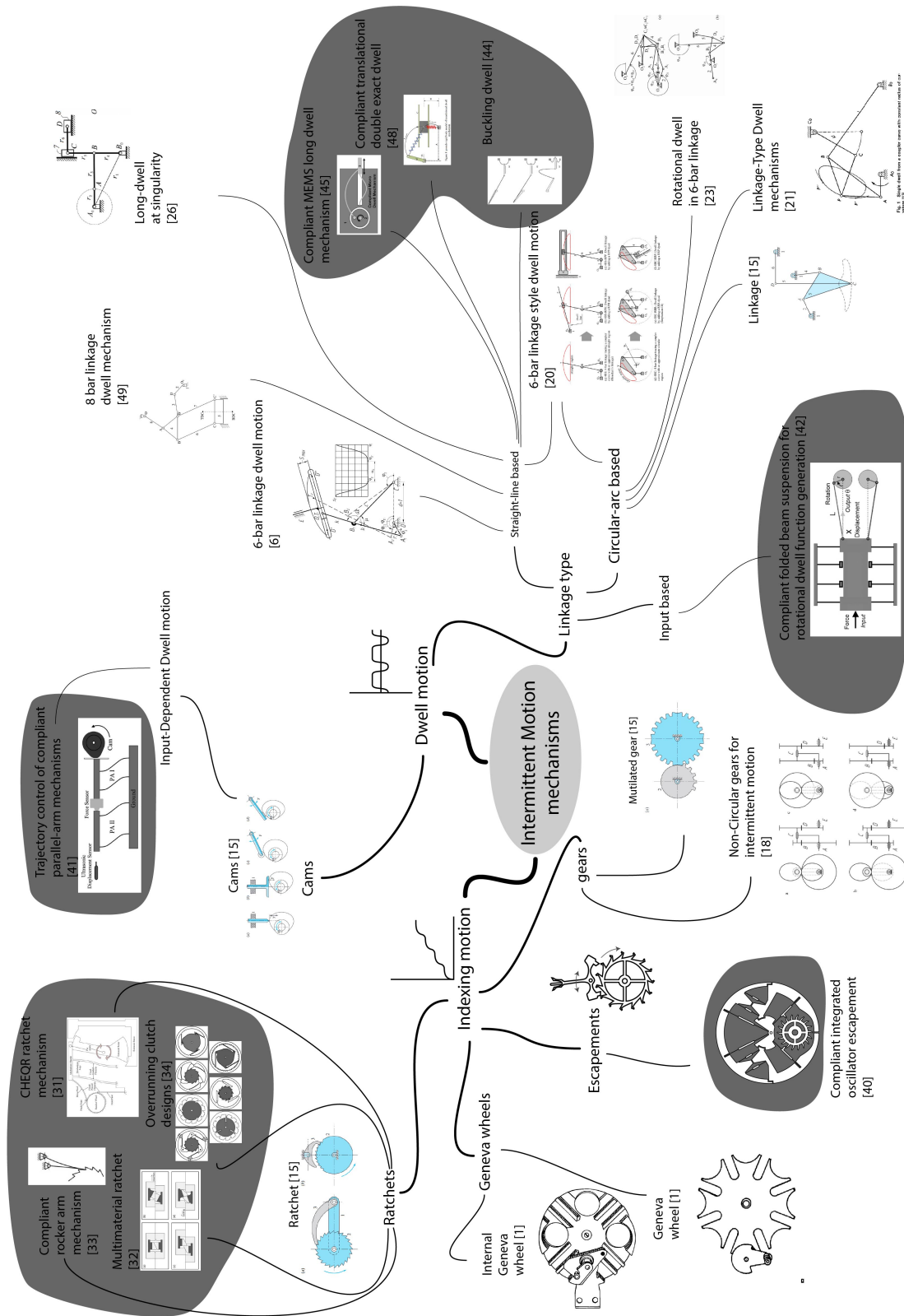


Fig. 21. Categorisation of intermittent motion mechanisms. This mindmap gives an overview of the found and considered intermittent motion mechanisms. The compliant mechanisms are highlighted with a dark gray background. Furthermore, a distinction is made between higher and lower kinematic mechanisms. [9], [15], [18], [20], [21], [23], [26], [31]–[34], [40]–[44], [48], [49]

TABLE IV  
DISCUSSING THE COMPLIANT VIABILITY OF TRADITIONAL MECHANISMS

	Ratchets	Geneva mechanisms	Gears
Partially compliant	x	x	x
Fully compliant			
Motivation	<p>Because the axis which is to be indexed requires infinite travel, it is impossible to make this mechanism compliant. However, as can be seen in fig. 8, there are some partially compliant solutions for the design of a ratchet system.</p>	<p>Similar to the ratcheting mechanism, due to the infinite travel along one axis which is required for an indexing mechanism, this system can not be made fully compliant. However, it may be possible to replicate a two-position geneva mechanism using a bistable mechanism.</p>	<p>Because of the nature of gears, it is practically impossible to make them fully compliant. The types of gear which provide intermittent motion are generally mutilated gears. These might be approximated using buckling beams.</p>
Partially compliant	Escapements	Cams	Linkages
Fully compliant	x	x	x
Motivation	<p>Escapements can not be made fully compliant, this is because this mechanism requires full rotation of the input axis. However, the oscillator part of the mechanism can be made compliant.</p>	<p>Similarly to ratchets, due to the sliding interaction it is impossible to replace this type of mechanism with a fully compliant mechanism. Thus, the follower is the part which could be replaced with a compliant mechanism. Alternatively to ratchets however, one could look for a linkage type counterpart to a cam mechanism and make this compliant.</p>	<p>Linkages can be replaced with a compliant mechanism, one could overlay the rigid members and replace the joints with compliant rotational joints for example. The challenge for this type of mechanism is that due to the nature of compliant mechanisms, the full rotation of the input crank becomes impossible. As a result one wants to ensure that the mechanism is produced in the correct initial position to capture the desired path.</p>



